

Durham E-Theses

Studies and computing techniques in the spectral characterisation of solids

Puteh, Rustam

How to cite:

Puteh, Rustam (1984) *Studies and computing techniques in the spectral characterisation of solids*, Durham theses, Durham University. Available at Durham E-Theses Online:
<http://etheses.dur.ac.uk/7181/>

Use policy

The full-text may be used and/or reproduced, and given to third parties in any format or medium, without prior permission or charge, for personal research or study, educational, or not-for-profit purposes provided that:

- a full bibliographic reference is made to the original source
- a [link](#) is made to the metadata record in Durham E-Theses
- the full-text is not changed in any way

The full-text must not be sold in any format or medium without the formal permission of the copyright holders.

Please consult the [full Durham E-Theses policy](#) for further details.

STUDIES AND COMPUTING TECHNIQUES
IN THE
SPECTRAL CHARACTERISATION OF SOLIDS

by

Rustam Puteh, B.Sc. (University of Malaya)

Graduate Society

The copyright of this thesis rests with the author.
No quotation from it should be published without
his prior written consent and information derived
from it should be acknowledged.

A Thesis submitted to the University of Durham

in candidature of the degree of

Doctor of Philosophy

June, 1984



13 AUG 1984

To my late father

i

ABSTRACT

A new rapid technique for the measurement of permittivity and dielectric loss has been developed by utilising the concept of Fourier methods of analysis. In the equipment developed an input signal, characterised by having known harmonic components, was fed (in a coaxial system) to a solid sample and the distorted output waveform could either be Fourier analysed by a computer whose output was programmed to give directly the variations of permittivity and dielectric loss with frequency or compared directly with reference waveforms stored in the computer. Trials made with standard materials showed that the results obtained by the Fourier computerised technique were in very good agreement with those obtained by the more conventional methods.

The Fourier technique, together with an improved cavity perturbation method at 9.4GHz., has been used to make an extended study of the dielectric properties of reaction bonded silicon nitride (RBSN). Attention was particularly directed to the situation in partially nitrated materials, a region which has not been fully explored in previous studies. The salient feature of the experimental results is the presence of a peak in the variation of permittivity with weight gain. This effect has been discussed in terms of structural and microstructural studies which have shown the presence of impurity phases of iron silicide (FeSi_2) and calcium silicide (CaSi_2) in addition to the expected silicon and voids.

ACKNOWLEDGEMENTS

I am most grateful to my supervisors, Dr. J.S. Thorp and Dr. B.L.J. Kulesza, for their unfailing guidance and assistance in the execution of this project and in the preparation of this thesis.

My sincere thanks to Professor G.G. Roberts for giving me access to the facilities of the Department, the technical staff of the Department, especially Mr. R.T. Harcourt, for his help in the sample preparation, and to Messrs. P. Friend, C. Savage, W. Mounsey and P.J.E. Richardson, for their help in the construction of apparatus.

I would like to thank Dr. G.J. Russell for the help and suggestions he gave in the structural and microstructural studies of RBSN.

I would also like to express my gratitude to the University of Malaya for the award of a scholarship and for the grant of study leave from October 1980 until June 1984.

Finally, to Rukiah, without whom this thesis would not exist, thank you.

CONTENTS

Part I

	Page
CHAPTER 1	
INTRODUCTION	
1.1 GENERAL FEATURES	1
1.2 SUMMARY OF THESIS	2
REFERENCES	6
CHAPTER 2	
TECHNIQUES FOR MEASURING DIELECTRIC PROPERTIES	
2.1 INTRODUCTION	8
2.2.1 BRIDGE TECHNIQUES	10
2.2.2 RESONANT CIRCUIT TECHNIQUES	12
2.2.3 TRANSMISSION LINE MEASUREMENTS	14
2.2.4 SLOTTED LINE TECHNIQUES	16
2.2.5 CAVITY PERTURBATION METHODS	17
2.3 TIME DOMAIN TECHNIQUES	20
2.3.1 INTRODUCTION	20
2.3.2 BASIC PRINCIPLES OF TDS METHODS	21
2.4 USE OF COMPUTER IN PERMITTIVITY MEASUREMENT	23
REFERENCES	25
CHAPTER 3	
THEORY OF FOURIER METHOD	
3.1 INTRODUCTION	29
3.2 FOUNDATION OF FOURIER ANALYSIS	30
3.3 DETERMINATION OF FOURIER COEFFICIENTS	32
3.4 THEORY OF THE DIELECTRIC TEST CIRCUIT	33
3.4.2 THE EQUIVALENT TEST CIRCUIT	34
3.5 SIGNIFICANCE OF THE DERIVED EQUATIONS	38
REFERENCES	41

	Page
CHAPTER 4	
EXPERIMENTAL FOURIER ANALYSIS TECHNIQUES SYSTEM	
4.1 INTRODUCTION	43
4.2 THE COMPLETE SYSTEM	43
4.3 CHOICE OF INPUT WAVEFORM	44
4.4 SAMPLE-HOLDER DESIGN	47
4.5 SAMPLING AND COMPUTING	47
4.6 TEST OF DATA ACQUISITION SYSTEM	50
REFERENCES	51
CHAPTER 5	
APPRAISAL OF THE FOURIER ANALYSIS TECHNIQUE	
5.1 INTRODUCTION	52
5.2 EARLY EXPERIMENT USING WAVE ANALYSER	53
5.3 RESULTS ON PURE MgO AND VITREOSIL	54
5.4 DISCUSSION AND CONCLUSION	55
REFERENCES	58
CHAPTER 6	
THE CRITERIA FOR AND APPRAISAL OF THE CAVITY PERTURBATION METHOD	
6.1 INTRODUCTION	59
6.2 THE PERTURBATION FORMULAE AND THE CRITERIA	59
6.3 DETAILS OF MEASUREMENT TECHNIQUES	62
6.4 APPRAISAL OF THE METHOD	64
6.4.1 MEASUREMENTS OF THE FREQUENCY SHIFT USING DIFFERENT LENGTHS OF SILICA ROD	64
6.4.2 MEASUREMENTS WITH STANDARD SAMPLES	65
6.5 DISCUSSION	66
REFERENCES	67

ν

Part II

	Page
CHAPTER 7	
PREPARATION AND GENERAL PROPERTIES OF REACTION BONDED SILICON NITRIDE (RBSN)	
7.1 INTRODUCTION	68
7.2 MATERIAL PREPARATION	70
7.2.1 CHEMICAL VAPOUR DEPOSITION (CVD)-Si ₃ N ₄	70
7.2.2 HOT PRESSED SILICON NITRIDE	70
7.2.3 REACTION BONDED SILICON NITRIDE (RBSN)	71
7.3 REACTION MECHANISMS OF RBSN	72
7.4 THE RBSN SAMPLES STUDIED	75
REFERENCES	79
CHAPTER 8	
EXAMINATION OF FULLY NITRIDED RBSN	
8.1 INTRODUCTION	83
8.2 DIELECTRIC MEASUREMENTS	84
8.3 ANALYSIS OF BULK CERAMIC PERMITTIVITY RESULTS	85
8.4 CONCLUSIONS	88
REFERENCES	90
CHAPTER 9	
EXAMINATION OF PARTIALLY NITRIDED RBSN	
9.1 RESULTS	91
9.1.1.1 FREQUENCY VARIATION OF ϵ' AND ϵ''	91
9.1.1.2 VARIATION OF MEASURED PERMITTIVITY WITH WEIGHT GAIN	93
9.1.2.1 STRUCTURAL AND MICROSTRUCTURAL STUDIES OF RBSN	95
9.1.2.2 X-RAY DIFFRACTION	96

	Page
9.1.2.3 REFLECTION HIGH ENERGY ELECTRON DIFFRACTION	101
9.1.2.4 SCANNING ELECTRON MICROSCOPE AND EDAX STUDY	105
9.2 DIELECTRIC THEORY OF COMPOSITE MATERIALS	110
9.3 CONCLUSIONS AND SUGGESTIONS	114
REFERENCES	115

CHAPTER 1

INTRODUCTION

1.1 GENERAL FEATURES

The present work had two main objectives, namely to develop a new, rapid technique for the measurement of permittivity and dielectric loss and then to apply this method, together with other suitable conventional or recently improved methods to the study of one ceramic system, Reaction Bonded Silicon Nitride (RBSN). The first objective arose because in the previous work, undertaken by the research group over several years, there had been a need to determine the frequency variation of ϵ' and ϵ'' over a very wide range of frequency in order to establish whether, in the systems under investigation e.g. doped magnesia, oxynitride glass, hot pressed silicon nitride and sialon ceramics, the main mechanism responsible for conductivity was hopping. This had necessitated the development, assembly and appraisal of several specific techniques e.g. low frequency bridge, Q-meter, coaxial line and cavity techniques, each of which covered a limited range of frequency. Obtaining experimental data over the whole frequency range thus required both familiarisation with all the respective techniques and the expenditure of a large amount of time spent in making the detailed measurements. It would clearly be advantageous to obtain similar information more rapidly and this idea leads first to the concept of utilising Fourier methods of analysis as an alternative. In principle an input signal characterised by having known harmonic components could be fed, in a coaxial system, to a solid sample; the



transmitted distorted waveform could then be Fourier analysed by a computer whose output could be programmed to give directly the ϵ' versus frequency and ϵ'' versus frequency data. A description of the development and appraisal of the new Fourier computerised technique which gives frequency coverage from 25MHz to about 1GHz forms the basis of the first half of this thesis. Trials made with standard reference materials showed that the Fourier method gave answers in very good agreement with those obtained by the more conventional methods. In the second part of the work described in the thesis this method, together with an improved cavity perturbation technique at 9.4GHz, have been used to make an extended study of the dielectric properties of RBSN. In this particular study attention was directed to the situation which arises in the partially nitrided materials, a region which has not been fully explored in previous studies. The overall structure of the thesis is outlined in the summary given in the next section.

1.2 SUMMARY OF THESIS

In Chapter 2 a review is given of some conventional techniques available for the measurement of ϵ' and ϵ'' . Several of these have been used previously in the High Frequency Measurements and Applications Group, usually in cases where a particular technique offered some specific advantage for unusual measurement situations. Comments are also given on the accuracy attainable with each method, particularly with regard to measurement of dielectric loss, time factors involved in making measurements and the degree of skill required of the researcher. The theory of the new

Fourier method is discussed in Chapter 3. This covers the basic assumptions made, the formulation and derivation of the appropriate theoretical expressions for the behaviour of the input and output waveforms, the calculation of specific formulae to determine ϵ' and ϵ'' and general considerations relating to the prediction of the type of distortion in the output signal to be expected with particular values of the pair of parameters, ϵ' and ϵ'' . It concludes by referring to the limitations of the method. The experimental side is dealt with in Chapter 4 which describes the Fourier method technique. Here a functional description of each component is given together with details of the data acquisition system and examples of the use of the system to calculate the harmonic components with a given known input pulse. Chapter 5 reports the appraisal studies made to establish the validity of the new Fourier method. Here some preliminary tests were made using a wave analyser because this could examine Fourier harmonic generation aspects alone (without at this stage involving the data acquisition and computing subsystem). Single crystal MgO was used as the standard reference material in this preliminary test. The results showed good agreement with the accepted values and the full tests of the whole system were completed using both MgO and Vitreosil. Chapter 5 also includes a discussion of the experimental errors associated with the new technique and its limitations. As already pointed out the upper frequency limit of the Fourier technique was about 1GHz and there was a need to consolidate a method for dielectric measurements in the microwave region, not least because of the increased

interest in material for microwave window and radome applications. In Chapter 6 the criteria for obtaining reliable, accurate measurements of ϵ' and ϵ'' by the microwave cavity perturbation technique are critically reviewed because this method, together with the newly developed Fourier harmonic analysis method, has been used in the dielectric studies described in Part II of the thesis.

In the second part of the research attention has been given solely to a study of the dielectric behaviour of fully and partially nitrided RBSN. The main features of the preparation together with the reaction mechanisms of the nitridation process and the general properties of this material are discussed in Chapter 7. For convenience the results of the fully and partially nitrided material have been considered separately. Thus in Chapter 8 the examination of fully nitrided RBSN is described. The use of the Wiener formula for composite dielectrics is introduced and the results, analysed on this more comprehensive basis, confirm and extend those reported previously. The silicon nitride theme is continued in the last chapter of Part II of the thesis (Chapter 9), which details an examination of partially nitrided RBSN, covering the whole weight gain range from 0% (silicon) to 64.5% (fully nitrided RBSN). This chapter includes, in addition to the dielectric data, an account of structural and microstructural studies made using X-ray diffraction, Reflection High Energy Electron Diffraction (RHEED) and a Scanning Electron Microscope (SEM) with an Energy Dispersive Analysis by X-ray (EDAX) facility. An important and hitherto unreported feature here is the

observation of a peak in the plot of ϵ' versus weight gain at around 22% weight gain. It is suggested that this cannot be explained on the basis of a three phase system (i.e silicon nitride, unnitrided silicon and voids) and an explanation is presented in terms of the effects of the impurities located and analysed by the structural and microstructural studies. In the concluding sections of both Part I and Part II some suggestions are made for future work on the techniques and applications respectively.

REFERENCES

- 1.1 "The dielectric constant of CaWO_4 , Nd/CaWO_4 and Gd/CaWO_4 "
J.S Thorp and E.A.E. Ammar
J. Mat. Science Vol.10, p918, (1975)
- 1.2 "Electrical conductivity in hot-pressed nitrogen ceramic"
J.S. Thorp and R.I. Sharif
J. Mat. Science Vol.11, p1494, (1976)
- 1.3 "Dielectric properties of hot-pressed nitrogen ceramic"
J.S. Thorp and R.I. Sharif
J. Mat. Science Vol.12, p2274, (1977)
- 1.4 "D.C electrical properties of hot-pressed nitrogen ceramic" - J.S. Thorp and R.I. Sharif
J. Mat. Science Vol.13, p441, (1978)
- 1.5 "The dielectric behaviour of single crystal MgO , Fe/MgO and Cr/MgO " - J.S. Thorp and N. Enayati-Rad
J. Mat. Science Vol.16, p255, (1981)
- 1.6 "High frequency dielectric properties of MgO , Fe/MgO and Cr/MgO " - J.S. Thorp, B.L.J. Kulesza, N.E. Rad and S.V.J. Kenmuir" - J. Mat. Science Vol.16, p1052, (1981)
- 1.7 "Dielectric properties of some oxy-nitride glasses"
J.S. Thorp and S.V.J. Kenmuir
J. Mat. Science Vol.16, p1409, (1981)
- 1.8 "Dielectric properties of single crystal Co/MgO "
J.S. Thorp, M.D. Hossain and S.V.J. Kenmuir
Solid State Communications Vol.38, p455, (1981)

- 1.9 " Some electrical characteristics of lithium and yttrium sialons" - R.I. Sharif, J.S. Thorp and S.A. Kavanagh - J. Mat. Science Vol.16, p211, (1981)
- 1.10 "The dielectric behaviour of Mg-Al-Si, Ca-Al-Si, Y-Al-Si and Nd-Al-Si oxynitride glasses" S.V.J. Kenmuir, J.S. Thorp and B.L.J. Kulesza J. Mat. Science Vol.18, p1725, (1983)
- 1.11 "Temperature dependence of dielectric constant of divalent doped MgO single crystals at 1kHz" J.S. Thorp and M.D. Hossain - Pakistan J. Sci. and Indust. Research - accepted for publication (1983)
- 1.12 "Coaxial line methods for measuring permittivity and dielectric loss" - B.L.J. Kulesza, J.S. Thorp and B. Ahmad - J. Mat. Science - accepted for publication (1983)
- 1.13 "High frequency dielectric properties of Mg-Al-Si, Ca-Al-Si and Y-Al-Si oxynitride glasses" - J.S. Thorp, B.L.J. Kulesza, B. Ahmad - J. Mat. Science - accepted for publication (1983)
- 1.14 "The permittivity and dielectric loss of RBSN" J.S. Thorp, B. Ahmad, B.L.J. Kulesza and T.G. Bushell J. Mat. Science - accepted for publication (1984)

CHAPTER 2

TECHNIQUES FOR MEASURING DIELECTRIC PROPERTIES

2.1 INTRODUCTION

A macroscopic description of the electrical properties of a dielectric is provided by the complex relative permittivity ($\epsilon_r = \epsilon' - j\epsilon''$). The significant variables on which ϵ_r depends, in decreasing order of importance, are the frequency, the temperature, the pressure and the intensity of the applied field. Thus the choice of the method depends principally on the frequency and because the whole field of dielectric spectroscopy covers a wide range of frequency, from about 0.0001Hz to about 100GHz, a large number of techniques are required. Measurement can either be made in the frequency or time domain. [2.1 - 2.10]

In the frequency domain techniques, measurements are made at one frequency at a time and a particular set of apparatus will only cover a certain frequency range. At low frequencies (0.001Hz to 1MHz) bridge techniques are most appropriate; they can give precise measurements of both the real component (ϵ') of dielectric constant and the conductivity. At higher frequencies (100kHz to 100MHz), a resonant circuit technique uses a similar procedure to the bridge technique; however the degree of precision tends to be less, particularly at the high frequency end of the range, mainly due to lead inductance problems. The transmission line (slotted) standing wave methods are used for the range of frequency from about 500MHz to about 9GHz but low loss material measurement is difficult as precision components and instrumentation are required. At still higher frequency

ranges (above 3GHz) the cavity perturbation method is usually employed to give the dielectric parameters.

In principle the application of transient methods is an attractive alternative to the point-by-point approach in the frequency domain. A single time domain signal, applied to the dielectric sample, will give results that cover a large frequency spectrum. This method has long been used in the frequency range from about 0.0001Hz to about 1kHz. By about 1969 due to the development of sampling oscillography, this method could be used to a much higher frequency. At present the frequency range covered by this method is from the kHz region up to about 15GHz. The accuracy of the method is at present comparable to that of the frequency domain techniques. The striking advantages are the lesser amount of equipment needed to cover the wide frequency range and the much shorter time required to carry out the measurements.

The need for skilled operators and the time taken in obtaining the dielectric properties of a material make conventional techniques increasingly incompatible with many present day applications; for example in the plants that manufacture modern synthetic insulating materials, where the results of a variation in a processed parameter may have to be evaluated quickly and frequently. For this reason, there is currently a great deal of interest in the development of fast techniques for dielectric spectroscopy. Such systems will permit the rapid evaluation and display of complex permittivity over a wide range of frequencies. The use of computers improved some of the known techniques to a certain extent but what is required is a completely new approach to

the dielectric measurement techniques so as to enable measurements to be done on the spot in a factory.

2.2.1 BRIDGE TECHNIQUES

In the frequency range of 0.008Hz to 2MHz, the dielectric properties of materials are usually determined by measuring the capacitance and the conductance of a sample held between a pair of micrometer electrodes. The principle of the Wheatstone bridge has for long been employed in measurements of conductance, inductance and capacitance. The design of these bridges depends not only on the type and precision of measurement required, but also on the frequency range needed; for example, the Scheiber bridge is capable of measuring in the frequency range of 0.008Hz to 2MHz and the Schering bridge covers the frequency range from 20Hz. to about 1MHz.

The electrode systems are made so that the effects due to fringing fields at the edge of the specimen are reduced and the entire system is contained in a metal shielding box to eliminate undesirable effects of stray field. Electrodes must be evaporated on the opposite polished surfaces of the specimens to ensure a good electrical contact over a well defined area between the specimen and the electrodes of the dielectric test jig; with many materials gold is used for this purpose. The usual arrangement for solids, comprises flat, parallel plates of known area and separation between which is inserted the sample, in the form of a parallel sided disc of diameter slightly less than that of the electrodes. If the diameter of the sample extends beyond the electrodes then corrections for edge effects are necessary.

In the bridge measurement techniques the dielectric material in the test jig can be represented either by a parallel combination of capacitance C_x and R_x or by its series combination of R and C . The parallel and series parameters are related by (Fig. 2.1a):

$$R = \frac{R_x}{1 + (\omega C_x R_x)^2} \quad ; \quad C = \frac{1 + (\omega C_x R_x)^2}{(\omega C_x R_x)^2} \quad \text{--- eq.2.1}$$

The capacitance C_x and resistance R_x values are measured by the bridge and the dielectric permittivity and loss are calculated from:

$$\epsilon' = \frac{C_x}{C_0} \quad ; \quad \epsilon'' = \frac{1}{C_0 R_x \omega} \quad \text{---eq.2.2}$$

where C_0 is the capacitance of the empty jig.

In the case of the Schering bridge, Fig.2.1b, C and R represent the series equivalent circuit of the dielectric, C_2 and C_3 are standard calibrated capacitors and the resistances R_1 and R_2 are equal. C_1 represent stray capacitance across R_1 . Initially without the dielectric present,

$$C = C_0 \quad ; \quad R = 0 \quad \text{---eq.2.3}$$

and the balance equations are:

$$C_0 = C_3 \quad ; \quad C_2 = 0 \quad \text{---eq.2.4a}$$

With the dielectric inserted, the equations become:

$$C = C_3' \quad ; \quad R = \frac{R_1 C_2}{C_3} \quad \text{---eq.2.4b}$$

$$\text{and } \text{Tan } \delta = \omega C_2 R_2 = \frac{\epsilon''}{\epsilon'} \quad \text{---eq.2.5}$$

Thus C_2 may be calibrated directly in terms of $\text{Tan } \delta$.

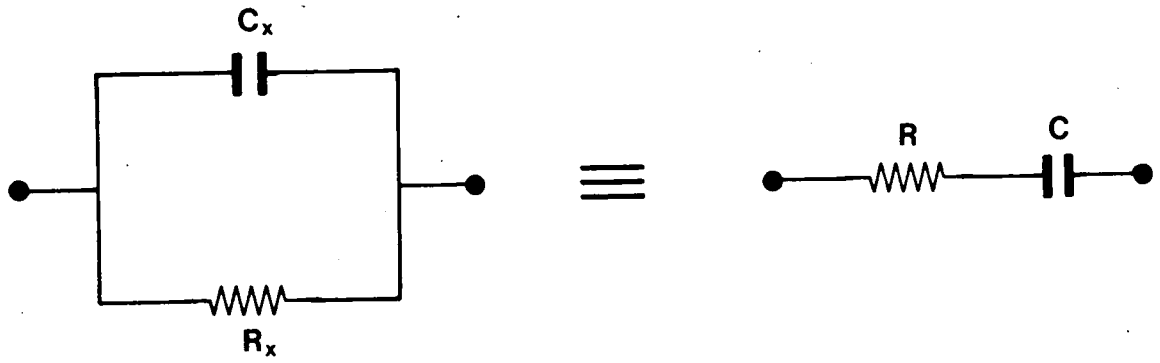


Fig. 2.1a Parallel and series equivalent circuits

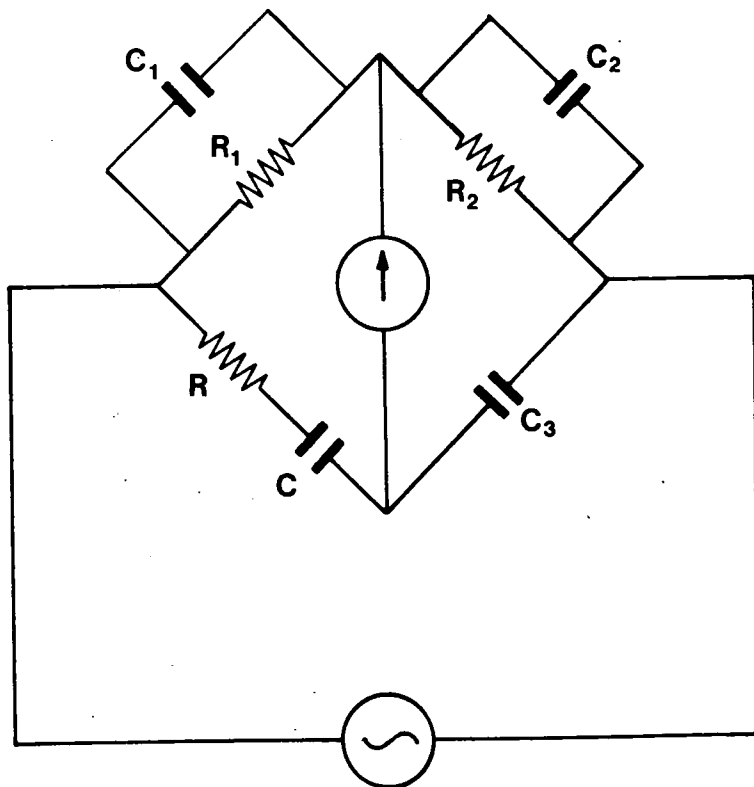


Fig. 2.1b Schering bridge

The value of ϵ' is given by:

$$\epsilon' = \frac{C}{C_0} = \frac{C_3}{C_3} \quad \text{--- eq. 2.6}$$

The accuracy attainable with the Schering bridge is quoted as $\pm 0.2\%$ in capacitance and $\pm 2\%$ in $\text{Tan}\delta$ for the whole range of frequency of 20Hz to 1MHz. The accuracy depends critically on the measuring jig in which the specimen is mounted. Errors are associated with the inductance and capacitance of the leads to the electrodes and the inaccuracies in the standard capacitors and resistors. The main drawback of the bridge technique is that it has to make the assumption of a simple parallel or series combination of capacitance and resistance as the representation for the dielectric. This assumption is only valid if the permittivity is independent of frequency and if the loss is due wholly to conductivity.

2.2.2 RESONANT CIRCUIT TECHNIQUES

The operation of bridges in the MHz region and upwards becomes increasingly difficult as the frequency is raised, since the admittances associated with stray capacitance increase in proportion to the frequency. It is usual to make the measurements using a resonant circuit of which the whole or part of the capacitance is the dielectric measuring cell. Resonant circuits can be designed to operate over the frequency range of around 50kHz to 300MHz and are capable of high accuracy, provided the loss is low. The equivalent circuit of a resonant circuit is shown in Fig.2.2.

Taking R as the total internal resistance of the circuit and L and C as the total inductance and capacitance

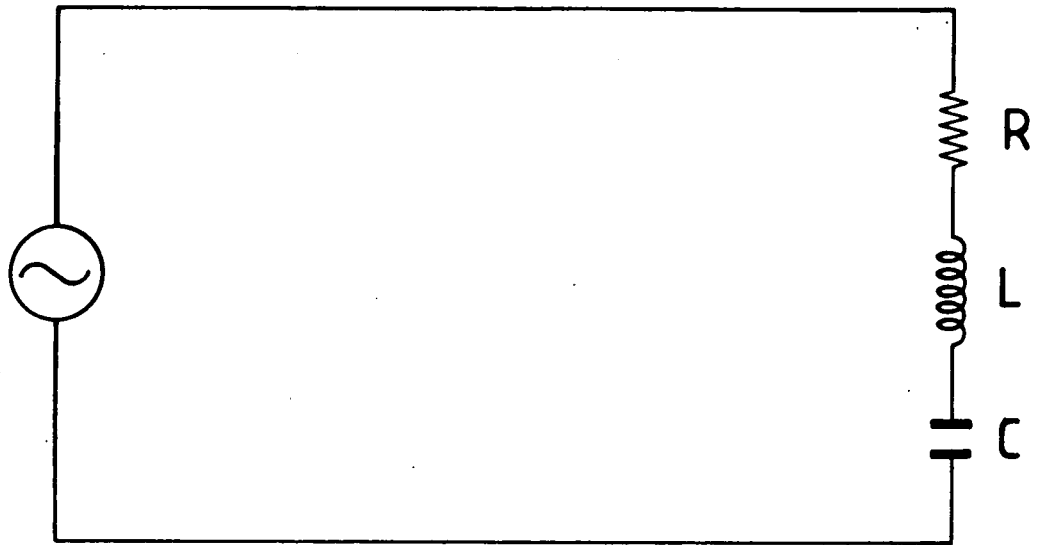


Fig. 2.2 Equivalent resonant circuit of Q-meter

respectively, resonance occurs at $\omega = \omega_r = 2\pi f_r$, where:

$$f_r = \frac{1}{2\pi\sqrt{LC}} \quad \text{--- eq.2.7}$$

An external e.m.f. with voltage E is injected at the resonant frequency f_r . At resonance the reactive components of the circuit are equal; $X_1 = X_c$ (where $X_1 = \omega L$ and $X_c = \frac{1}{\omega C}$)

The total impedance of the circuit is:

$$Z = R + j\left(\omega L - \frac{1}{\omega C}\right) \quad \text{--- eq.2.8}$$

At resonance:

$$Z = R$$

The magnification (Q-factor) of the circuit is defined as:

$$Q = \frac{X}{R} \quad \text{--- eq.2.9}$$

where $X = X_1 = X_c$ at resonance.

If the test jig is connected to the circuit with the spacing of the electrodes exactly equal to the thickness of the sample, the air gap capacitance will be C_0 and the total capacitance of the circuit at resonance, C_t , is given by:

$$C_t = C_1 + C_0 + C_h + C_l \quad \text{--- eq.2.10}$$

where

C_1 = variable capacitor of the circuit without sample,

C_0 = capacitance of the testing jig without sample,

C_h = capacitance of the sample holder (electrodes),

C_l = capacitance of the connecting leads.

Putting the sample between the electrodes, the total capacitance at resonance will be:

$$C_t = C_2 + C_s + C_h + C_l \quad \text{--- eq.2.11}$$

where

C_2 = variable capacitor of the circuit with sample,

C_s = capacitance of testing jig with sample.

Equating:

$$C_1 - C_2 = C_s - C_0 \quad \text{--- eq.2.12}$$

The relative permittivity of the sample, neglecting the edge effect, is given by:

$$C_s = \epsilon' C_0 \quad \text{--- eq.2.13}$$

Substituting:

$$C_1 - C_2 = C_0(\epsilon' - 1)$$

which gives:

$$\epsilon' = \frac{C_1 - C_2}{C_0} + 1 \quad \text{--- eq.2.14}$$

The loss $\text{Tan}\delta$ is given by:

$$\text{Tan}\delta = \frac{Q_1 - Q_2}{Q_1 \times Q_2} \frac{C_1}{C_1 - C_2} = \frac{\epsilon''}{\epsilon'} \quad \text{--- eq.2.15}$$

where Q_1 and Q_2 are the Q values of the circuit with the sample out of and in the testing jig respectively. At higher frequencies a correction has to be applied for circuit inductance L_r , using the relation:

$$C_{\text{effective}} = \frac{C^*}{1 + \omega^2 L_r C^*} \quad \text{--- eq.2.16}$$

where C^* refers to C_1 and to C_2 in turn. This correction amounts at most to about 8%. The resonance circuit technique becomes difficult as the frequency goes beyond 75MHz. because of the difficulty in obtaining sufficiently thin, large diameter specimens.

2.2.3 TRANSMISSION LINE MEASUREMENTS

For frequencies greater than 100MHz, the resonant circuit technique cannot be employed due to the impossibility of realising lumped circuit elements. Distributed circuit analysis must be employed. Numerous methods of measuring dielectric properties are available at

these frequencies and can be divided into total reflection and total transmission methods. In both cases the permittivity of the sample is expressed in terms of the measured values of complex reflection and transmission coefficient.

Two waves travelling in opposite directions will interact to produce a standing wave pattern. The minima and maxima occur alternately along the line with a separation of $\frac{\lambda}{4}$. The voltage standing wave ratio is defined as:

$$S = \frac{E_{\max.}}{E_{\min.}} \quad \text{--- eq.2.17}$$

and is related to the reflection coefficient, p by:

$$|p| = \frac{S - 1}{S + 1} \quad \text{--- eq.2.18}$$

where

$$p = \frac{E_r}{E_i} = |p| \exp(-j\theta) \quad \text{--- eq.2.19}$$

in which E_r and E_i represent the reflected wave and the incident wave respectively.

Measurement of voltage minima and maxima of the standing wave will give the magnitude of the reflection coefficient. The separation of the first minimum from the face of the sample will depend on the wavelength and the thickness of sample, i.e insertion of a dielectric shifts the minimum of the standing wave toward the end. Thus, by finding the location of the first minimum, x , (the distance from the face of the material to the first minimum) the phase angle of p can be determined from:

$$\theta = 2\beta x - \pi \quad \text{--- eq.2.20}$$

where β is the phase constant given by $\frac{2\pi}{\lambda}$

and λ is the wavelength of the standing wave.

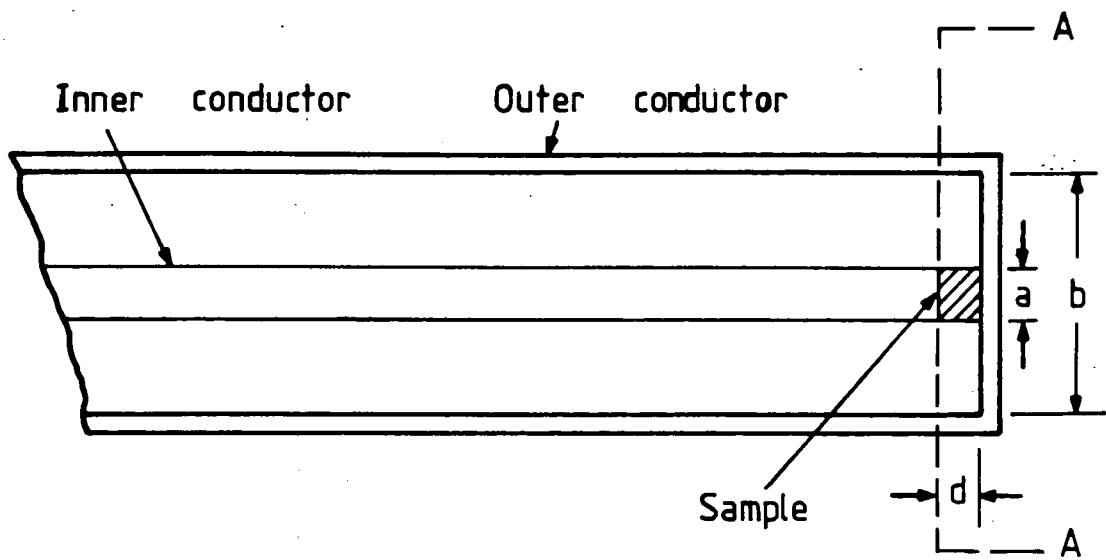
2.2.4 SLOTTED LINE TECHNIQUES

In these methods the permittivity is either calculated from measurements of the input impedance or the reflection coefficient on the input side of the sample holder. The reference frame is usually defined to be at the input interface of the dielectric sample. There are many possible sample configurations that can be used, depending upon the range of frequency and the nature and availability of the sample. A summary of many possible configurations and their equivalent circuits was described by A.B.Ahmad[2.15]. These techniques can be used for measurement of the complex dielectric constant over the range of frequencies from about 500MHz to 9GHz.

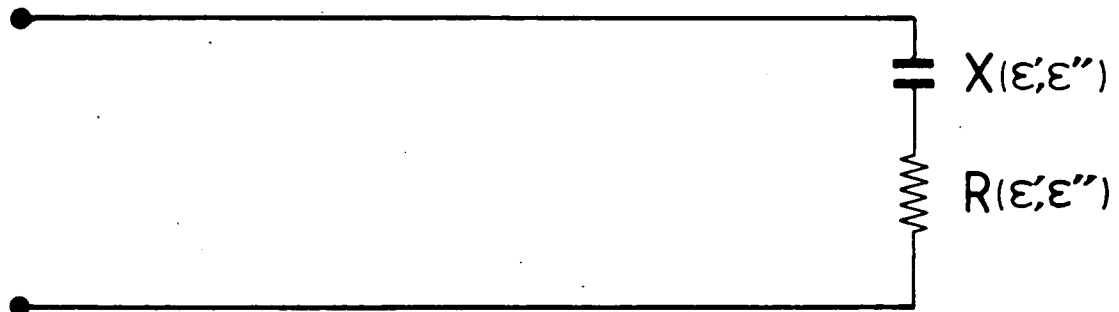
In the lumped capacitance method which was originally suggested by Westphal and later developed by Stuchly, a small shunt capacitor terminating a coaxial line section is used as a sample holder (Fig. 2.3). The permittivity of the substance filling the test capacitor (jig) can be calculated from the input reflection coefficient. The reflection coefficient at the A-A plane is related to the permittivity of the material in the test capacitor by the following expression:

$$p = |p| \exp(-j\theta) = \frac{1 - j\omega C_0 Z_0 \epsilon^*}{1 + j\omega C_0 Z_0 \epsilon^*} \quad \text{--- eq.2.21}$$

where C_0 is the capacitance of the test capacitor, Z_0 is the characteristic impedance of the transmission line and ϵ^* is the complex relative permittivity of the material in the capacitor [2.11].



a)



b)

Fig. 2.3 a) Coaxial line with sample

b) Equivalent circuit of sample

The real and imaginary parts of the complex relative permittivity are given by:

$$\epsilon' = \frac{2|p|\sin\theta}{C_0 Z_0 (|p|^2 + 2|p|\cos\theta + 1)} \quad \text{--- eq.2.22a}$$

$$\epsilon'' = \frac{1 - |p|}{C_0 Z_0 (|p|^2 + 2|p|\cos\theta + 1)} \quad \text{--- eq.2.22b}$$

The magnitude of the reflection coefficient, $|p|$ can be obtained indirectly by measuring the Voltage Standing Wave Ratio (VSWR). There are various methods available for measuring VSWR, depending on its magnitude. All the methods can be grouped into three classes i.e:

- a) the direct method, which uses the VSWR indicator,
 - b) the attenuation method, which measures the difference in decibels between the minimum and maximum,
 - c) the graphical method used mainly for high values of VSWR.
- The direct method is least troublesome and can be made suitable for measurement of high VSWR.

The attenuation method requires a precision variable attenuator and the accuracy with this method is rather less. The graphical method can determine higher VSWR but the process is very tedious and time consuming.

2.2.5 CAVITY PERTURBATION METHODS

The most essential instrument used in this technique is a cavity resonator. A cavity resonator is an enclosed space which is capable of oscillating and storing energy. It is analogous to a low frequency resonant circuit consisting of an inductance, a capacitance and a resistance. The technique involves inserting a small piece of dielectric material inside the resonant cavity. It is placed at the end

of a thin silica rod so that the specimen is suspended in the position of maximum electric field. The resultant shift of the resonant frequency of the cavity gives the real part of the complex dielectric constant and the change in the Q-factor gives the imaginary part.

The Q factor is defined as:

$$Q = 2\pi \frac{\text{Energy stored per cycle}}{\text{Energy dissipated per cycle}} \quad \text{--- eq.2.23}$$

It is usually approximated to the ratio of the resonant frequency to the bandwidth of the half power point (i.e at 0.707 of the voltage or current maximum) i.e:

$$Q = \frac{f_0}{\Delta f} \quad \text{--- eq.2.24}$$

The cavity has to be matched to the waveguide and this is done by two coupling screws that act like stub tuners. To match the cavity impedance, the tuners are adjusted in such a way that the normalised input impedance (with respect to Z_0) of the system is unity.

There are three kinds of Q-factor associated with the cavity and they are related by:

$$\frac{1}{Q_1} = \frac{1}{Q_u} + \frac{1}{Q_e} \quad \text{--- eq.2.25}$$

in which:

$$Q_1 = \frac{\omega_0 L}{R + Z_0} \quad \text{is the loaded Q i.e the loss}$$

of the cavity and the coupling are taken into account,

$$Q_u = \frac{\omega_0 L}{R} \quad \text{is the unloaded Q i.e loss}$$

in the cavity alone,

$$Q_e = \frac{\omega_0 L}{Z_0} \quad \text{is the external } Q \text{ i.e loss}$$

due to the external circuit (coupling).

By definition the coupling parameter B is defined as:

$$B = \frac{Z_0}{R} = \frac{Q_u}{Q_e} \quad \text{--- eq.2.26}$$

In order for the cavity to be matched to the waveguide;

$$R = Z_0 \quad \text{i.e } B = 1$$

Therefore the matching condition is:

$$Q_u = Q_e = 2Q_1 \quad \text{--- eq.2.27}$$

Tuning the cavity can either be achieved by:

a) Displaying the resonance curve on an oscilloscope; when the matching condition is approached the displayed curve becomes sharper and the bottom of it reaches up to the base line. This method can be tedious because the two matching screws can have many possible combinations.

b) VSWR method; when the cavity is matched to the waveguide the VSWR approaches unity. To obtain a good match a VSWR of less than 1.05 is required.

When a small piece of dielectric material is introduced into the cavity, the resonant frequency and the Q-factor of the cavity change. The relationship between these changes and the properties of the dielectric material are deduced from perturbation theory. This was first proposed by Casimir [2.20] and it was further extended and developed by Waldron [2.21] and others. The relationships for a sample in a rectangular cavity are given as:

$$\frac{\Delta f}{f} = -2(\epsilon' - 1) \frac{V_s}{V_0} \quad \text{--- eq.2.28}$$

and

$$\frac{1}{Q} = \frac{1}{Q_s} - \frac{1}{Q_0} = 4 \epsilon'' \frac{V_s}{V_0} \quad \text{--- eq. 2.29}$$

where V_s = volume of sample,

V_0 = volume of cavity,

Q_s = Q value with the sample in the cavity,

Q_0 = Q value of the cavity without sample.

The negative sign indicates that Δf is negative i.e by introducing a sample the resonant frequency of the cavity is lowered. Measurement of the Q of the unperturbed and perturbed cavity as well as the shift in frequency will determine the values of ϵ' and ϵ'' of the material inside the cavity. The cavity is assumed to be unperturbed when the silica rod is inserted inside the cavity.

This method is a well known tool and the only limitations are that the frequency shift should be much less than 1% and that the volume of the sample introduced into the cavity should not alter appreciably the field inside the cavity. However very high loss material cannot be measured by this method as it will flatten the Q curve of the cavity. The estimated accuracy obtained by this method is about 10%. A detailed lay-out of this technique is presented in Chapter 6.

2.3 TIME DOMAIN TECHNIQUES

2.3.1 INTRODUCTION

The whole field of dielectric spectroscopy covers the range of frequencies from about 0.0001Hz to 100GHz . In the frequency domain, to cover these ranges, a large number of laborious techniques and pieces of instrumentation are required.

Time domain transient methods are the alternative and because the time domain signal usually covers a large frequency spectrum, it is obvious that transient methods are less time consuming and less laborious. These methods have been used for a long time to study slow relaxation processes, such as for polymeric material to give information about dielectric properties in the frequency range from about 0.0001Hz to 1kHz. The study of fast relaxation processes was introduced by about 1969 and it originated from a technique called " Time Domain Reflectometry ". At present both reflection and transmission methods are used; thus the transient methods are now collectively known as the Time Domain Spectroscopy (TDS) method.

The development of TDS methods was carried out in various fields by many workers. In physical chemistry it was started by Fellner - Feldeg [2.25] and in the field of electrical engineering, Nicolson [2.26] and Bagozzi [2.27] independently developed a similar technique. Later Sugget et al [2.28] improved the original methods to obtain a higher accuracy and also managed to increase the frequency range up to 15GHz. Fellner - Feldeg and De Loor et al [2.29] extended the technique to lower frequencies. The frequency range covered by this technique, at present is from about 1kHz to more than 15GHz.

2.3.2 BASIC PRINCIPLES OF TDS METHODS

The change in propagation properties of a step voltage in a lossless coaxial line is the basis of all TDS methods. When the step voltage propagates along the line, its shape remains unchanged as long as the propagation properties of

the line remain the same but it will be partly reflected and partly transmitted at the interface of the section of the line with different propagation characteristics. The insertion of a dielectric sample in the line will change the propagation properties of the line and will therefore distort the shape of the step voltage. The equipment required for these techniques basically must comprise:

- a) fast rise time step generator (about 1 picosecond),
- b) sampling system (to transform the signal to a longer time scale),
- c) low loss coaxial line,
- d) display unit e.g oscilloscope or X- Y plotter.

The measurements are made by propagating the fast rise-time waveform through the delay line network containing a section with the dielectric sample. At the air-dielectric interface, partial reflection and partial transmission of the incident wave occurs. The resultant transmitted and reflected waveforms carry the necessary information from which the frequency dependence behaviour of the dielectric sample (that is responsible for the change in the characteristic impedance of the line) can be determined. The delay line network acts as a time window to select the required waveform and to eliminate the unwanted reflections. The selected waveform propagates to the sampling system to be displayed on the oscilloscope. The waveform is then Fourier transformed and this information is used to obtain the dielectric properties of the material under test.

Basically there are two groups of methods i.e single response methods and multiple response methods. In the

single response methods only a single reflection or a single transmission (or combination) is considered and in the multiple response methods an infinite number of reflections or transmissions (or both) are considered. The placement of the sample with respect to the sampling head and the sample's size further subdivide the two main methods into many possible techniques. The direct reflection method theoretically requires the sample to be infinite. This is because only the reflection against the first interface is taken into account, which means that the reflected time domain decay has to be virtually complete before reflections from the end of the sample reach the sampling head as well. There are many other different techniques available depending upon the sample size and the relative position of the sample with respect to the sampling head. A detailed summary of the high frequency time domain methods in dielectric spectroscopy is given by Van Gemert [2.8].

2.4 USE OF COMPUTER IN PERMITTIVITY MEASUREMENT

Digital electronics has one great advantage in its ability to store and access data at will. Computer technology has come to a stage that it is cheap and its versatility makes it an important part in any experimental system. In fact most experimental arrangements for research are computer controlled to facilitate the acquisition of data and also to minimise human error. In permittivity measurements, to take advantage of computer techniques, two approaches can be considered. Firstly the automation of existing steady state (frequency domain) techniques; for example automatically balanced bridges.

Secondly, automation of the step-response methods; so that the current-time response to a step voltage can be read into the computer and Fourier transformation subsequently completed at will to obtain the properties of the material under test. The former techniques suffer from the disadvantages that phase detectors and sweeping oscillators covering the required frequency range are almost impossible to obtain and, more important, that the rate of sweep must be slow in comparison with the period of the exciting wave. Thus measurements at the low frequency end can be time consuming. The automation of step-response does not suffer from this problem; excitation is by a simple voltage step function and the response is measured by a current detector and data covering a range of frequencies will be obtained within the duration of the step.

REFERENCES

- 2.1 "High frequency dielectric measurement"
J. Chamberlain and G.W. Chantry
Science & Technology Press - London (1972)
- 2.2 "Introduction to microwave theory"
H.A. Atwater - McGraw Hill Electrical and Engineering
Series - New York (1962)
- 2.3 "Introduction to microwave theory and measurement"
A.L. Lance - McGraw Hill - New York (1964)
- 2.4 "Microwave techniques"
H. Mooijweer - MacMillan (Philips Technical Library)-
London (1971)
- 2.5 "Dielectric materials, measurements and application"
IEE Conference Publication Number 129 - (1975)
- 2.6 "Dielectric materials, measurements and application"
IEE conference Publication Number 177 - (1979)
- 2.7 "Universal bridge - Operating instructions"
Wayne Kerr (B 224) -Publication TP43
- 2.8 "High frequency time domain methods in dielectric
spectroscopy" - M.J.C. Van Gemert
Philips Research Report 28 - p 530-573 - (1973)
- 2.9 "The Q-meter in theory and practice"
Marconi Instrument Ltd., St. Albans, Herts., England
- 2.10 "Technique of microwave measurements" - C.G. Montgomery
McGraw Hill Radiation series 11 - New York (1947)

- 2.11 "A lumped capacitance method for the measurement of the permittivity and conductivity in the frequency and time domain - A further analysis"
M.A. Rzepecka, S.S. Stuchly
IEEE Trans. on Instrum. and Meas. Vol.IM 24,p27-32,(1975)
- 2.12 "Time domain techniques for measuring the conductivity and permittivity spectrum of materials"
O.M. Bucci, G. Cortucci, G. Franceschetti, C. Savarese, R. Tiberie - IEEE Trans. on Instrum. and Meas. Vol.IM21, p237-243, (1972)
- 2.13 "A thin sample method for the measurement of permeability, permittivity and conductivity in frequency and time domain" -H. Fellner- Feldegg
The Journal of Physical Chem. Vol.76 No.15 p2116, (1972)
- 2.14 "Measurement of instrinsic properties of materials by time domain techniques" - A.M. Nicolson, G.F. Ross
IEEE Trans. on Instrum. and Meas. Vol. IM19, p377, (1979)
- 2.15 "Improved wideband coaxial methods for dielectric measurement on Nitrogen Ceramic" - A.B. Ahmad
Ph.D thesis - University of Durham (1983)
- 2.16 "Time domain spectroscopy of dielectric materials"
R.H. Cole - IEEE Trans. on Instrum. and Meas. Vol.IM25, p371-375, (1976)
- 2.17 "Evaluation of dielectric behaviour by time domain spectroscopy" - 1. Dielectric response by real time analysis.; 2. Complex permittivity - Robert H.Cole
Journal of Physical Chem. Vol.79 No.14 pl459-1474

- 2.18 "A microprocessor controlled time-domain Spectrometer"
B.R. Parisien and S.S. Stuchly
IEEE Trans. on Instrum. and Meas. Vol.IM28, p269, (1979)
- 2.19 "A combined total reflection-transmission method in
application to dielectric spectroscopy"
S.S. Stuchly and M. Matuszewski
IEEE Trans. on Instrum. and Meas. Vol.IM27, p285, (1978)
- 2.20 "On the theory of electromagnetic waves in resonant
cavities" - H.B.G. Casimir, Philips Research Reports
No.6, p162, (1951)
- 2.21 "Perturbation theory of resonant cavities"
R.A. Waldron - The Institution of Electrical
Engineering Monograph No.373E, (1960)
- 2.22 "Current status of time-domain metrology in material
and distributed network research"
H.M. Cronson and G.F. Ross
IEEE Trans. on Instrum. and Meas. Vol.IM21, p495, (1972)
- 2.23 "Note on cavity perturbation theory"
E.G. Spenser, R.C. Lecraw, L.A. Ault
Journal of Applied Physics Vol.28, No.1, p130, (1956)
- 2.24 "An instrument for continuously measuring capacitance
changes" - B.Z. Kaplan, Ysiah Sagy, D.M. Jacobson
IEEE Trans. on Instrum. and Meas. Vol.IM27, p43, (1978)
- 2.25 "The measurement of dielectrics in the time domain"
H. Fellner-Feldegg - The Journal of Physical Chem.
Vol.75, No.3, p616, (1969)

- 2.26 "Broad-band microwave transmission characteristic from a single measurement of transient response"
A.M. Nicolson - IEEE Trans. on Instrum. and Meas.
Vol.IM17, No.4, p395, (1968)
- 2.27 "Determination of the dielectric relaxation time in a Debye binary liquid by pulse measurements"
R.P. Bagozzi, W.R. Ives, N.S. Nahman - Progress Radio Sci. Vol.2, p257, (1971)
- 2.28 "Dielectric relaxation study by time domain"
A. Sugget, P.A. Mackness, M.J. Tait, G.M. Young
Nature, Vol.228, p456, (1970)
- 2.29 "Measurement of dielectric permittivity with Time Domain Reflectometry. Extension of the method to lower relaxation frequencies" - G.P. DeLoor, M.J.C. Van Gemert, H. Gravesteyn - Chem. Physics Letters
Vol.18, p295, (1973)
- 2.30 "Recent advances in broad-band UHF and VHF transmission line methods for moisture content and dielectric constant measurement" - W.J. Chudobiak, B.A. Syrett, H.M. Hafez - IEEE Trans. on Instrum. and Meas. Vol.IM28, No.4, p284, (1979)
- 2.31 "Wide range dynamic complex dielectric constant measurements using microprocessor control techniques"
C. Akyel, R.G. Basario - IEEE Trans. on Instrum. and Meas. Vol.IM28, No.4, p472, (1979)

CHAPTER 3

THEORY OF FOURIER METHOD

3.1 INTRODUCTION

The development of techniques for measuring dielectric properties of materials has long been carried out and there are various techniques available both in the frequency and the time domain. Generally each technique is difficult and tedious to carry out and skilled operators are required to make the measurements. Usually a dielectric measuring rig is set up by the operator using some established technique; measurements can only be carried out after the various components required have been assembled and enough skill has been acquired. The fact is, there is no commercial instrument that enables dielectric measurements to be done on the spot. Standard bridges, Q-meters or slotted line are available and can be adapted for dielectric measurement. However most of these standard techniques are tedious and very time-consuming and there are many dielectric measurements that require on the spot assessment; for example, in the chemical and biological sciences [3.1] (dielectric effects associated with molecular movement, electronic properties of organic and biological polymeric systems) or on a factory line manufacturing dielectric material. The use of microwave energy in cooking appliances requires a detailed and continuous assessment of the variation of dielectric properties with moisture content at different temperatures for all the electrical insulating components used.

The Fourier method attempts to introduce a closed-loop system in which results can be obtained within minutes of

the introduction of the sample in the sample holder. Measurements are made in the time domain and Fourier analysis is used for time-to-frequency domain transformation. Data acquisition is achieved with the aid of a computer which simultaneously performs the required calculation. The dielectric properties of the material under test can be obtained almost instantaneously by comparing the distorted output waveform of the sample with the stored waveforms in the computer. The time taken to determine the required parameters will be the time taken for the computer to search through its file for the appropriate waveform that matches the experimental waveform of the sample. The frequency range covered by this technique is from the MHz to the GHz region.

3.2 FOUNDATION OF FOURIER ANALYSIS

If the variation of a quantity repeats itself at some basic frequency, ω , then the disturbance can be considered as being built up from a set of harmonically varying disturbances having repetition frequencies equal to multiples of the basic frequency. Thus if the function $f(t)$ represents the quantity that varies with time and if T is the basic repetition period, i.e. $f(t + T) = f(t)$, then the Fourier series expansion of $f(t)$ is given by:

$$f(t) = a_0 + \sum_{n=1} a_n \cos(n\omega t) + \sum_{n=1} b_n \sin(n\omega t) \quad \text{--- eq. 3.1}$$

where

$$a_0 = \frac{1}{T} \int_0^T f(t) dt \quad \text{--- eq. 3.2}$$

$$a_n = \frac{2}{T} \int_0^T f(t) \cos(n\omega t) dt \quad \text{--- eq. 3.3}$$

$$b_n = \frac{2}{T} \int_0^T f(t) \cos(n\omega t) dt \quad \text{--- eq. 3.4}$$

Equation 3.1 is the Fourier series representation of the **periodic** function $f(t)$ and a_0 , a_n and b_n are the Fourier coefficients. Some conditions must be satisfied for the expression to be valid i.e the integral $\int f(t)dt$ must be finite and $f(t)$ must be piecewise continuous and piecewise monotonic. These conditions are generally known as the Dirichlet's conditions [3.3], and these conditions are met by practically all of the functions which are of interest in the physical sciences.

The Fourier series in equation 3.1 can be written in the complex form using the relation:

$$\cos(\theta) + j\sin(\theta) = \exp(j\theta) \quad \text{--- eq. 3.5}$$

The complex Fourier series is given by :

$$f(t) = \sum_{-\infty}^{+\infty} c_n \exp(jn\omega t) \quad \text{--- eq. 3.6}$$

where c_n is given by:

$$c_n = \frac{1}{T} \int_0^T f(t) \exp(-jn\omega t) dt \quad \text{--- eq. 3.7}$$

Alternatively, c_n can be derived from the coefficients in the trigometric Fourier series, i.e:

$$c_n = \frac{1}{2} \sqrt{a_n^2 + b_n^2} \exp(-j\theta_n) \quad \text{--- eq. 3.8}$$

and $\theta_n = \text{ARCTAN}\left(\frac{b_n}{a_n}\right) \quad \text{--- eq. 3.9}$

All the output waveforms obtained by this technique can be transformed to their spectra through the Fourier transformation. The time-to-frequency domain transformation is necessary for reasons which will be explained in section 3.4.

3.3 DETERMINATION OF FOURIER COEFFICIENTS

The waveforms dealt with in the measurements are periodic but complicated; the mathematical functions representing them are unknown. Thus determination of the corresponding Fourier series has to be done numerically. Numerical evaluation of Fourier coefficients is undertaken by sub-dividing a period of the waveform into M equally spaced sections along the time axis. If the period of the waveform is T then $T = M \Delta t$, where Δt is the interval (Fig. 3.1). Suppose t_m is the time at the end of the m^{th} time interval i.e. $t_m = m \Delta t$ for $1 < m < M$ and Δt can be worked out, as shown below:

Since

$$T = \frac{2\pi}{\omega} = M \Delta t \quad \text{--- eq. 3.10}$$

therefore

$$\Delta t = \frac{2\pi}{M\omega} \quad \text{--- eq. 3.11}$$

Substituting Δt for dt , T for $\frac{2\pi}{\omega}$ and $m\Delta t$ for t into equations 3.1, 3.2 and 3.3, the numerical Fourier coefficients can be written as:

$$a_0 = \frac{1}{M} \sum_{m=1}^M f(m\Delta t) \quad \text{--- eq. 3.12}$$

$$a_n = \frac{1}{M} \sum_{m=1}^M f(m\Delta t) \cos(nm\Delta t) \quad \text{--- eq. 3.13}$$

and

$$b_n = \frac{1}{M} \sum_{m=1}^M f(m\Delta t) \sin(nm\Delta t) \quad \text{--- eq. 3.14}$$

The numerical evaluation of the Fourier coefficients is done with the help of a computer (described in Chapter 4).

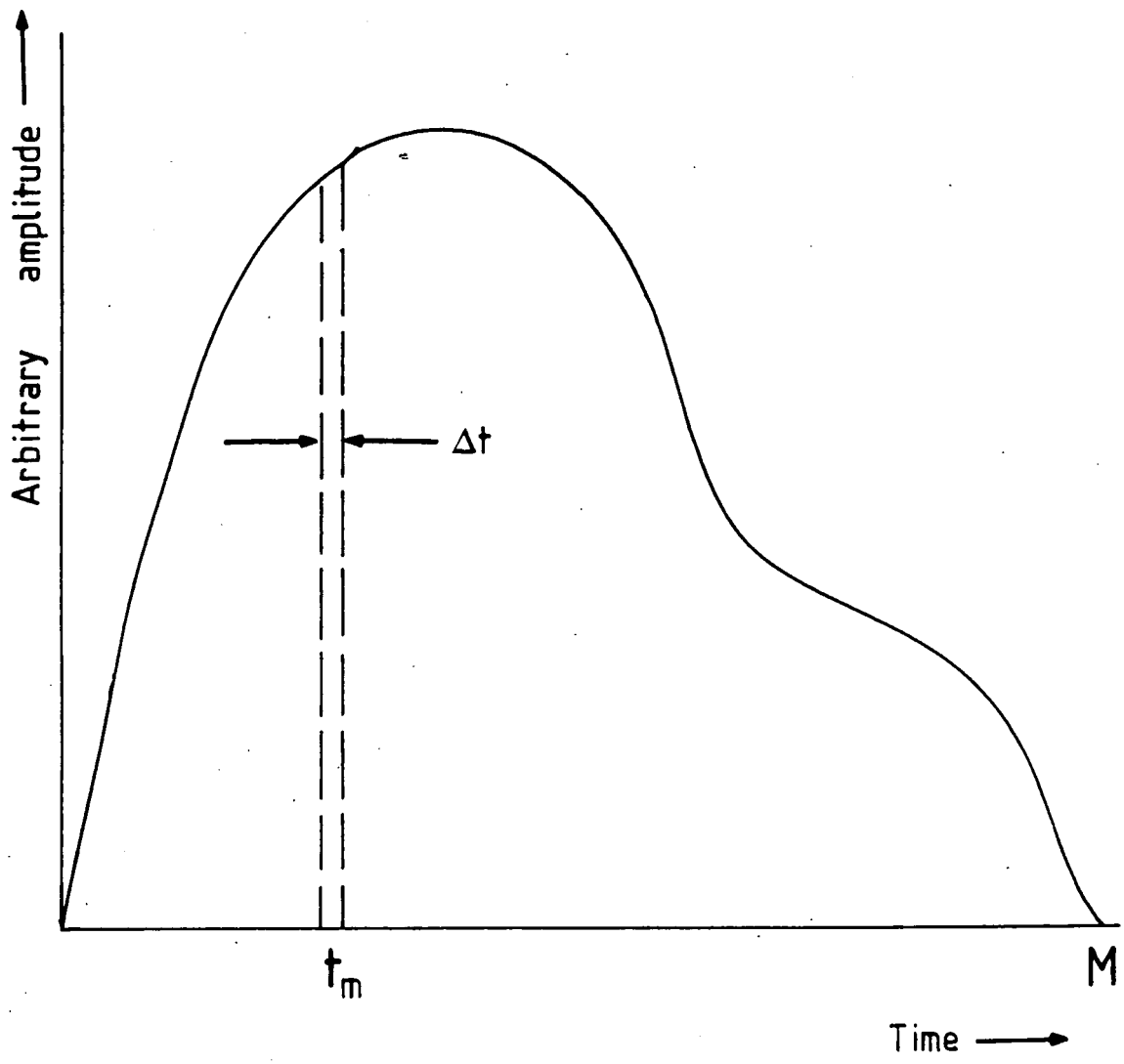


Fig. 3.1 Part of a periodic waveform

3.4 THEORY OF THE DIELECTRIC TEST CIRCUIT

This technique uses the fact that the response of a linear system to an input containing harmonics itself also contains harmonics at the corresponding frequencies [3.6]. Thus instead of using a single frequency input signal, a square wave (or any periodic signal that contains harmonics) is used to drive the circuit under study. Therefore, instead of getting a result at a particular frequency, a spectrum of results at all the harmonic frequencies of the input signal is obtained in one single run. A wide range of frequencies can be covered in a very short time as compared to all known methods and, since this new technique uses computer techniques for data acquisition, it is less tedious and can be easily adapted into other systems.

The signal (harmonics) is propagated in a low loss coaxial line that forms part of the dielectric test circuit. The shape of the waveform should remain unchanged throughout the line unless there is a change in the line characteristic. The dielectric in the sample holder is considered as having a linear, passive characteristic; having an input on one side and output on the other. It transforms the input, $v_i(t)$, into an output $v_o(t)$.

From linear response theory [3.7], $v_i(t)$ and $v_o(t)$ are related by a convolution equation:

$$v_o(t) = \int_0^t v_i(t-t')h(t')dt' \quad \text{--- eq. 3.15}$$

where $h(t)$ is the system's transfer function.

Applying the deconvolution procedure:

$$v_o(\omega) = v_i(\omega)H(\omega) \quad \text{--- eq. 3.16}$$

where $v_o(\omega)$, $v_i(\omega)$ and $H(\omega)$ are Fourier transforms of $v_o(t)$, $v_i(t)$ and $h(t)$ respectively.

e.g:

$$H(\omega) = \int h(t)\exp(-j\omega t) \quad \text{--- eq. 3.17}$$

Thus if we let the spectrum of the input signal be denoted by $V_i(\omega)$ (which defines its magnitude and phase characteristic) and let the modification to this spectrum, caused by the dielectric in the sample holder, be denoted by the complex function $H(\omega)$, the output spectrum will be given by $V_o(\omega)$. Relation 3.16 is an important property of the frequency domain approach i.e. it enables one to work out the spectrum of the output signal or waveform from the product of the input spectrum and the system's frequency response, $H(\omega)$. There is no simple relationship of this sort existing in the time domain. It is also possible to work out how a particular waveform is modified as it passes through a system. First the spectrum of the input waveform must be worked out by doing Fourier transformation. Multiplication of the input spectrum by the frequency response of the system will give the output spectrum. The output time function is obtained by applying inverse Fourier transformation procedure to the spectrum of the output signal. This process is difficult and lengthy but with the aid of a computer it can be done easily.

3.4.2 THE EQUIVALENT TEST CIRCUIT

The equivalent circuit of the apparatus used in this technique is shown in Fig. 3.2. The input signal is a square-wave with a repetition rate of about 25MHz and the impedance of the line is 50 Ohms. From circuit theory, the output voltage $V_o(\omega)$ of the circuit is given by:

$$V_o(\omega) = V_i(\omega) \cdot \frac{j\omega CR_1}{1 + j\omega C(R_1 + R_s)} \quad \text{--- eq. 3.18}$$

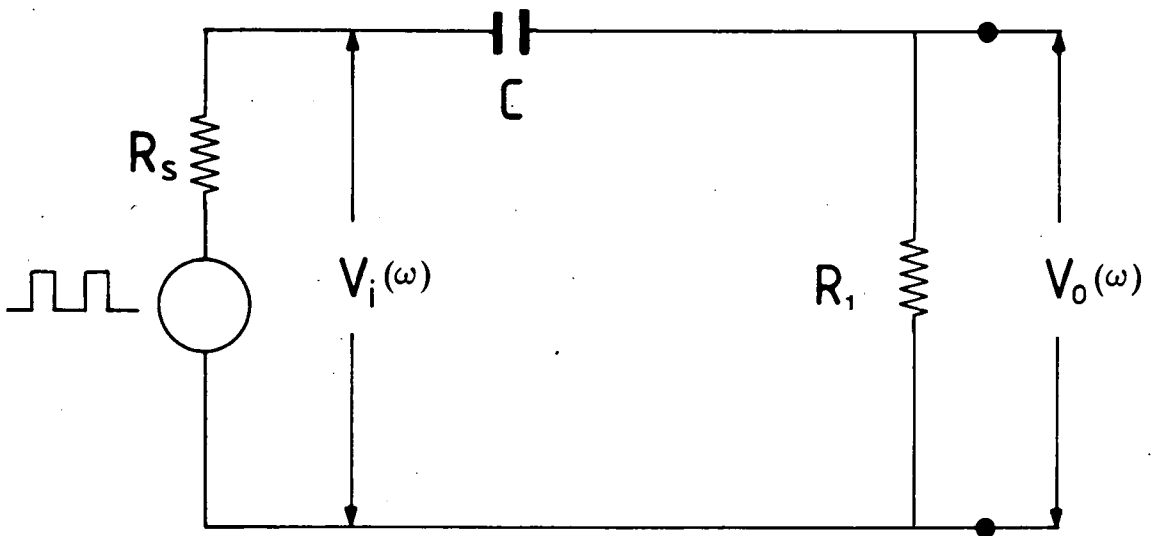


Fig. 3.2 Equivalent circuit of Fourier technique

where

$V_i(\omega)$ = spectrum of the input signal,

R_1 = load resistance of the detector used (50 Ohms),

R_s = source resistance (50 Ohms),

C = capacitance of the sample holder.

The capacitance of the sample holder is given by:

$$C = \epsilon_0 \frac{A}{d} (\epsilon' - j\epsilon'') \quad \text{--- eq. 3.19}$$

where

$\epsilon_0 = 8.854 \times 10^{-12}$ F/m (electric constant),

A = area of the capacitor,

d = gap between the capacitor plates.

With an empty sample holder (air gap) $C = C_0$, and the output voltage $V_a(\omega)$ becomes:

$$\begin{aligned} V_a(\omega) &= V_i(\omega) \times \frac{j\omega C_0 R_1}{1 + j\omega C_0 R_1} \quad \text{--- eq. 3.20a} \\ &= V_i(\omega) \times \frac{\omega C_0 R_1}{[1 + \omega^2 C_0^2 R_1^2]^{1/2}} \exp\left(j\frac{\pi}{2} - j\text{ARCTAN}(\omega C_0 R_1)\right) \\ &= |V_a(\omega)| \exp(j\theta_a) \end{aligned}$$

where

$$R_t = R_1 + R_s$$

With the sample inserted the output voltage $V_d(\omega)$ is:

$$V_d(\omega) = V_i(\omega) \times \frac{j\omega C_0 R_1 (\epsilon' - j\epsilon'')}{1 + j\omega C_0 R_t (\epsilon' - j\epsilon'')} \quad \text{--- eq. 3.20b}$$

Multiplying the right hand side by $\frac{\epsilon' + j\epsilon''}{\epsilon' + j\epsilon''}$ and rearranging:

$$|V_d(\omega)| = |V_i(\omega)| \times \frac{\omega C_0 R_1}{\left[\left(\frac{\epsilon'}{\epsilon'^2 + \epsilon''^2} \right)^2 + \left(\frac{\epsilon''}{\epsilon'^2 + \epsilon''^2} + \omega C_0 R_1 \right)^2 \right]^{1/2}}$$

$$\theta_d(\omega) = \frac{\pi}{2} - \text{ARCTAN} \frac{\epsilon'' + \omega C_0 R_1 (\epsilon'^2 + \epsilon''^2)}{\epsilon'}$$

The **transfer function**, $H(\omega)$, for equations 3.20a and 3.20b are given by:

$$\left| H_a(\omega) \right| = \frac{\omega C_0 R_1}{[1 + \omega^2 C_0^2 R_1^2]^{1/2}} \quad \text{--- eq. 3.21a}$$

$$\Theta_a(\omega) = \frac{\pi}{2} - \text{ARCTAN}(\omega C_0 R_1)$$

$$\left| H_d(\omega) \right| = \frac{\omega C_0 R_1}{\left[\left(\frac{\epsilon'}{\epsilon'^2 + \epsilon''^2} \right)^2 + \left(\frac{\epsilon''}{\epsilon'^2 + \epsilon''^2} + \omega C_0 R_1 \right)^2 \right]^{1/2}} \quad \text{--- eq. 3.21b}$$

$$\Theta_d(\omega) = \frac{\pi}{2} - \text{ARCTAN} \frac{\epsilon'' + \omega C_0 R_1 (\epsilon'^2 + \epsilon''^2)}{\epsilon'}$$

In Fig.3.3 the variations of the functions given in equations 3.21a and 3.21b with angular frequency are shown graphically. Thus the plots for the amplitude of the **transfer function**, $H(\omega)$ for air and also for different values of ϵ' ($\epsilon''=0.001$) are shown in Fig.3.3a. The variation of the phase angle for different values of ϵ' is given in Fig.3.3b.

Dividing the two complex voltages shows that the ratio of the amplitudes is:

$$\left| \frac{V_d(\omega)}{V_a(\omega)} \right| = \frac{(1 + \omega^2 C_0^2 R_1^2)}{\left[\left(\frac{\epsilon'}{\epsilon'^2 + \epsilon''^2} \right)^2 + \left(\frac{\epsilon''}{\epsilon'^2 + \epsilon''^2} + \omega C_0 R_1 \right)^2 \right]^{1/2}} \quad \text{--- eq. 3.22a}$$

and the phase angle difference gives:

$$\Theta_d(\omega) - \Theta_a(\omega) = \text{ARCTAN}(\omega C_0 R_1) - \text{ARCTAN} \frac{\epsilon'' + \omega C_0 R_1 (\epsilon'^2 + \epsilon''^2)}{\epsilon'} \quad \text{--- eq. 3.22b}$$

The variation of the phase angle difference with the loss factor, ϵ'' , ($\epsilon' = 10$) is shown in Fig 3.4.

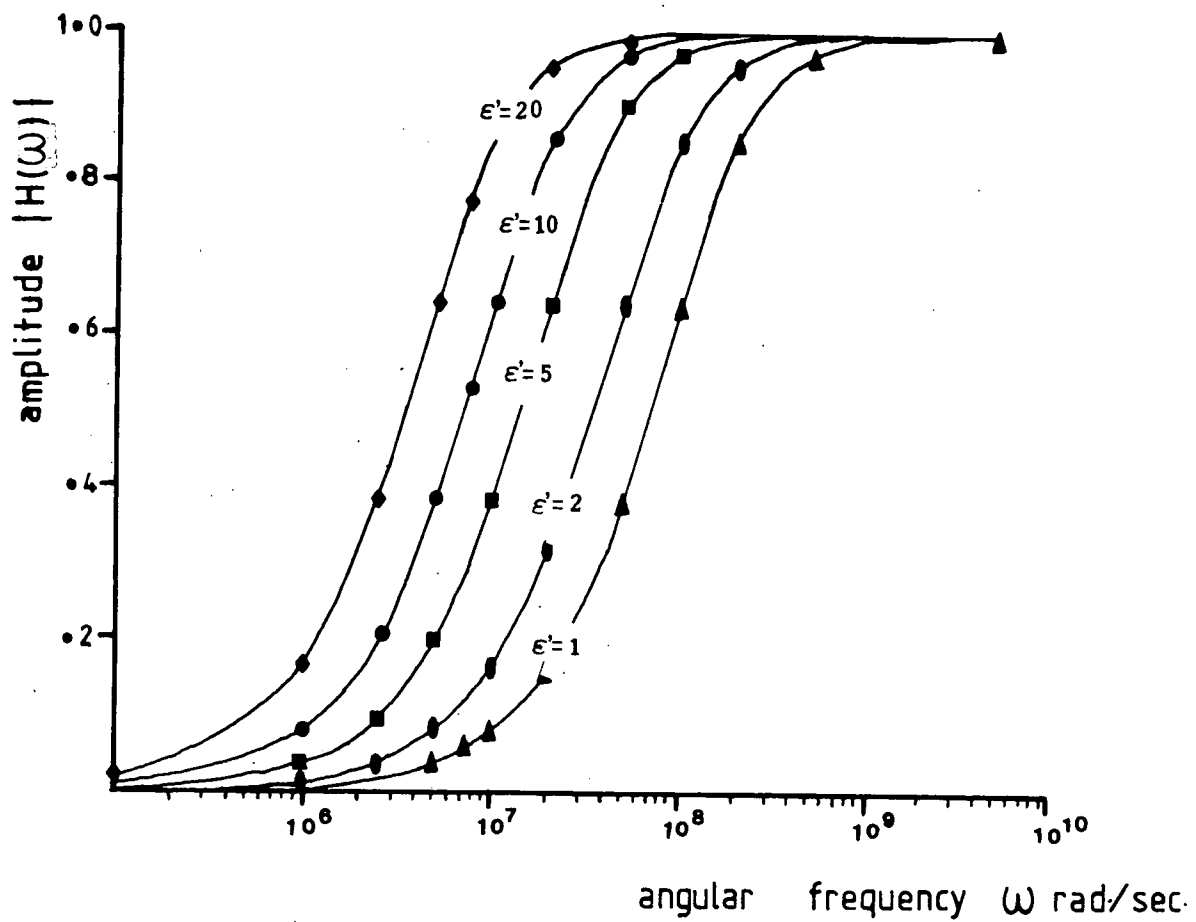


Fig. 3.3a Variation of transfer function (amplitude)

with ω for different values of ϵ' ($\epsilon'' = 0.001$)

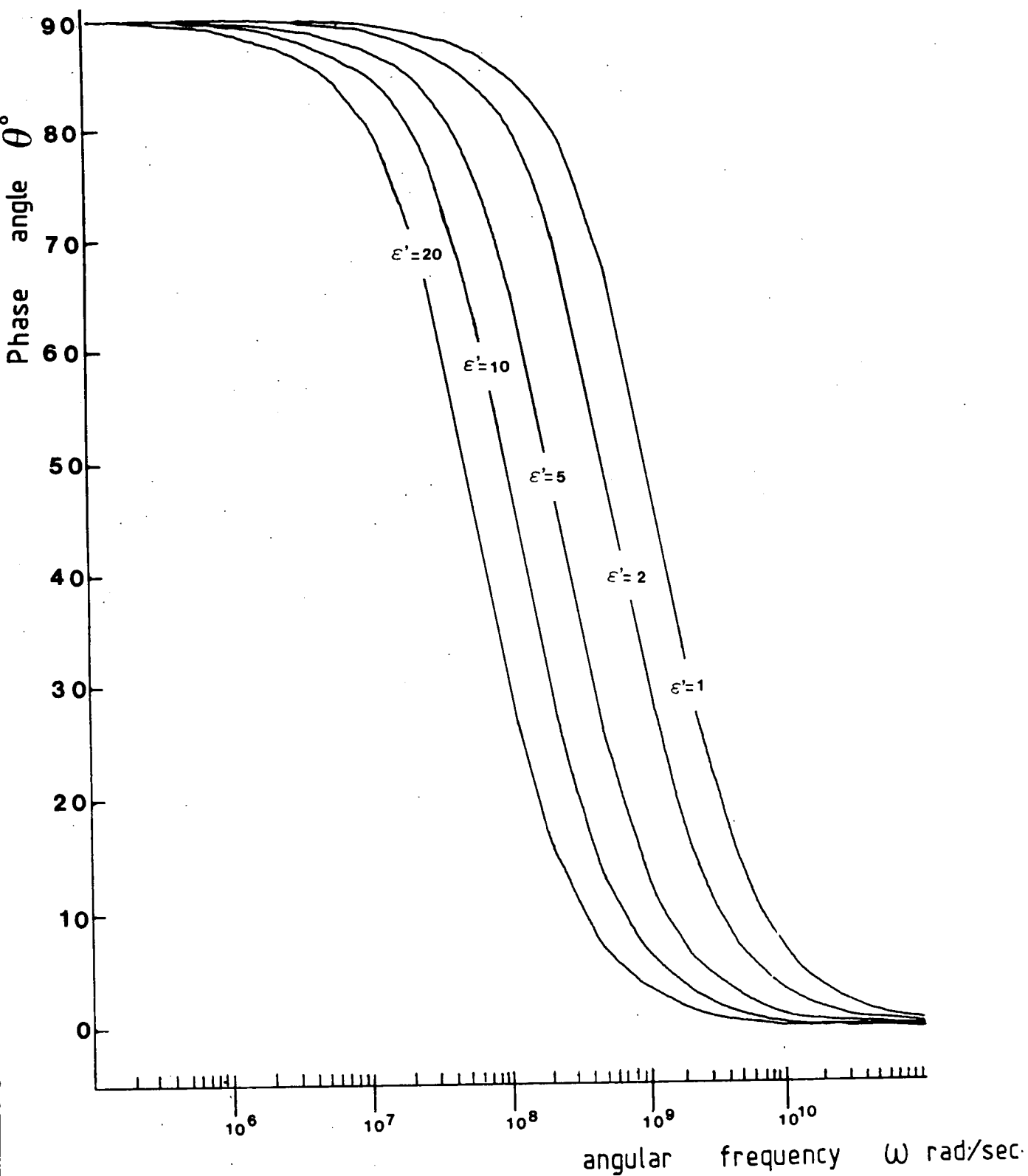


Fig. 3.3b Variation of transfer function (phase angle)

with ω for different values of ϵ' ($\epsilon'' = 0.001$)

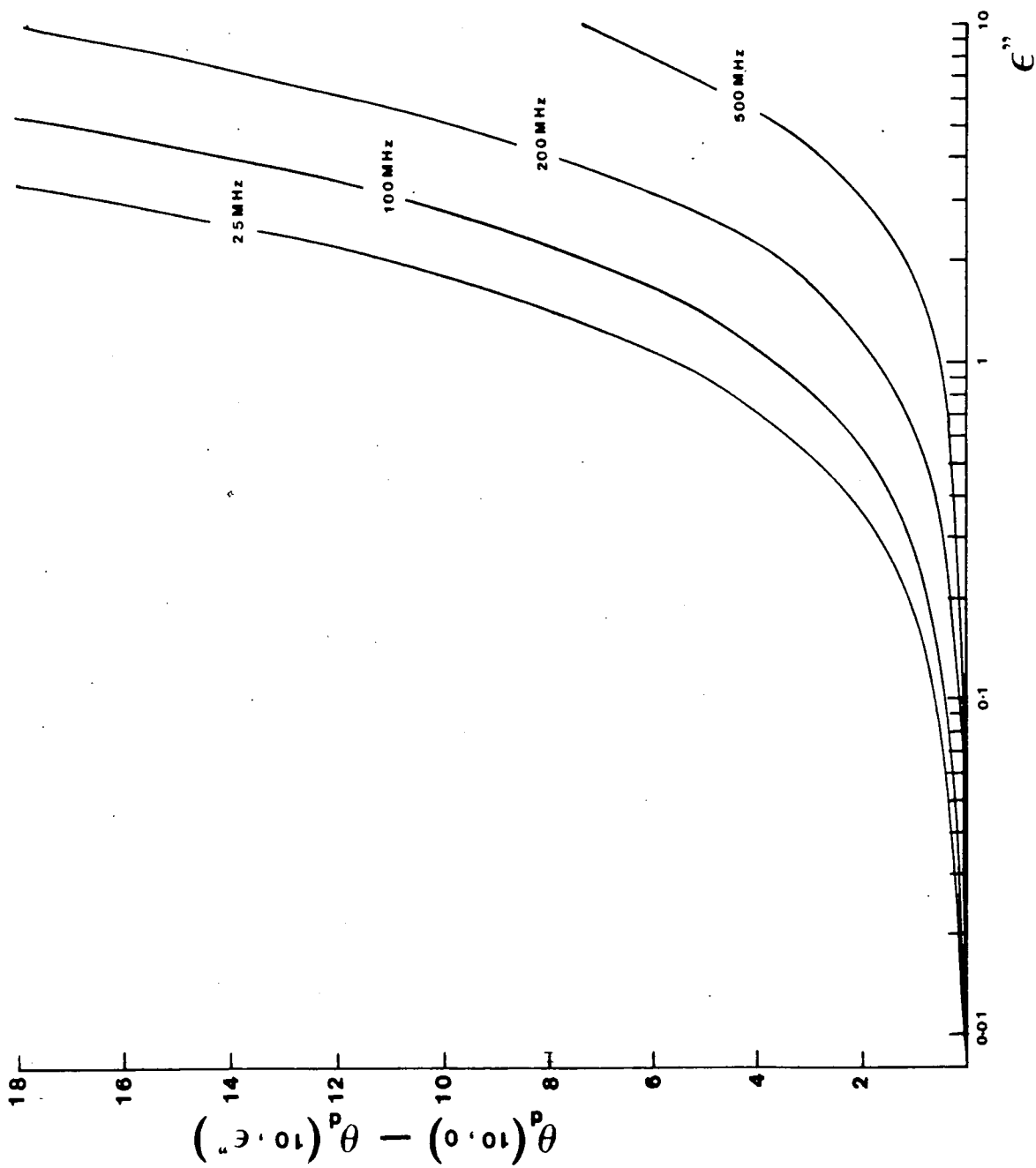


Fig. 3-4 Variation of phase angle difference with ϵ'' ($\epsilon' = 10$)

Equations 3.22a and 3.22b can be rearranged to give the formulae required to calculate the values of ϵ' and ϵ'' . Sometimes approximations are possible, for example, for a good insulator (i.e. $\epsilon'' \ll \epsilon'$), we can make the approximation:

$$\epsilon''^2 \ll \epsilon'^2$$

Therefore equations 3.22a and 3.22b become:

$$\left| \frac{V_d(\omega)}{V_a(\omega)} \right| = \frac{1 + \omega^2 C_0 R_t}{\left[\frac{1}{\epsilon'^2} + \left(\frac{\epsilon''}{\epsilon'} + \omega C_0 R_t \right)^2 \right]^{1/2}} \quad \text{--- eq. 3.23a}$$

$$\Theta_d(\omega) - \Theta_a(\omega) = \text{ARCTAN}(\omega C_0 R_t) - \text{ARCTAN} \frac{\epsilon''}{\epsilon'} + \omega C_0 R_t \epsilon'^2 \quad \text{--- eq. 3.23b}$$

From equation 3.23b:

$$\epsilon'' = \epsilon' \text{TAN}[\text{ARCTAN}(\omega C_0 R_t) - (\Theta_d(\omega) - \Theta_a(\omega))] - C_0 R_t \epsilon'^2 \omega$$

Substituting into equation 3.23a:

$$\epsilon' = \left| \frac{V_d(\omega)}{V_a(\omega)} \right| \left\{ \frac{1 + \text{TAN}^2[\text{ARCTAN}(\omega C_0 R_t) - (\Theta_d(\omega) - \Theta_a(\omega))]}{1 + (\omega C_0 R_t)} \right\}^{1/2}$$

If the thickness of the sample is not equal to the air gap:

$$\epsilon' = \left| \frac{V_d(\omega)}{V_a(\omega)} \right| \left\{ \frac{C_0}{C_0'} \frac{1 + \text{TAN}^2[\text{ARCTAN}(\omega C_0 R_t) - (\Theta_d(\omega) - \Theta_a(\omega))]}{1 + (\omega C_0 R_t)} \right\}^{1/2} \quad \text{--- eq. 3.24a}$$

and

$$\epsilon'' = \epsilon' \text{TAN}[\text{ARCTAN}(\omega C_0 R_t) - (\Theta_d(\omega) - \Theta_a(\omega))] - C' R_t \epsilon'^2 \omega \quad \text{--- eq. 3.24b}$$

where:

$$C_0' = \frac{\epsilon_0 A}{d'}$$

and

d' = thickness of sample.

3.5 SIGNIFICANCE OF THE DERIVED EQUATIONS

Equations 3.21 and 3.22 are the frequency transfer functions for an air gap and for materials having different values of ϵ' and ϵ'' . The air gap (and hence the thickness of sample) was taken to be 3×10^{-4} m. and the diameter of the inner conductor of the sample holder was 6.204×10^{-3} m.. The graphs in Fig. 3.3a show that the circuit transmits high frequency signals and blocks the low frequency signals. The transmitted signal experiences both a reduction in magnitude and a change in phase angle (see Fig. 3.3b). However at very high frequencies the signals are transmitted with negligible modification to their amplitude and phase. Every pair of values of ϵ' and ϵ'' has its characteristic transfer function and thus will modify the input waveform differently i.e for a particular input waveform different pairs of values of ϵ' and ϵ'' will cause different modifications and the output will have a distinct shape corresponding to the values of ϵ' and ϵ'' .

The output waveform for different values of ϵ' and ϵ'' can be obtained by multiplying the frequency transfer function with the input spectra at the corresponding harmonic frequency (eq.3.20b). Then, by performing an inverse Fourier transformation on the sum of the products at each harmonic frequency, the output waveform can be obtained. This waveform characteristically defines ϵ' and ϵ'' ; by comparing it with the experimental waveform, the values of ϵ' and ϵ'' for the material under study can be obtained simultaneously. Thus by storing all the possible family of waveforms for different pairs of values of ϵ' and ϵ'' in the computer file, an operator just has to change the sample and

the computer will make the comparison and give out the respective values of ϵ' and ϵ'' for each of the samples inserted in the test jig. Initially calibration is necessary i.e the input waveform (e.g. Fig. 3.5) has to be measured and analysed and the family of waveforms for different values of ϵ' and ϵ'' have to be worked out for the particular input waveform. Some typical output waveforms (corresponding to the input waveform shown in Fig. 3.5) for different values of ϵ'' are shown in Fig. 3.6a for $\epsilon'=4$ and in Fig. 3.6b for $\epsilon'=10$; a corresponding plot showing output waveforms for different values of ϵ' (with $\epsilon''=0.001$) is shown in Fig. 3.6c.

The dielectric properties of a material vary with frequency depending on the dominant conduction mechanism that the material experiences due to the introduction of an electromagnetic field. Thus, for example, in materials that obey the Universal law of dielectric response [3.9 - 3.14] the variations of ϵ' and ϵ'' with frequency obey the relations:

$$\epsilon' - \epsilon_{\infty} \propto \omega^{n-1}$$

$$\epsilon'' \propto \omega^{n-1}$$

in which $0.7 < n < 1$

These relations can be included in the frequency transfer function and will accordingly modify the function to give its characteristic output waveform. Thus, not only can the dielectric constants at harmonic frequencies be obtained in a single run, but also the exponent n in the Universal law can be worked out simultaneously. Alternatively, a dipolar material will show a different variation in the transfer function and give different output waveforms.

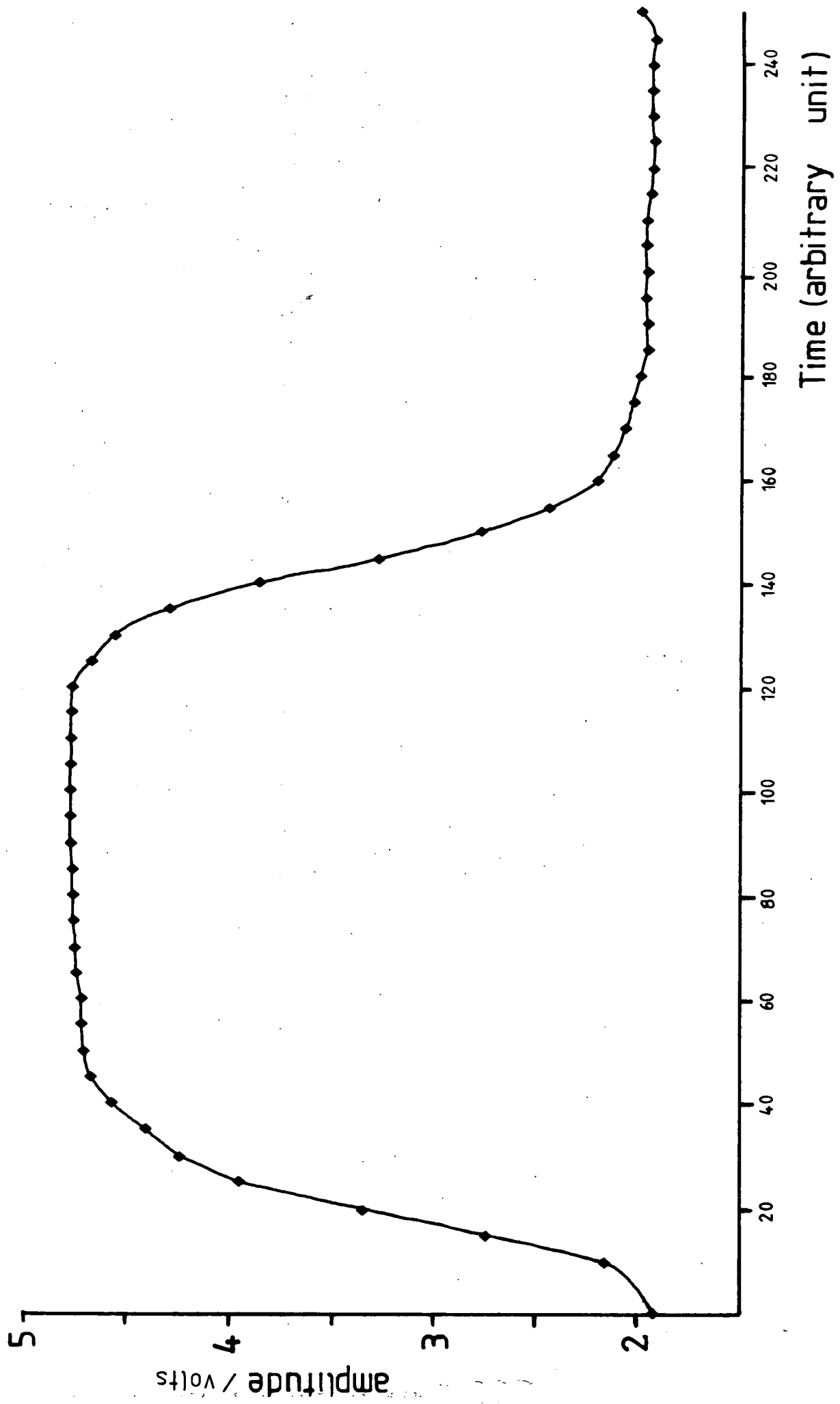


Fig. 3.5 Experimental input waveform.

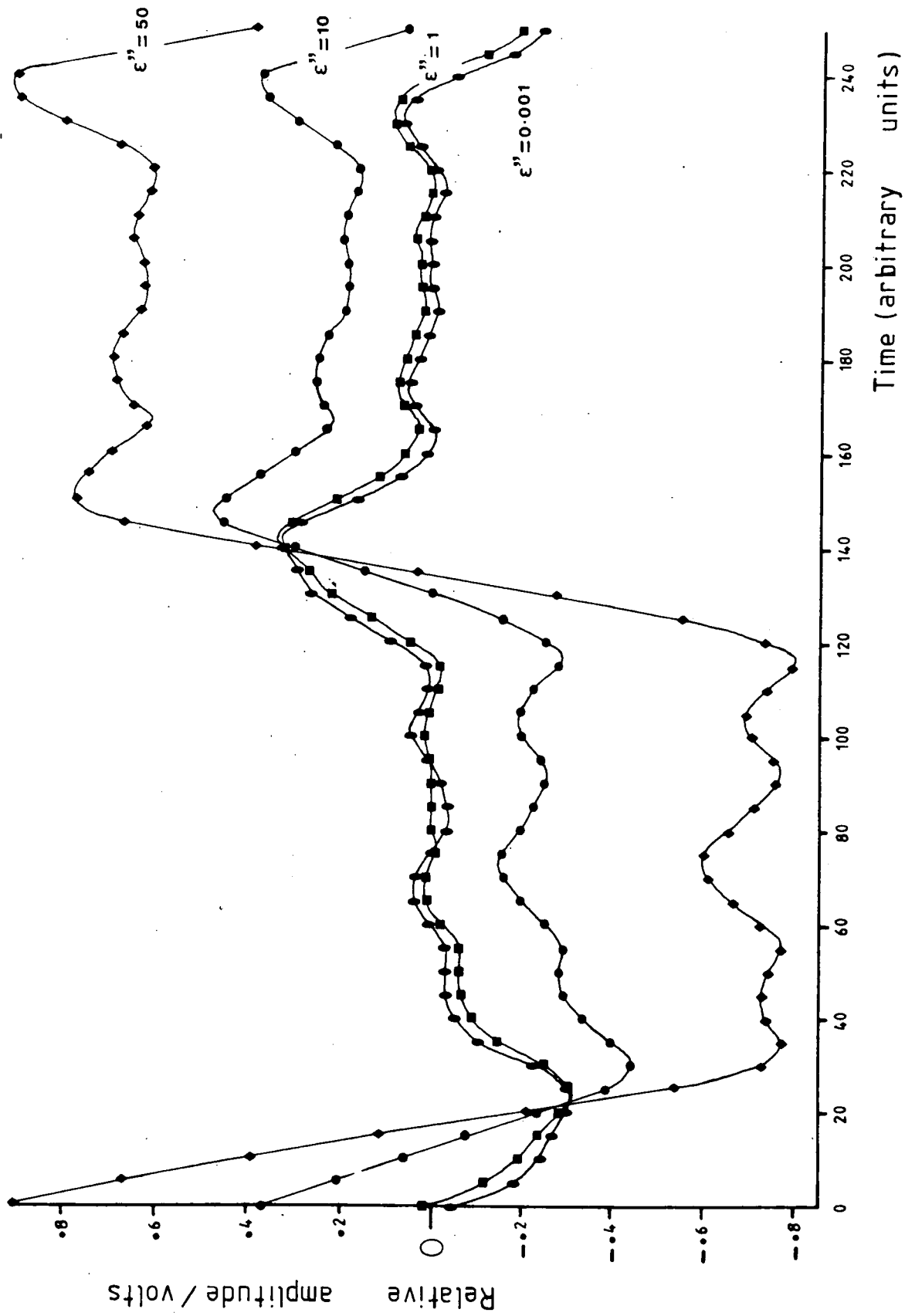


Fig. 3.6a Theoretical output waveform for different values of ϵ'' ($\epsilon' = 4$)

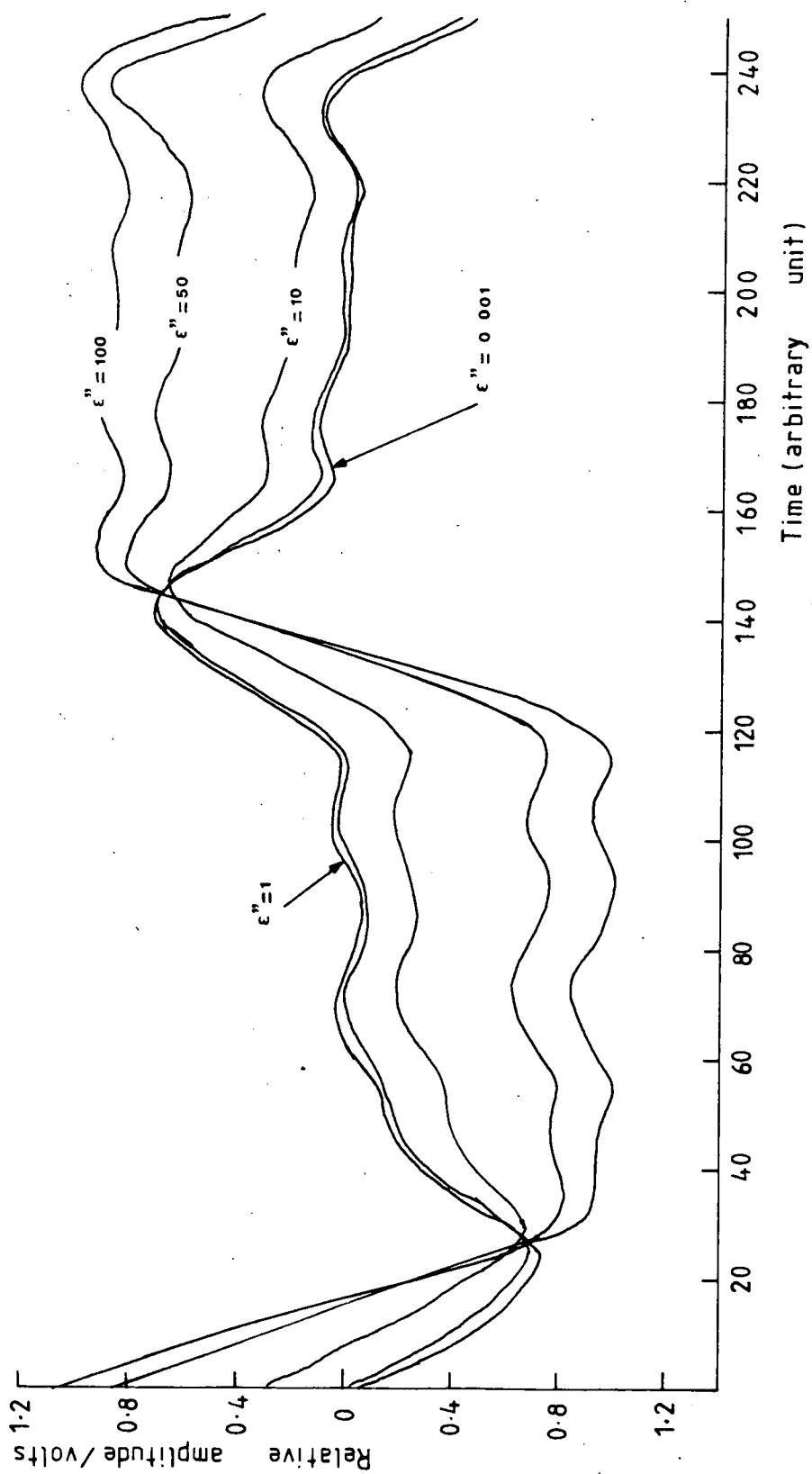


Fig. 3.6b Theoretical output waveform for different values of ϵ'' ($\epsilon' = 10$)

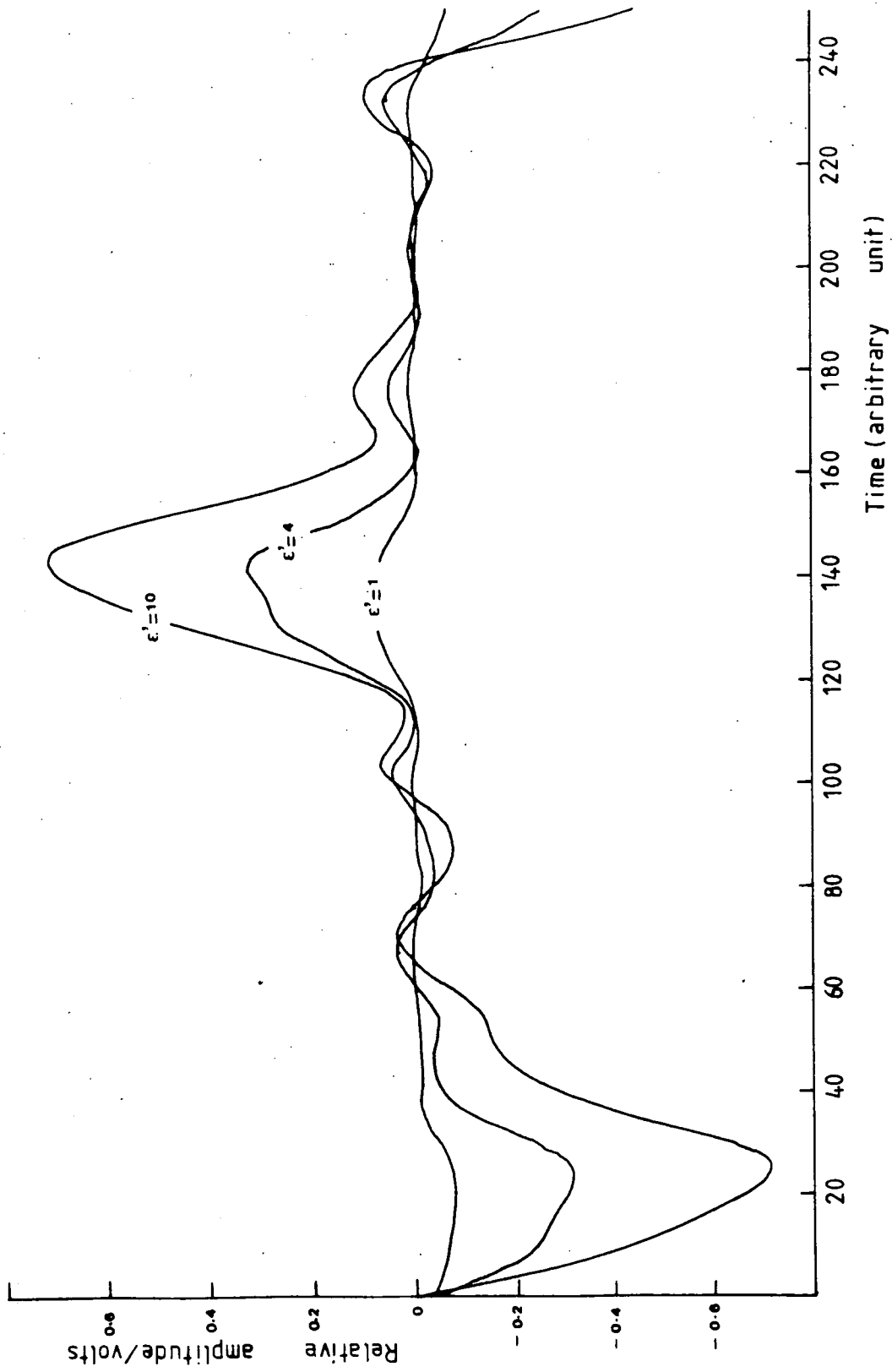


Fig. 3.6c Theoretical output waveform for different values of ϵ' ($\epsilon'' = 0.001$)

The suitability of the method for loss measurements can be assessed by referring to Fig. 3.7 and 3.8. In Fig. 3.7 the theoretical output waveforms for different values of ϵ'' are shown on an expanded scale of relative amplitude, taking the fixed value of $\epsilon'=4$. From this, taking sample point 50, the relative amplitudes were derived for different values of ϵ'' ; this plot is shown in Fig. 3.8. The experimental significance of this is that, in the range of ϵ'' from 0.1 to about 0.02 (i.e a range representing quite lossy materials) the amplitude difference can be measured fairly easily using conventional instrumentation. However for $\epsilon'' < 0.02$ (corresponding to materials which are becoming much more insulating) the amplitude difference, which now amounts to only a few tenth of a millivolt, is much more difficult to measure precisely. This gives an indication of the limitation of the technique. Further, equations 3.24a and 3.24b were used to check that the equivalent circuit and its mathematical representation were correct. A number of well-known dielectrics were used in the measurements and the results have been compared with standard values. These results are shown in Chapter 5.

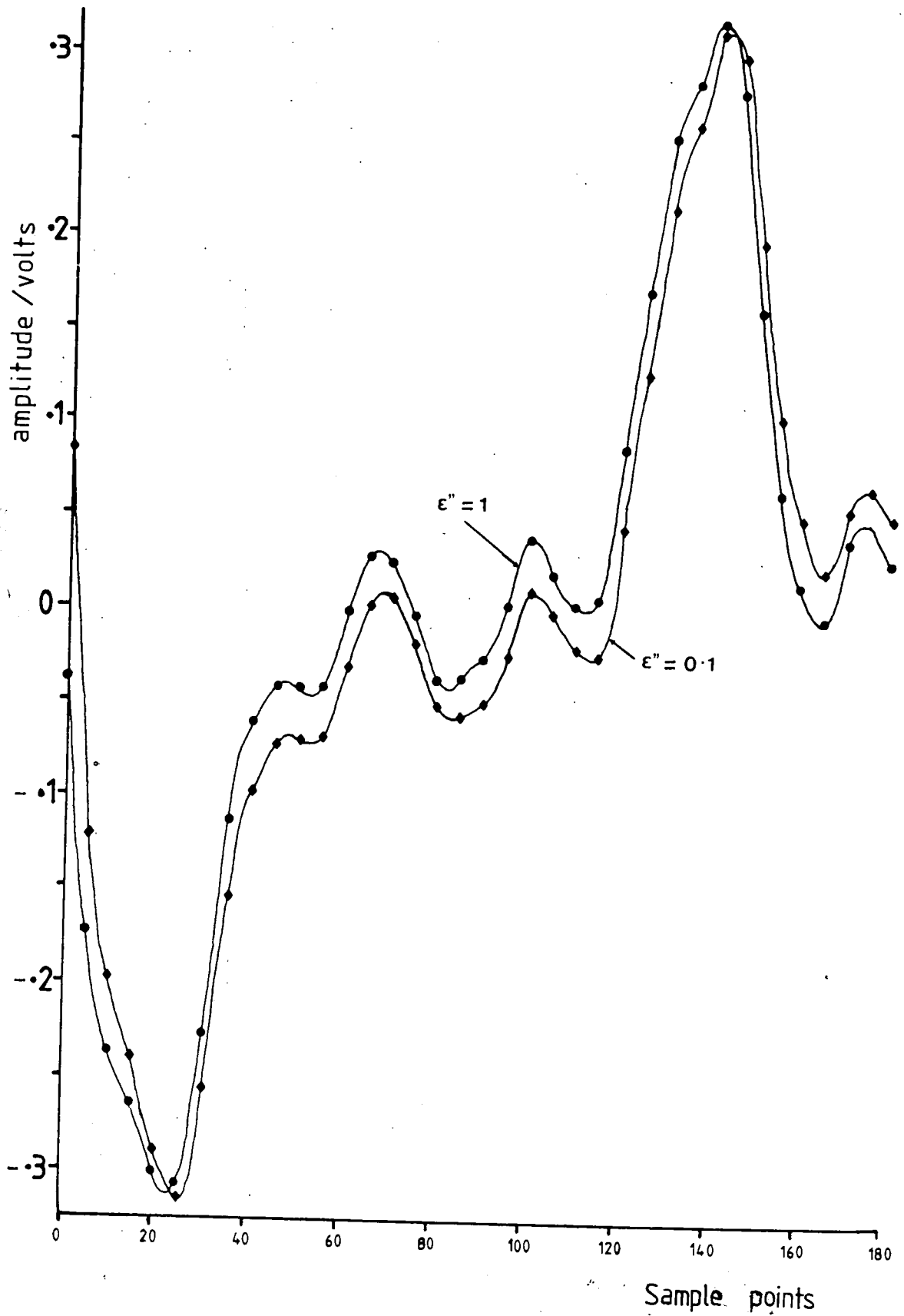


Fig. 3.7 Theoretical output waveform for different values of ϵ'' — expanded scale; ($\epsilon' = 4$)

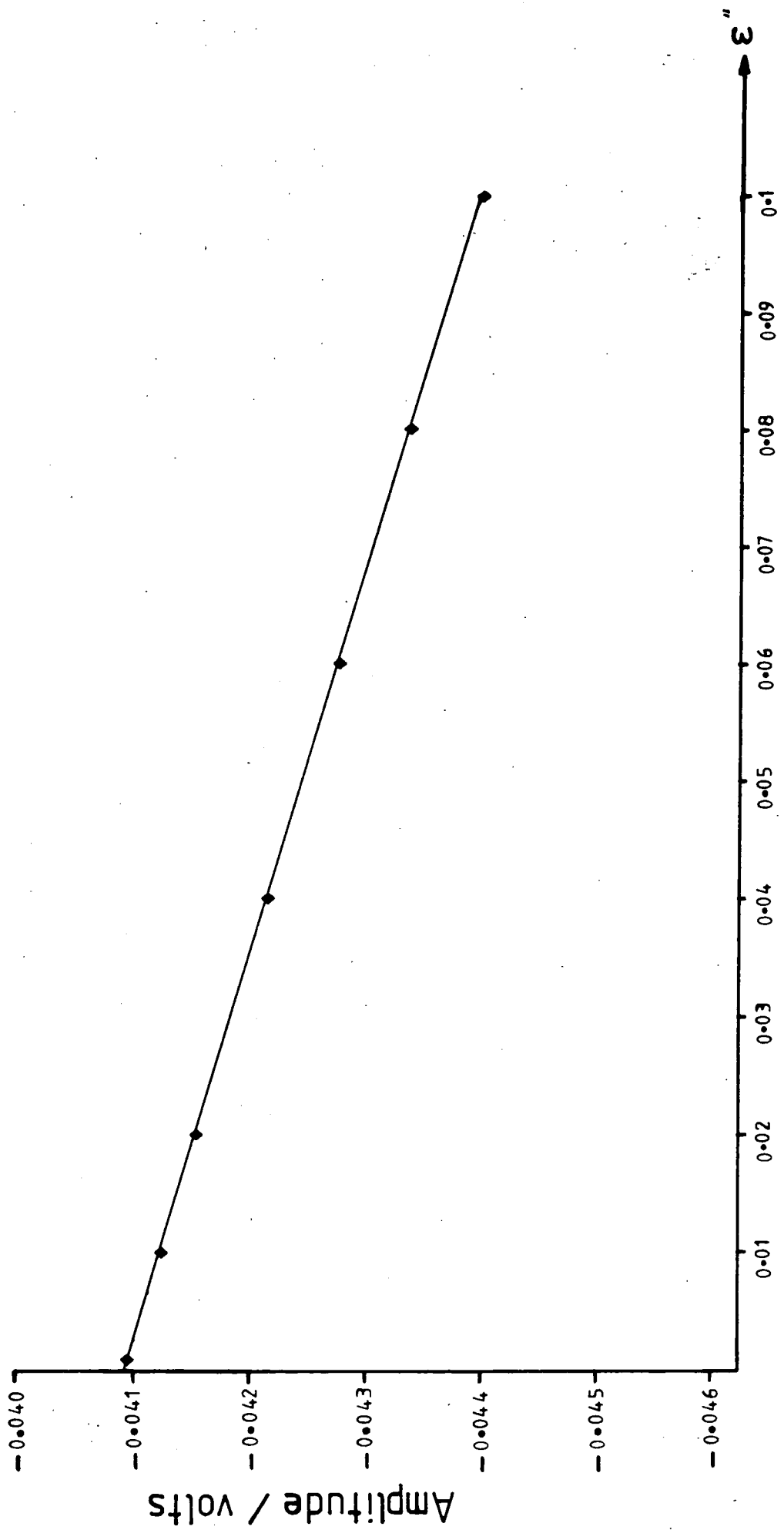


Fig. 3.8 Variation of amplitude with ϵ'' at sampling point 50
 ($\epsilon' = 4$)

REFERENCES

- 3.1 "A time-domain technique for measurement of dielectric properties of biological substances"
M.F. Iskandar and S. Stuchly - IEEE Trans. on Instrums. and Meas., Vol.IM21, No.4, p425, (1972)
- 3.2 "Time domain measurements for determination of dielectric properties of agricultural materials"
B.P. Kwok, S.O. Nelson, E. Bahar - IEEE Trans. on Instrums. and Meas., Vol.IM28, No.2, p109, (1979)
- 3.3 "An introduction to Fourier analysis" - R.D. Stuart - Methuen's Monograph (John Wiley & Son), N.York, (1961)
- 3.4 "Signal analysis" - A. Papoulis, McGraw Hill, N.York, (1977)
- 3.5 "Fourier transform of discrete data rendered continuously by use of polynomial interpolation"
K. Watanabe and K. Shimada - Electrical Engineering in Japan, Vol.95, No.5, p111, (1979)
- 3.6 "An introduction to the analysis and processing of signal" - P.A. Lynn, MacMillan, London, (1973)
- 3.7 "Dielectric and electronic properties of biological materials" - R. Pethig, John Wiley & Sons, N.York, (1979)
- 3.8 "Dielectric properties and molecular behaviour"
N.E. Hill, W.E. Vaughan, A.H. Price
Van Nostrand Reinhold Company, N.York, (1969)
- 3.9 "The Universal dielectric response - Review article"
A.K. Jonscher - Nature, Vol.267, p673, (1977)

- 3.10 "On the origin of the Universal dielectric response in condensed matter" - K.L. Ngai, A.K. Jonscher, C.T. White
Nature, Vol.277, p185, (1979)
- 3.11 "Physical basis of dielectric loss" - A.K. Jonscher
Nature, Vol.253, p717, (1975)
- 3.12 "Review - A new understanding of the dielectric relaxations of solids" - A.K. Jonscher
J. Mat. Science, Vol.16, p2037, (1981)
- 3.13 "Characterization of dielectric materials" - R.M. Hill
J. Mat. Science, Vol.16, p118, (1981)
- 3.14 "Hopping losses in polarisable dielectric media"
A.K. Jonscher - Nature, Vol.250, p191, (1974)
- 3.15 "Physics of dielectric solids" - C.H.L. Goodman
Conference series No.58, Institute of Physics,
Bristol, London, (1980)
- 3.16 "Dielectrics - intermolecular forces - optical rotation"
(Documents on modern physics) - R.H.Cole
(J.W. Kirkwood collected works, Vol.2) - Gordon and
Breach Science Publishers, N.York, (1965)

EXPERIMENTAL FOURIER ANALYSIS TECHNIQUES SYSTEM

4.1 INTRODUCTION

The need for the calculation of the dielectric parameters to be made in the frequency domain (eq. 3.16) requires the time domain signal to be transformed into its frequency domain equivalent. Thus the main task in the assembly of the Fourier analysis method of dielectric measurement is to build a data acquisition system to read the data points for one period of the output signal into the computer. The computer used is an 8-bit computer, therefore all the interfacing was completed using 8-bit converters. When data points (up to 256 points) are read into the computer they can be analysed and the computer will perform all the calculations giving out the final parameters required. A sampling adapter (Bradley Type 158) has been used in the data acquisition system. This unit transforms the high frequency signal into its low frequency presentation. To enable the computer to read the data points, the signals from the sampling adapter were digitized using an 8-bit analogue-to-digital converter. An 8-bit digital-to-analogue converter, controlled by the computer, was used to drive the external scanning voltage of the sampling adapter. This effectively divided the time-axis into M equal intervals (maximum 256) and synchronized the reading in of the sample points into the computer.

4.2 THE COMPLETE SYSTEM

The block diagram for the complete assembly of the

Fourier analysis technique of dielectric measurement of materials is shown in Fig. 4.1. All the connections used were coaxial with 50 ohm impedance. The signal source is a pulse generator which drives the test circuit at the fundamental and harmonic frequencies. Fifty ohm attenuators were used at both ends of the test circuit to ensure impedance matching. The sample is placed in a gap in the inner conductor of a coaxial sample-holder and the experiment consists of measuring the distortion of the output waveform caused by the introduction of the sample in the holder. This is achieved by passing the high frequency waveform through the sampling adapter unit. The sampling adapter is capable of reading signals up to 1GHz fairly easily and with very careful tuning its range could be extended to 1.2GHz . It transforms the high frequency signal into a low frequency equivalent at less than 100kHz . This unit has three operating modes, i.e automatic, manual and external scanning modes; each of these can provide the scanning voltage for the time-axis required to synchronize the display of all the waveforms. The signals from the sampling adapter were digitized by an analogue-to-digital converter and subsequently the computer read in data points for one period of the output waveform. The signals were stored in the computer file and can be processed and analysed to give out the required dielectric parameters.

4.3 CHOICE OF INPUT WAVEFORM

The basis of the Fourier series is that a complex periodic waveform may be analysed into a number of harmonically related sinusoidal waves. Thus, apart from pure

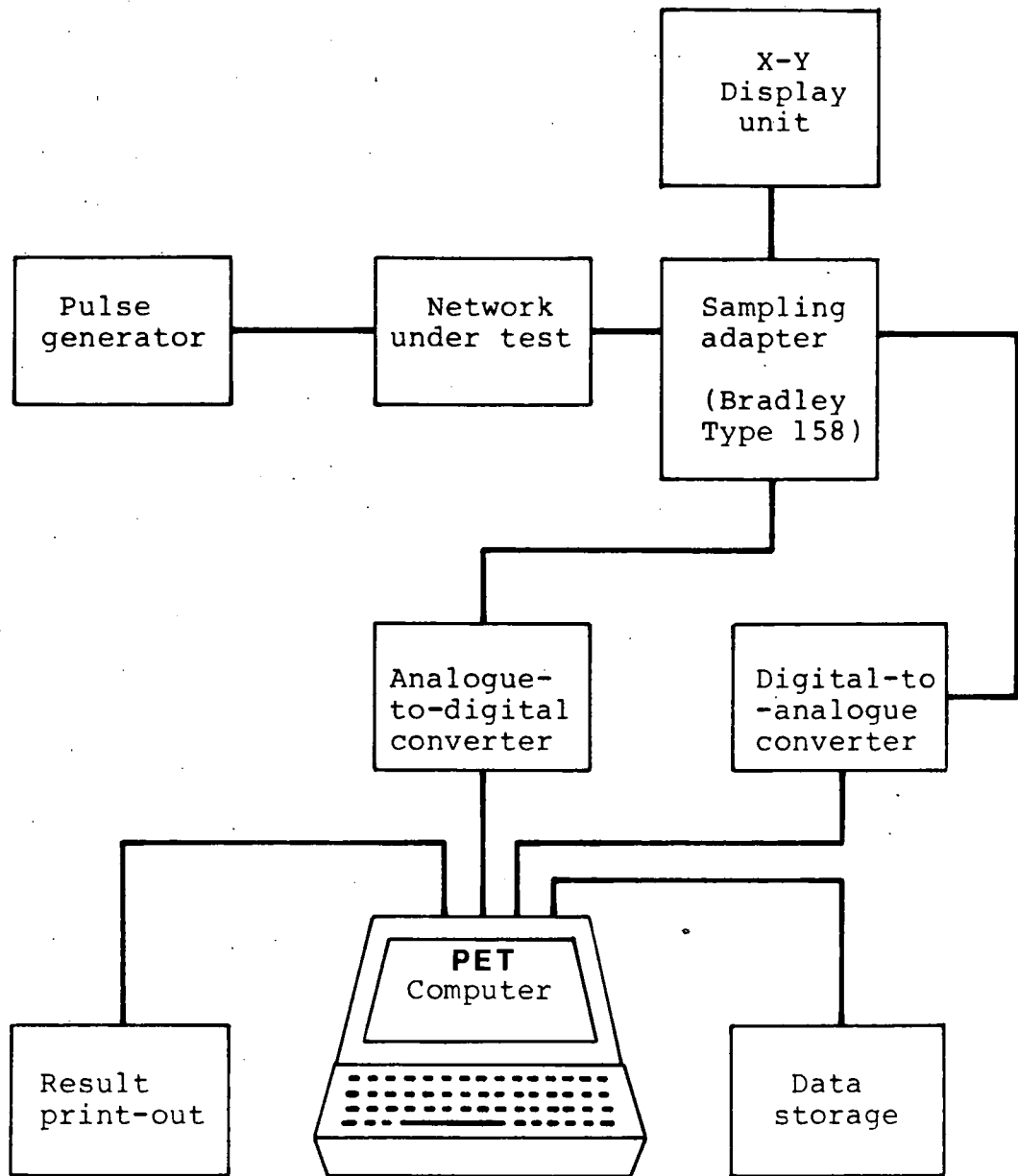


Fig. 4.1 Block diagram of experimental assembly for

Fourier analysis technique.

sinusoids, any waveform contains harmonics and in principle can be used as the input waveform for this technique. However, a number of factors must be taken into consideration when choosing the most desirable input waveform. Firstly, as the impedance of the measuring circuit is 50 ohm, it would be advantageous if the signal source had the same impedance in order to avoid mismatching. Secondly, the harmonic output of the input waveform varies with the shape of the waveform, i.e some particular shape of waveform may give higher harmonic output levels than other shapes. The choice would be for the one that would give the largest harmonic output at high harmonic frequencies. Table 4.1 shows some simple shapes of waveform which either are available from commercial equipment or can easily be made. The Table shows that the rectangular shaped waveform would give higher output harmonic levels than any other shape shown. The range of frequency coverage can be much more easily controlled by changing the fundamental frequency of the input waveform than by measuring the output at very high harmonic frequencies. Thus, it will be advantageous if the fundamental frequency of the input waveform can be varied easily.

The input waveform used in the present measurements is obtained from a pulse generator (Tektronik Type 2101) which is capable of producing a pulse output with repetition frequencies ranging from 25Hz to 25MHz, continuously variable between the calibrated steps. The output voltage of the unit is 10 volts and it has a characteristic impedance of 50 ohm. This particular type of generator was chosen

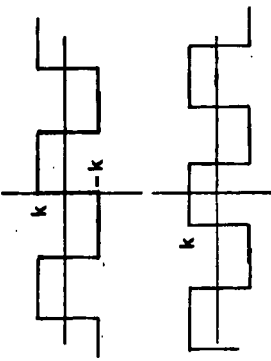
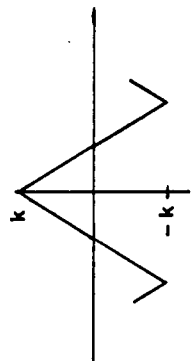
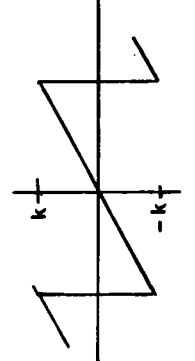
no.	wave equation	wave shape	series representation
1 Square wave a) Sine series b) Cosine series	$f(x) = \begin{cases} -k, & -L < x < 0 \\ k, & 0 < x < L \end{cases}$ $f(x) = \begin{cases} k, & x < \frac{1}{2}L \\ -k, & \frac{1}{2}L < x < L \end{cases}$		$f(x) = \frac{4k}{\pi} \left[\sin \frac{\pi x}{L} + \frac{1}{3} \sin \frac{3\pi x}{L} + \dots \right]$ $f(x) = \frac{4k}{\pi} \left[\cos \frac{\pi x}{L} - \frac{1}{3} \cos \frac{3\pi x}{L} + \dots \right]$
2 Triangular wave	$f(x) = \begin{cases} \frac{2k}{L}(\frac{L}{2} - x), & -L < x < 0 \\ \frac{2k}{L}(\frac{L}{2} + x), & 0 < x < L \end{cases}$		$f(x) = \frac{8k}{\pi^2} \left[\cos \frac{\pi x}{L} + \frac{1}{3} \cos \frac{3\pi x}{L} + \dots \right]$
3 Saw-tooth wave	$f(x) = \frac{kx}{L}, \quad -L < x < L$		$f(x) = \frac{2k}{\pi} \left[\sin \frac{\pi x}{L} - \frac{1}{2} \sin \frac{2\pi x}{L} + \dots \right]$

Table 4-1 Example of input waveform.

because it gave larger harmonic outputs than other non-sinusoidal signal generators and also provided wide frequency coverage.

4.4 SAMPLE-HOLDER DESIGN

The geometry of the coaxial line leads to particularly simple forms for the electric and magnetic fields, i.e for the TEM mode the electric field is entirely radial and the magnetic field forms a series of concentric circles around the inner conductor. A capacitive gap in the inner conductor of the coaxial line can be used as a sample-holder for measurements at both radio and microwave frequencies. When a sample is introduced into the sample-holder, the series capacitance is given by $C_0 \epsilon^*$ where ϵ^* is the complex relative permittivity of the sample and C_0 is the series capacitance of the empty sample-holder calculated from the inner conductor and air gap dimensions.

The sample-holder, Fig. 4.2, used in this work was constructed from brass. The diameter of the inner conductor was 6.20mm. and the internal diameter of the outer conductor was 14.29mm.. Theoretically this would give a characteristic impedance very close to 50 ohm. The details of the construction and performance of the sample-holder used in this work are given in Ahmad's thesis [4.3].

4.5 SAMPLING AND COMPUTING

The Fourier analysis technique for dielectric measurements involves detecting small changes in the shape of the output waveform. In the present measurements the fundamental frequency of the input waveform is about 25MHz .

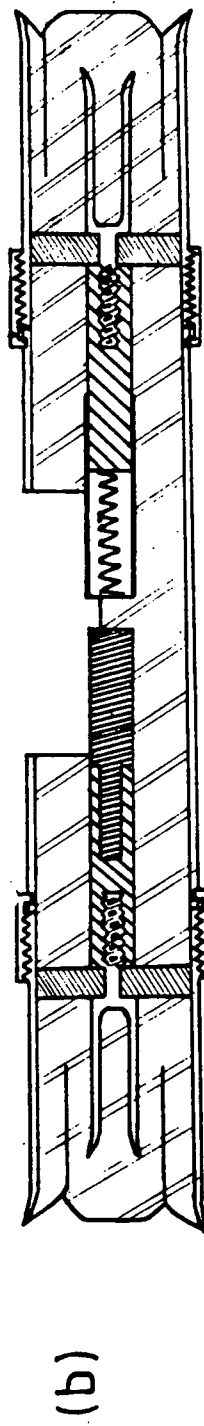
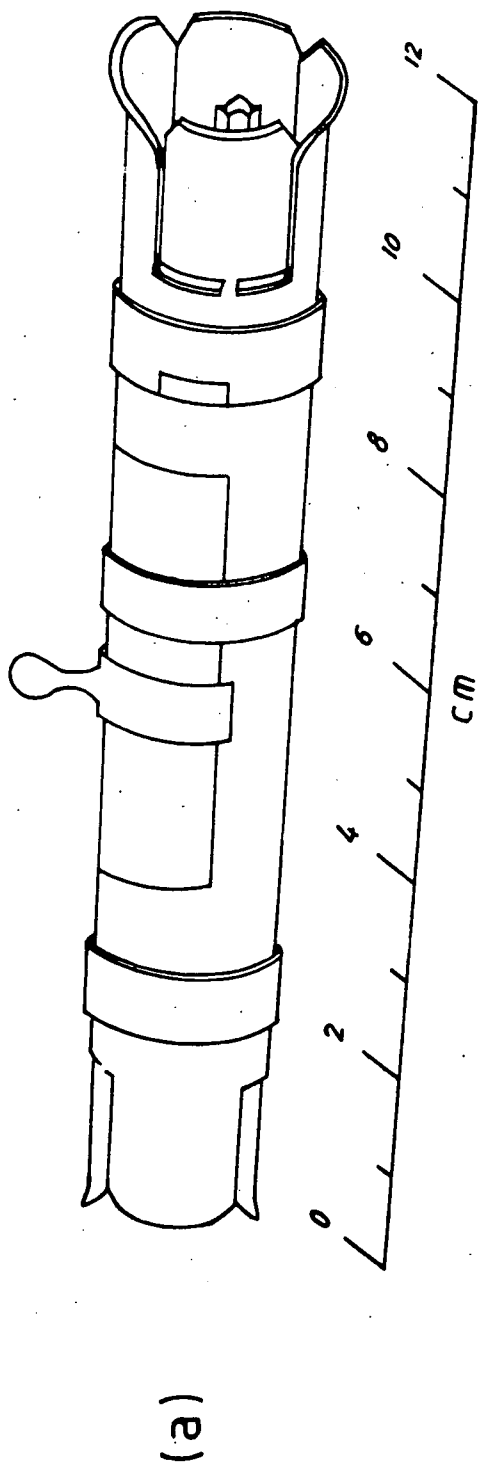


Fig. 4.2 (a) External view and (b) cross-section of sample-holder used in this work

Signals of this frequency can be displayed on oscilloscopes with bandwidths up to 25MHz, but the display would not represent the true output waveform as higher harmonics of the waveform would not be detected by the oscilloscope. The process of sampling the signal effectively expands the time-axis of the output waveform, i.e. sampling the output waveform transforms the high frequency signal from the high to low frequency range, and the low frequency signal can subsequently be displayed without loss of information. In the present work, the Bradley sampling adapter Type 158 was used for this purpose. This unit is capable of displaying signals with rise-times as fast as 0.5 nanoseconds and the equivalent bandpass is from direct current to beyond 1GHz.. The output from this unit is a signal whose frequency components range from d.c. to about 100kHz, depending upon the nature of the signal going into it. This output signal can easily be displayed on an ordinary oscilloscope or X-Y display unit. The signal gain of the adapter is calibrated from X1 to X50, which gives an overall maximum sensitivity of 10mV. per division. The signal input impedance is 50 ohm and the maximum input and output signal amplitudes are ± 2 volts.

The facilities provided by the sampling adapter were fully utilized in the data acquisition system of the assembly. The horizontal scan of the unit can be operated either with automatic, manual or external operation. In the automatic mode the unit will scan automatically and the number of sample points can be varied (between 100 to 1000) by using the SAMPLES/SCAN control. The manual mode enables

the operator to control manually the horizontal scan of the oscilloscope. Thus a display may be traced very slowly or, if desired, the sweep may be stopped at any point on the display. Use of the external operation mode required an external scanning voltage to be applied to the EXT. SCAN sockets. In the present data acquisition system, the external operation mode was used in order to overcome the synchronisation problem. An 8-bit digital-to-analogue converter, controlled by the computer supplies the external scanning voltage and an 8-bit analogue-to-digital converter reads in the amplitude of the signal at various scanning points. All the data points can then be stored to be processed to give out the required parameters.

The time taken to read in one period of a waveform is about one minute and with a computer that has a disk storage facility this data can be stored into its file in less than a minute. Thus the Fourier analysis technique can make measurements at two minute intervals. The actual calculation to produce the required parameters can either be completed at a subsequent time or simultaneous operation can be achieved by linking the computer to several others which will make the required calculations and comparisons to produce the required parameters. The advantages of this system will enable it to be used , for example, on a factory line to monitor the production output; another area of potential application is in biological research where measurements at very short time intervals are always required.

4.6 TEST OF DATA ACQUISITION SYSTEM

The data acquisition part of the assembly was tested by using a known pulse as an input. A rectangular pulse with a pulse duration (τ) of about one-fifth of the repetition period T (i.e. $\tau/T = 1/5$) was used; the pulse repetition frequency was 2.5MHz. The sample points were read into the computer and were Fourier analysed to give out the amplitude and phase spectra. These results are plotted in Fig. 4.3. The theoretical amplitude and phase spectra for a perfect (infinite rise time) pulse with $\tau/T = 1/5$ are included in Fig. 4.3 for comparison purposes. It can be seen that there is a good fit and this proves that the system is working very well. However the pulse used did not have the ideal theoretical shape but had a rise time of about 5 nsec.; furthermore the τ/T ratio was not exactly equal to 1/5. Consequently this test could not check the accuracy of the reading in of the data points. Nevertheless, this test proves that the data acquisition system is collecting data correctly and that the computer programs used to calculate the amplitude and phase spectra are correct. The complete appraisal of the whole assembly used to measure the dielectric properties of reference materials will be presented in Chapter 5.

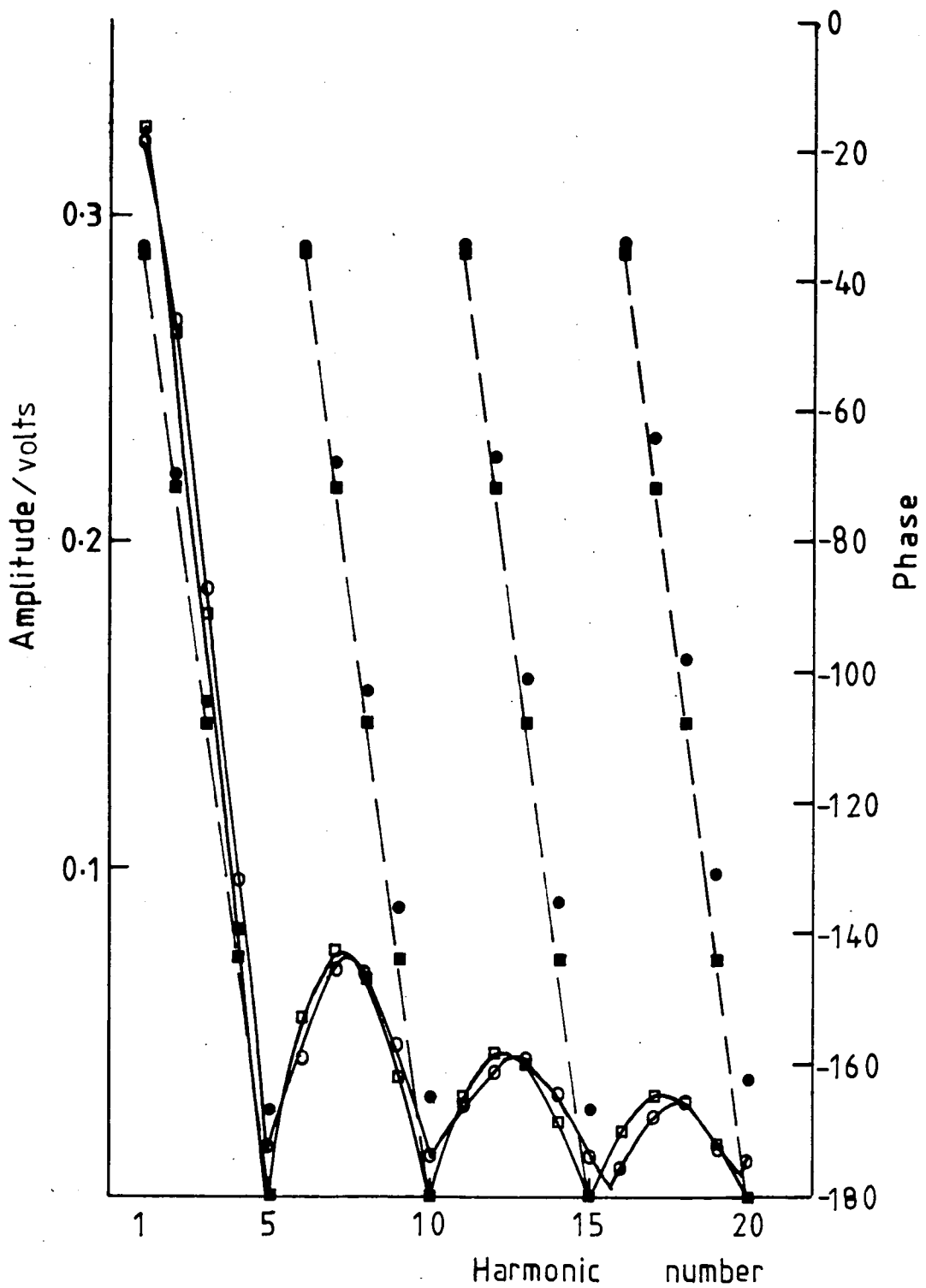


Fig. 4.3 Amplitude and phase spectra; (□) theoretical amplitude, (○) measured amplitude, (■) theoretical phase angle, (●) measured phase angle.

REFERENCES

- 4.1 "Computer augmented oscilloscope system" - P.E. Stuckert
IEEE Trans. on Instrum. and Meas. Vol.IM18, No.4, p299
(1969)
- 4.2 "Random sampling oscilloscopy" - G.J. Frye, N.S. Nahman
IEEE Trans. on Instrum. and Meas., p8, March (1964)
- 4.3 "Improved wideband coaxial methods for dielectric
measurements on nitrogen ceramics" - A.B. Ahmad
Ph.D Thesis - University of Durham (1983)
- 4.4 "Spectrum analyser measurements" - D. Welch
Tektronik Inc. Oregon, (1969)
- 4.5 "Spectrum analysers: Complicated measurements are
simplified" - K. Kitada
JEE, p52, August (1977)
- 4.6 "Fourier transform of discrete data rendered
continuously by use of polinomial interpolation"
K. Watanabe and K. Shimada
Electrical Engineering in Japan Vol.95, No.5, (1975)

CHAPTER 5

APPRAISAL OF THE FOURIER ANALYSIS TECHNIQUE

5.1 INTRODUCTION

Theoretically, the idea of obtaining a spectrum of results at harmonic frequencies has been shown in Chapter 3 to be feasible. However, many practical problems have to be overcome before a complete operating system can be built to give truly reliable results. The first problem was to determine whether the signal source could give out enough power to drive the test circuit at the required harmonic frequencies. The harmonic amplitudes were measured quite simply by using both a wave analyser and a spectrum analyser and the input level was adjusted accordingly. Further, the complete system involves a data acquisition section that uses a computer and this requires interfacing the measuring rig to the computer to enable it to read in all the data points. Thus, the assembly of the complete system is a tedious process; therefore the principle of the Fourier analysis approach was first tested in the frequency domain using the wave analyser. Here pure magnesium oxide (MgO) single crystal was used as a standard reference sample. The close agreement obtained between these experimental measurements and the accepted value justified the assembly of the complete Fourier analysis equipment. The complete system was also tested using two reference samples, namely pure MgO and vitreosil (pure SiO_2). The capabilities and limitations of this technique are discussed together with the factors which govern the accuracy attainable with the present system. Some suggestions to improve the system are put forward.

5.2 EARLY EXPERIMENT USING WAVE ANALYSER

The circuit diagram for this measurement is similar to that of Fig. 3.2 but instead of doing the measurement in the time domain, a wave analyser was used. The circuit was first tested using sinusoidal waves at various frequencies ranging from 1MHz to about 300MHz. Square waves with repetition frequency of about 2.5MHz were then introduced into the circuit and the value of permittivity at frequencies up to the 50th. harmonic was measured. Next, the repetition frequency of the square wave was increased to 25MHz and similar measurements were carried out. However, as the upper frequency limit of the wave analyser available was about 300MHz, only the first 12 harmonics could be measured.

In the calculation of the permittivity of the material tested, equation 3.22a was used. However, the wave analyser could only measure the amplitude of the signal fed into the circuit. As the material under study (pure MgO) was known to be very nearly lossless, a further assumption was made i.e:

$$\frac{\epsilon''}{\epsilon'} \ll C_0 R_t \quad \text{--- eq. 5.1}$$

By using this assumption equation 3.22a can be reduced to:

$$\epsilon' = \left| \frac{V_d}{V_a} \right| \frac{1}{\left[1 + \omega^2 C_0^2 R_t^2 \left(1 - \left| \frac{V_d}{V_a} \right|^2 \right) \right]^{1/2}} \quad \text{--- eq. 5.2}$$

The results from these early measurements are presented in Fig. 5.1 and the close agreement with the expected values shows that all the parts of the system except the data acquisition section work well.

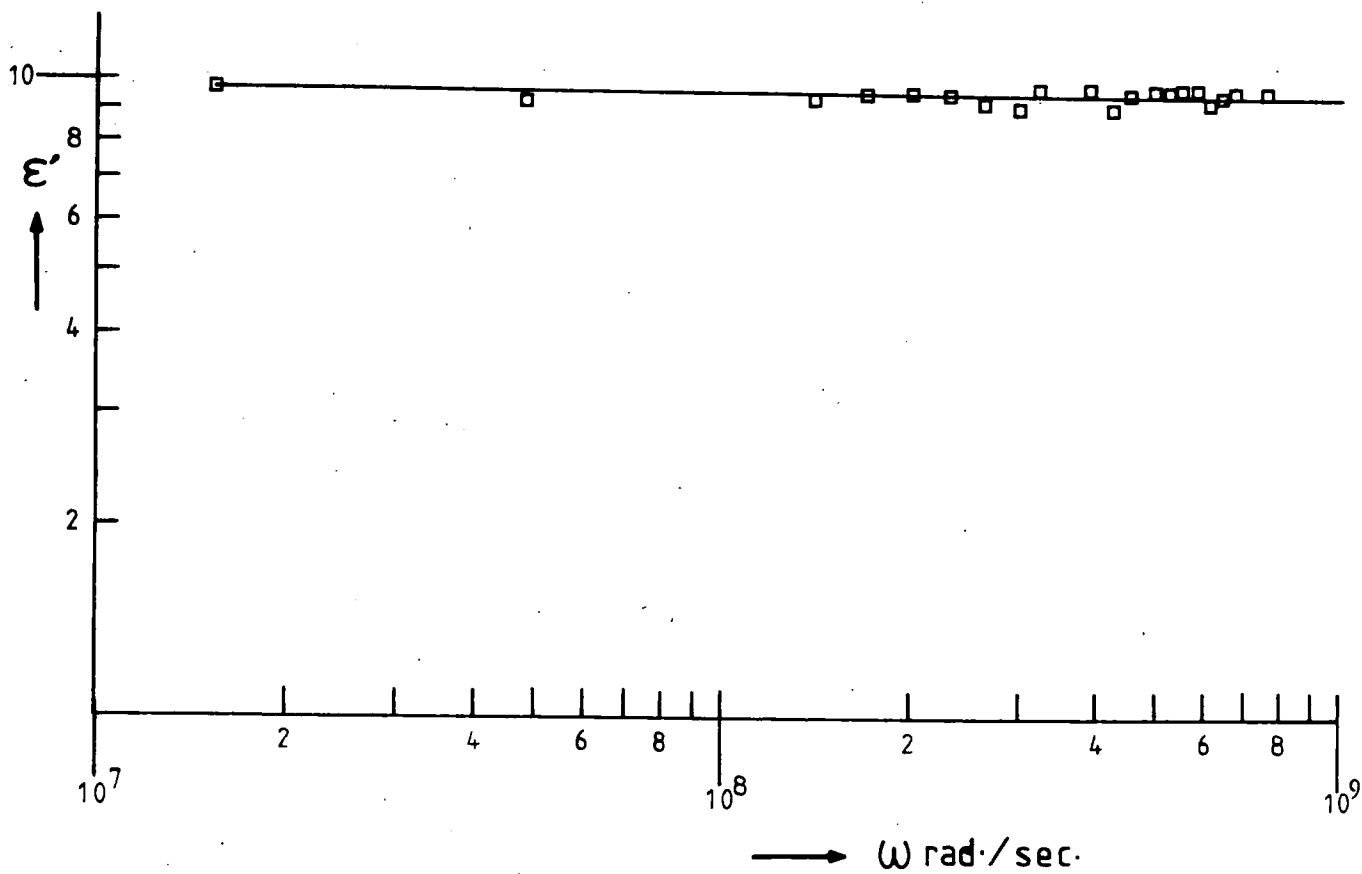


Fig. 5.1 Variation of ϵ' with ω for MgO measured

with wave analyser

5.3 RESULTS ON PURE MgO AND VITREOSIL

The close agreement between the measurements on pure MgO obtained by the early experiments using the wave analyser and the accepted values justified the assembly of the complete Fourier analysis system to measure the dielectric properties of materials. The block diagrams and detailed descriptions of each component of the system have been presented and discussed in Chapter 4. However, here the complete system was tested using two reference samples, namely pure MgO and vitreosil. Both samples were in the form of circular discs about 0.3mm. thick. It was observed that by evaporating gold electrodes on both sides of the sample, the results of the measurements give a better agreement with the standard value for the material under study.

The output waveform for an empty (air) sample-holder together with those for pure MgO and vitreosil are shown in Fig. 5.2. All the three output waveforms were Fourier analysed by the computer to give out the amplitude and phase values at each harmonic frequency. These values were then used (by the computer) to calculate the dielectric properties of pure MgO and vitreosil. The results of the final calculations are presented in Fig. 5.3, for the variation of ϵ' with frequency and in Fig. 5.4 for the variation of ϵ'' with frequency. The accuracy of the results was ± 0.5 and the n value deduced from the gradient of the log-log plot of ϵ' against frequency (for vitreosil) was 1.009 ± 0.01 . The permittivity over this frequency range measured by the Fourier technique was 3.78 and this value is in very good agreement with the reported value of 3.84. The value of dielectric loss was 0.005 ± 0.005 . For the other

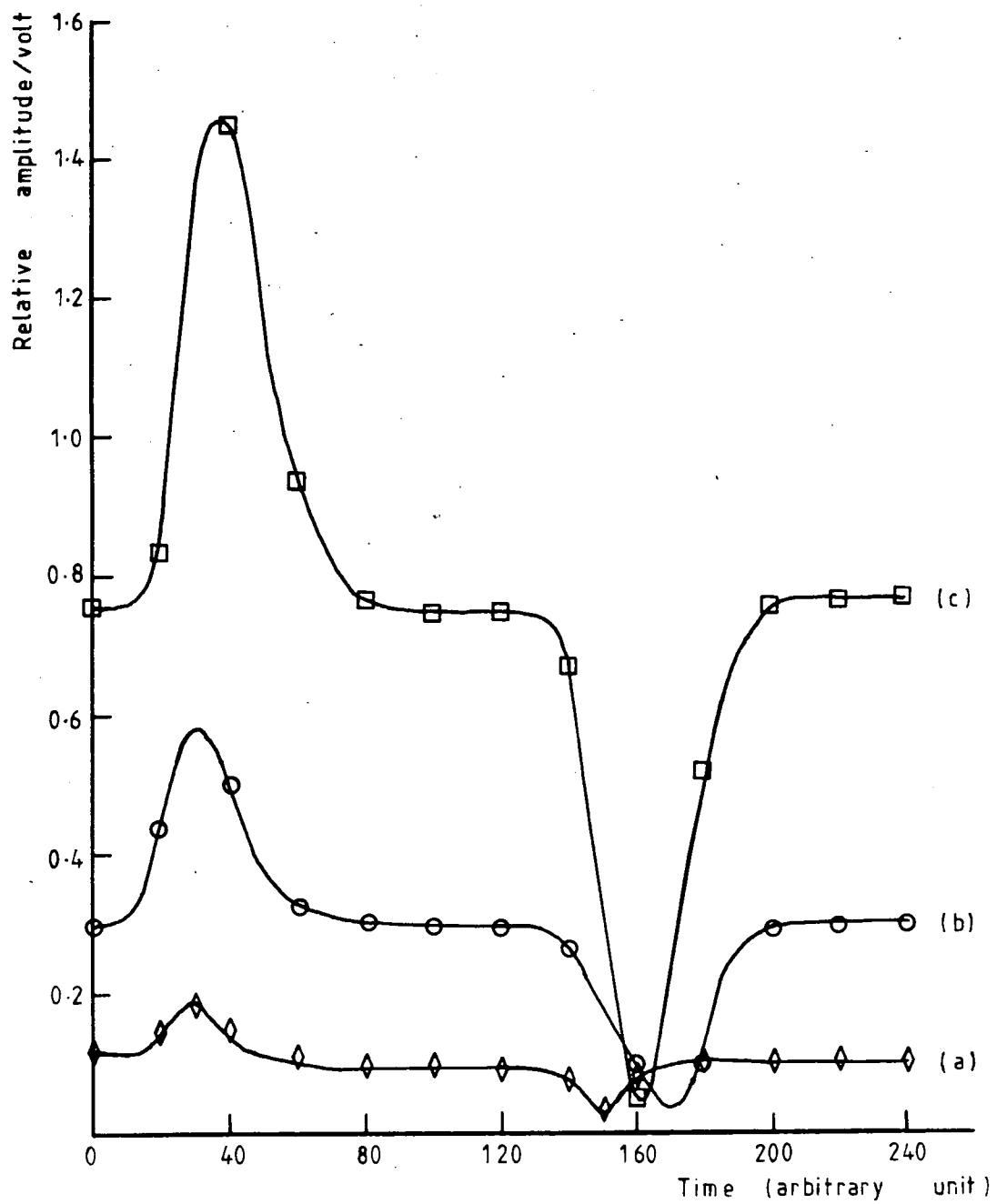


Fig. 5.2 Output waveforms for: a) Air (◇), b) Vitreosil (○) and c) pure MgO (□).

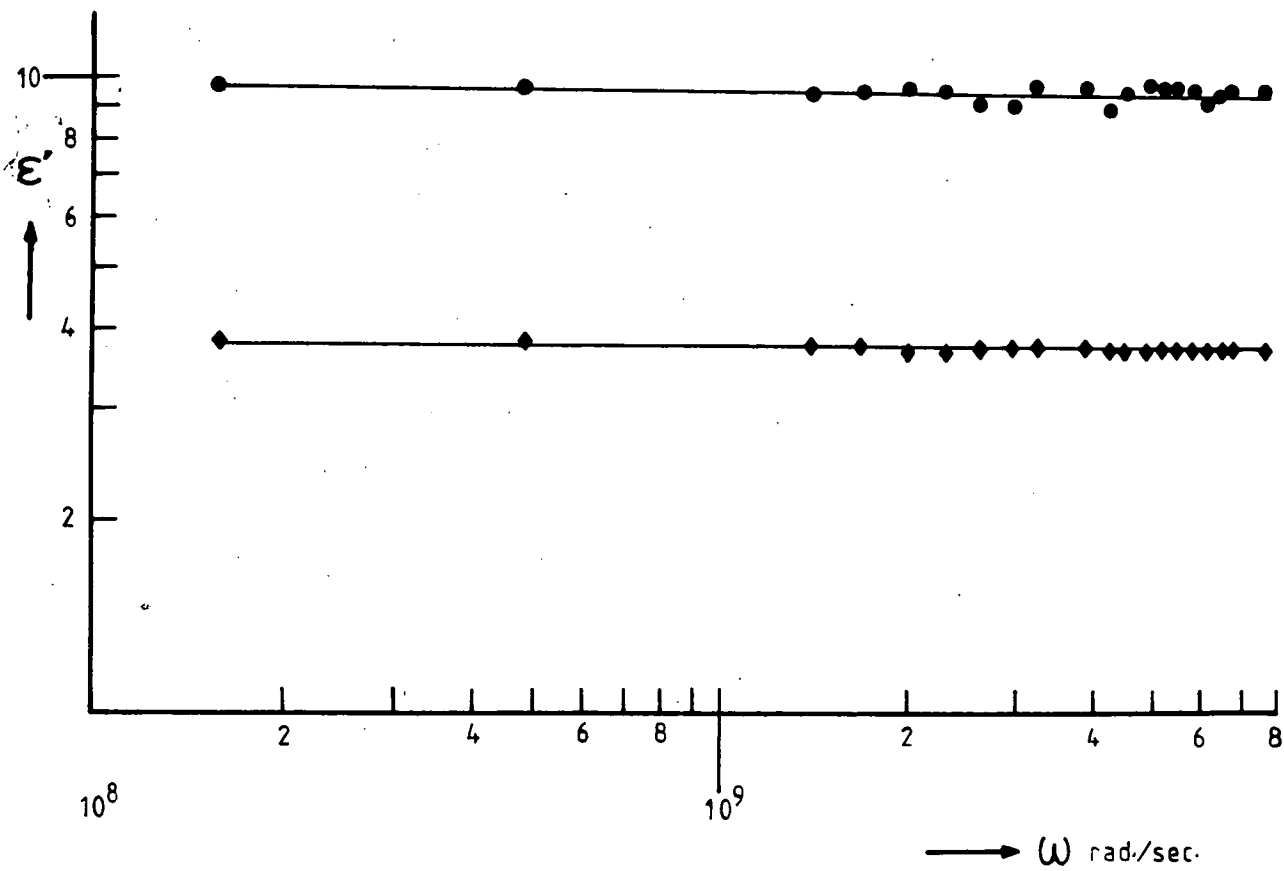


Fig. 5.3 Variation of ϵ' with angular frequency;

a) Vitreosil (♦) and b) pure MgO (●).

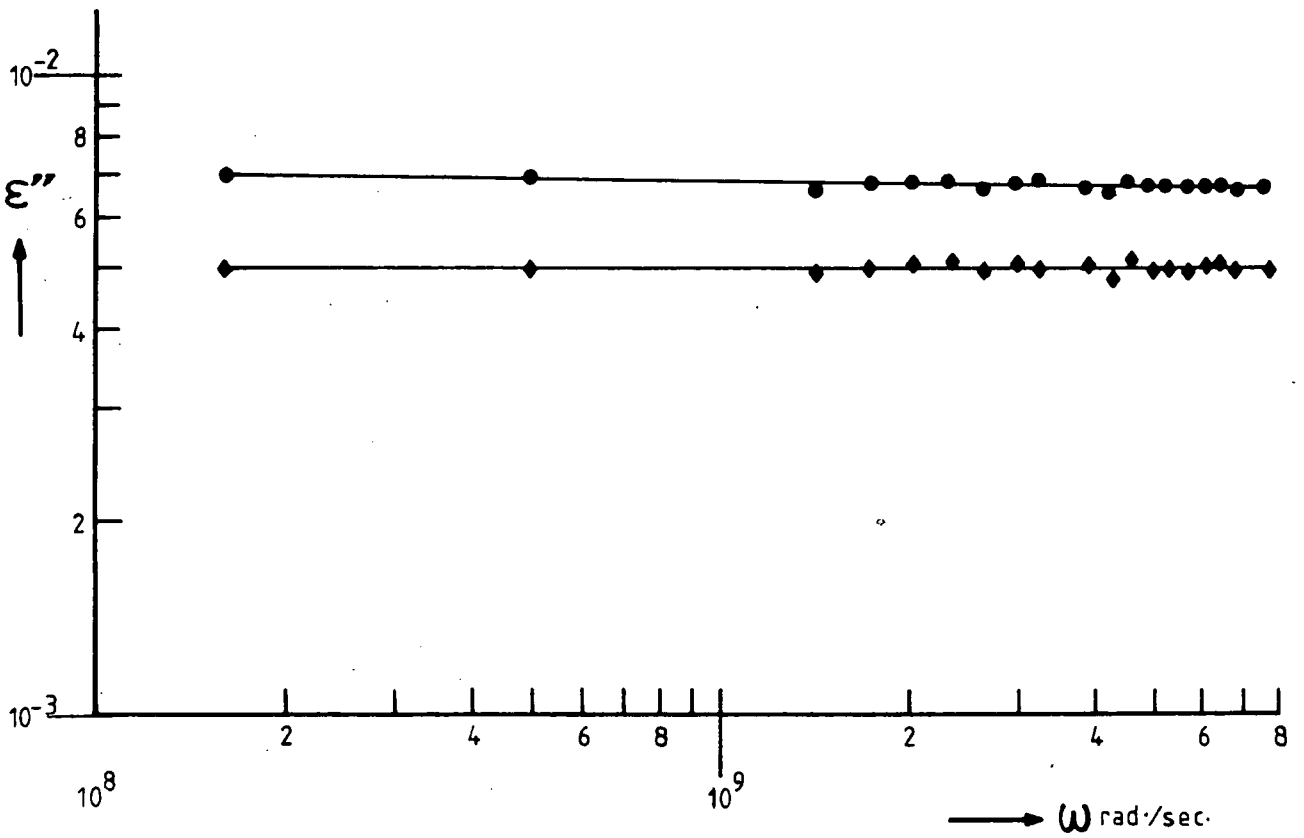


Fig. 5.4 Variation of ϵ'' with angular frequency;

a) Vitreosil (\blacklozenge) and b) pure MgO (\bullet).

material, pure MgO, the permittivity was found to be $\epsilon' = 9.55 \pm 0.5$ and the value of the dielectric loss was 0.007 ± 0.005 . The gradient n of the log-log plot was 0.98 ± 0.01 and all these values are in complete agreement with the previously reported data.

5.4 DISCUSSION AND CONCLUSION

The appraisal of this technique was carried out by transforming the time domain output signal into its equivalent frequency domain representation. This process was carried out by using a Fourier analysis method. Here the transformation was made as a means of checking the results at each harmonic frequency although the required information was in fact available in the output waveform. This process is not necessary once the validity of the technique has been established. Since all the information is contained in the output waveform it is therefore possible to obtain the parameters required just by comparing the output waveform with that of standard calculated waveforms corresponding to different sets of parameters. Thus the computer can be made to calculate all the output waveforms for different sets of values of ϵ' , ϵ'' and n and store these data points in its file. The dielectric parameters of a material can then simply be determined by comparing the output waveform, when the sample is inserted in the sample-holder, with the stored waveforms in the computer. The process of comparing the measured output waveform with the calculated one can be performed by the computer as well. Therefore the computer can be programmed to make all the calculations and comparisons and would give out the final parameters i.e ϵ' ,

ϵ'' and the gradient of the log-log plot of either ϵ' or ϵ'' with frequency. Thus, once the technique has been fully established, measurement of the dielectric properties of materials can be made with ease.

The accuracy of the measurement of ϵ'' for highly insulating material (i.e. $\epsilon'' < 0.01$) can be further improved. From the plot in Fig. 3.8 it can be seen that to measure ϵ'' in the region of 10^{-3} the data acquisition system must be able to read voltage or current differences of less than 10^{-4} volts/or amps.. The present assembly is an 8-bit system i.e the analogue-to-digital system can only read in 256 data points and it is calibrated to read in the range of ± 2 volts. However the signal can be amplified X50 by the sampling adapter. Therefore, the accuracy attainable by the present 8-bit system corresponds to 3×10^{-4} volts. A 10-bit data acquisition system (1024 data points) would be able to measure to an accuracy of about 7×10^{-5} volts; this would enhance the accuracy of ϵ'' measurements. To build a 10-bit or 12-bit data acquisition system would need a much more complex interfacing technique when using an 8-bit computer. Despite this, the system could thus be further improved and the major limitation will then become the stability of the sampling system.

It has been shown that the Fourier analysis technique enables measurements of the dielectric properties of materials to be made with ease. In addition it can provide a closed-loop system which would allow a continuous assessment of the dielectric properties of materials to be made. The method could be extended on the one hand to permit loss

measurements to be made on nearly lossless materials (an area which is difficult when using conventional techniques) and on the other hand to study lossy materials because with these the distortion of the waveform will become greater and therefore amenable to analysis.

REFERENCES

- 5.1 "A microprocessor controlled time-domain spectrometer"
B.R. Parisien and S.S. Stuchly - IEEE Trans. on Instrum.
and Meas. Vol.IM28, No.4, p269, (1979)
- 5.2 "A high sensitivity narrow band time-domain
reflectometer" - N.A.M. Mackay and S.R. Penstone
IEEE Trans. on Instrum. and Meas. Vol.IM23, No.2, p155,
(1974).
- 5.3 "Real time measurement of microwave parameters and e.m
fields" - R.J. King - IEEE Trans. on Instrum. and Meas.
Vol.IM21, Mo.1, p2, (1972)
- 5.4 "Current status of time-domain metrology in material
and distributed network research" - H.M. Cronson and
G.F. Ross - IEEE Trans. on Instrum. and Meas. Vol.IM21,
No.4, p495, (1972).
- 5.5 "Wide frequency range dielectric spectrometer"
P.J. Hyde - Proc. IEE Vol.117, No.9, p1891, (1970).
- 5.6 "A method of digital loss angle measurement"
A. Krywaznin, P. Madej and J. Ociepka - J. of Physics E,
Scientific instruments Vol.16, No.9, p823, (1983)
- 5.7 "Frequency analysis of data using a microcomputer"
F.R. Ruckdeshel - BYTE publication Inc., p11, Dec.(1979)
- 5.8 "Fourier transform of discrete data rendered
continuously by use of polynomial interpolation"
K. Watanabe, K. Shimada - E.E in Japan Vol.95, p111,(1975)

CHAPTER 6

THE CRITERIA FOR AND APPRAISAL OF THE CAVITY PERTURBATION METHOD

6.1 INTRODUCTION

The detailed derivation of the perturbation formula which gives the frequency shift has been discussed by Waldron [6.1] and others [6.2, 6.3]. By taking the frequency shift to be complex, the real part as well as the imaginary part of the dielectric parameters of the sample under study can be measured. The exact field equations can be obtained for cavities of simple shape. However if the shape of the sample is not ellipsoidal, approximations have to be made. The theoretical relationship between the frequency shifts and the properties of the material is accurate and exact. However to make full use of this inherent accuracy in measurements on a material, it is necessary to choose the size and shape (geometry) of the sample very carefully. Thus the purpose of this Chapter is to present a detailed consideration of how the accuracy inherent in perturbation formulae may be fully utilized in practice.

6.2 THE PERTURBATION FORMULAE AND THE CRITERIA

In the unperturbed state (empty cavity) Maxwell's equations are in the form:

$$\begin{aligned}\nabla \times H_1 &= \omega_1 \epsilon_1 E_1 \\ \nabla \times E_1 &= \omega_1 \epsilon_1 H_1\end{aligned}\quad \text{--- eq. 6.1}$$

where

$$\epsilon_1 = \epsilon_1' - j\epsilon_1'', \quad \mu_1 = \mu_1' - j\mu_1'', \quad \omega_1 = \omega_1' + j\omega_1''$$

and, on the introduction of the small sample (characterised by ϵ_1 and μ_1) into the cavity, the fields and the resonant

frequency are modified so that:

$$\begin{aligned}\nabla \times H_2 &= \omega_2 \epsilon_2 E_2 \\ \nabla \times E_2 &= \omega_2 \epsilon_2 H_2\end{aligned}\quad \text{---- eq. 6.2}$$

Assuming that for the empty cavity, $\epsilon_1 = 1$, $\mu_1 = 1$ and that the walls of the cavity are perfectly conducting, it can be shown [6.1] that:

$$\frac{\omega_2 - \omega_1}{\omega_1} = \frac{-(\epsilon_2 - 1) \int_{V_s} E_1 \cdot E_2 dV - (\mu_2 - 1) \int_{V_s} H_1 \cdot H_2 dV}{\int_{V_c} (E_1 \cdot E_2 + H_1 \cdot H_2) dV}\quad \text{--- eq. 6.3}$$

where

$$\omega_2 = \omega_2' + j\omega_2''$$

V_s = volume of the sample

V_c = volume of the cavity.

The real and imaginary parts of the dielectric constant and the permeability are quantities measurable in terms of the real and imaginary parts of the frequency shift, the imaginary part of the frequency shift being related to the cavity Q.

The field E in the empty cavity is presumed to be known and only the perturbed field E_2 in the sample volume V_s remains as an unknown which can be determined with knowledge of the sample's geometry and of E_1 . If the sample is such that its surface is everywhere tangential to the (unperturbed) electric field lines in the cavity, then the electric field must be continuous across the boundary. It follows [6.3] from this that, very nearly:

$$E_2 = E_1 \quad \text{--- eq. 6.4}$$

Thus for a rectangular or cubical cavity with the sample having the geometrical shape of a rod, placed as shown in

Fig. 6.1, the perturbation formulae can be worked out [6.4] and result in the expressions:

$$\frac{\Delta f}{f_0} = - \frac{2(\epsilon' - 1)V_s}{V_c}$$

and

--- eq. 6.5

$$\Delta \left(\frac{1}{Q} \right) = \frac{4\epsilon'' V_s}{V_c}$$

where

Δf = frequency shift

f_0 = resonant frequency of the unperturbed cavity.

In the literature, the criteria for the derivation of the perturbation formulae state that the radio-frequency in the cavity with and without the sample are approximately equal. Furthermore, the criteria require the changes in the stored energy in the cavity, upon introduction of the sample, to be small. These criteria are very stringent and usually violated to some extent in experiments. Spencer et. al. [6.2] showed a weaker but sufficient criterion for all commonly encountered Q-values. This criterion only requires the changes in the overall geometrical configuration of the radio frequency field be small upon introduction of the sample, i.e the energy stored in the sample should be a small fraction of the total energy stored in the cavity in the perturbed condition. Experimentally, this means that providing measurements are made with small samples only the percentage change in the real part of the frequency need be small, i.e:

$$\frac{\Delta \omega}{\omega} \ll 1$$

The range of values of $\Delta \omega$ for which the criteria for

the validity of the perturbation formulae are satisfied, have to be determined for a particular sample shape used. Here, a circular silica rod and two reference samples (magnesium oxide single crystal and vitreosil) in the form of rectangular rods have been used. By varying the length of the circular silica rod introduced into the cavity and measuring the frequency shift, the necessary experimental conditions for satisfying the criteria can then be determined. The two reference samples were then used to check the validity of eq. 6.5.

6.3 DETAILS OF MEASUREMENT TECHNIQUES

Fig. 6.1 shows the cavity and the sample arrangement for the measurement of dielectric properties at 9.4GHz . It is important that the sample can be inserted and removed from the cavity without significantly changing the Q of the unperturbed cavity. The cavity may be taken apart, the sample inserted and the cavity reassembled. This is acceptable provided that the repeated reassembly does not significantly alter the Q of the unperturbed cavity. Also, if the cavity is to be dismantled there must be no microwave current flowing in the wall across the mechanical joints otherwise the Q value obtained for the unperturbed cavity could not be regained. To overcome this problem the sample is inserted through a suitably placed hole. An ordinary silica rod was observed to shift the resonant frequency of the cavity and lowered the Q of the cavity quite significantly. However, a very thin Lindemann glass rod (of the type used in X-ray powder diffraction) when fully inserted into the empty cavity gives a frequency shift

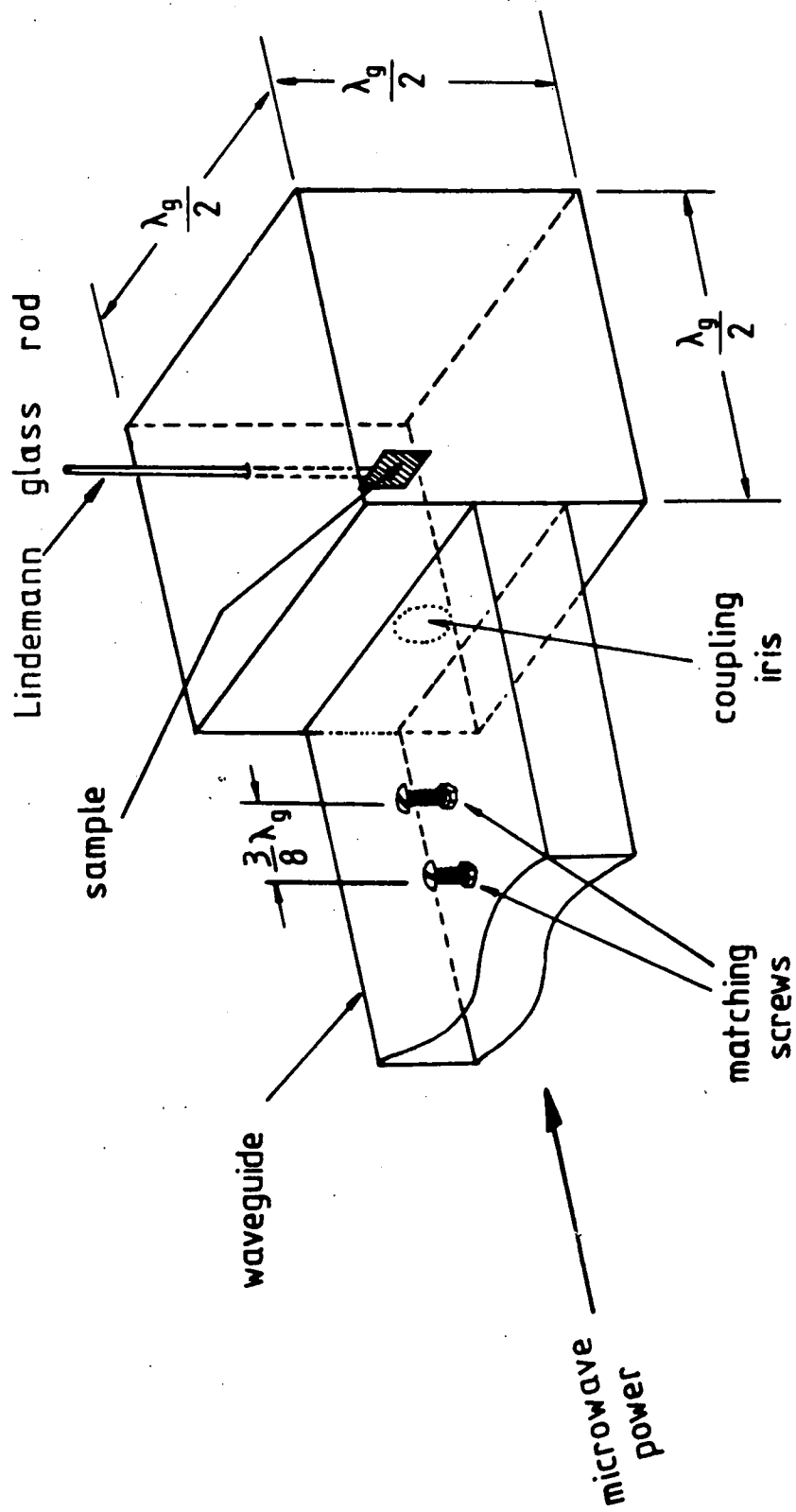


Fig. 6.1 Cavity and sample arrangement for measurement of dielectric properties at 9.34 GHz

of about 1MHz. and the Q of the cavity remained unchanged. Care has also to be taken in mounting the specimen. For example, it was found that the glue (Durofix) used previously by some other workers to stick the sample onto the glass rod was very lossy ;also the amount used had to be quite large. Here, as an alternative, vacuum grease has been used because it was discovered that only a thin layer was required and that it was virtually lossless. A micrometer is used to lower the glass rod into the cavity. This ensures that the sample under study is placed at the same position in the cavity. Only after eliminating all other factors can the changes when the sample is inserted be safely assumed to be caused by the sample alone.

Fig. 6.2 shows the block diagram of the experimental arrangement used in the cavity perturbation method. The power supply for the reflex klystron has its own modulation, therefore an external ramp generator is not required. However a dual trace oscilloscope (D66) with automatic synchronisation had to be used to obtain a stable display of both traces (incident and reflected). The arrangement consisted of the following components:

- 1) power supply with internal modulation unit,
- 2) reflex klystron,
- 3) attenuator,
- 4) isolator,
- 5) directional coupler (incident power),
- 6) directional coupler (reflected power),
- 7) cavity
- 8) attenuator

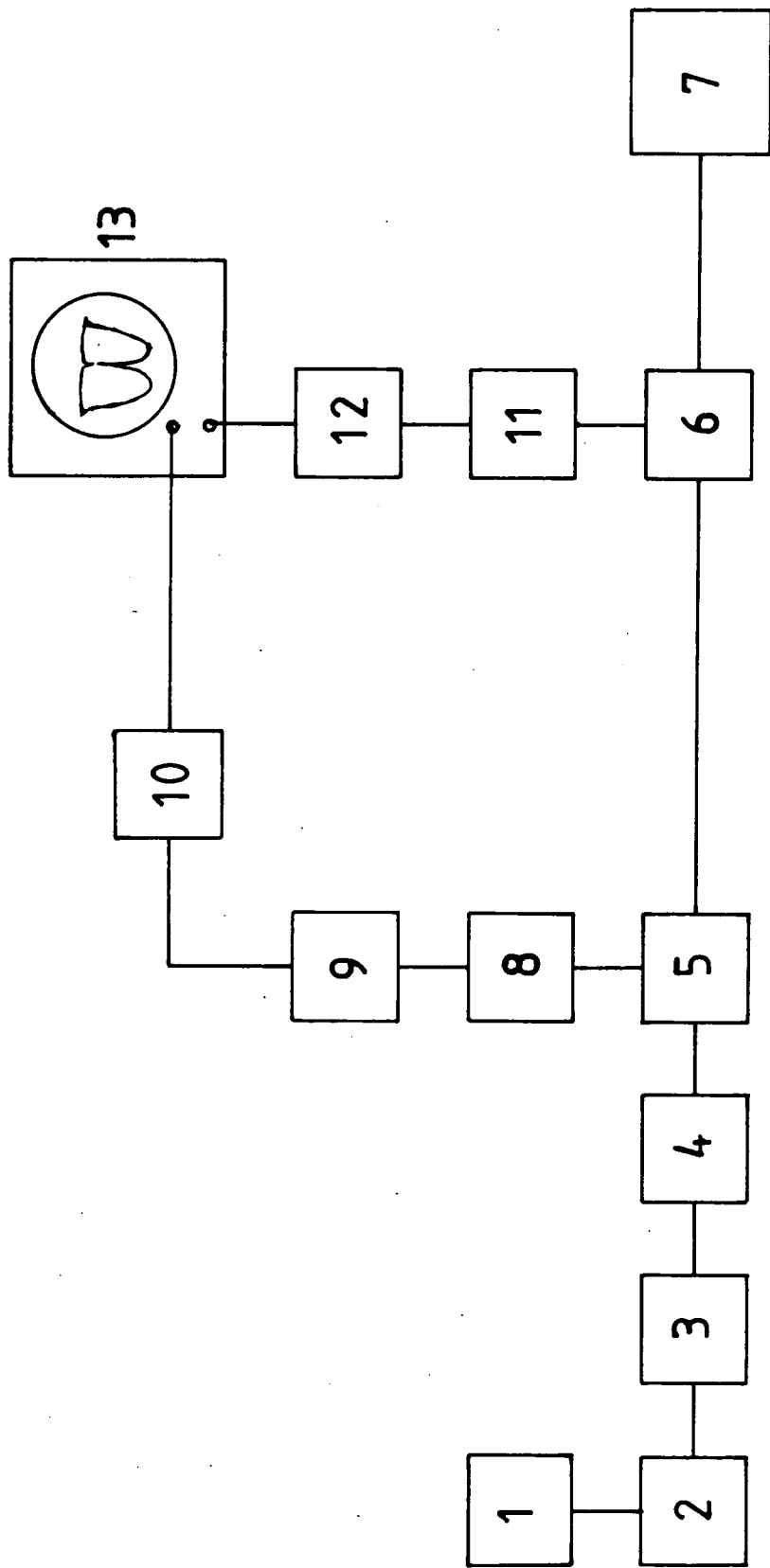


Fig. 6-2 Block diagram of experimental assembly for the cavity perturbation method.

- 9) wavemeter,
- 10) crystal detector,
- 11) attenuator,
- 12) crystal detector,
- 13) dual trace oscilloscope.

6.4 APPRAISAL OF THE METHOD

6.4.1 MEASUREMENTS OF THE FREQUENCY SHIFT USING DIFFERENT LENGTHS OF SILICA ROD

An ordinary silica rod, about 0.5mm. in diameter and about 3cm. in length was mounted on the end of the micrometer. By turning the micrometer the silica rod could be introduced by known distances into the cavity. The resonant frequency and the Q of the cavity were determined for each insertion length. Fig. 6.3 shows the plot of the length of the rod inside the cavity against the resonant frequency. Initially the Q of the cavity decreased significantly when the rod was just introduced into the cavity; further increase in length of the rod inside the cavity produced only a small further reduction in Q -value. However, it can be seen from the plot in Fig. 6.3, that the resonant frequency is directly proportional to the length of the rod inside the cavity; as the length of the rod is proportional to its volume, the frequency shift is therefore directly proportional to the volume of the rod inside the cavity.

This observation is consistent with equation 6.5, i.e when ϵ' is constant for the whole length of the silica rod, the frequency shift, Δf , is proportional to the volume of the sample, V_s . It was observed also that even when the

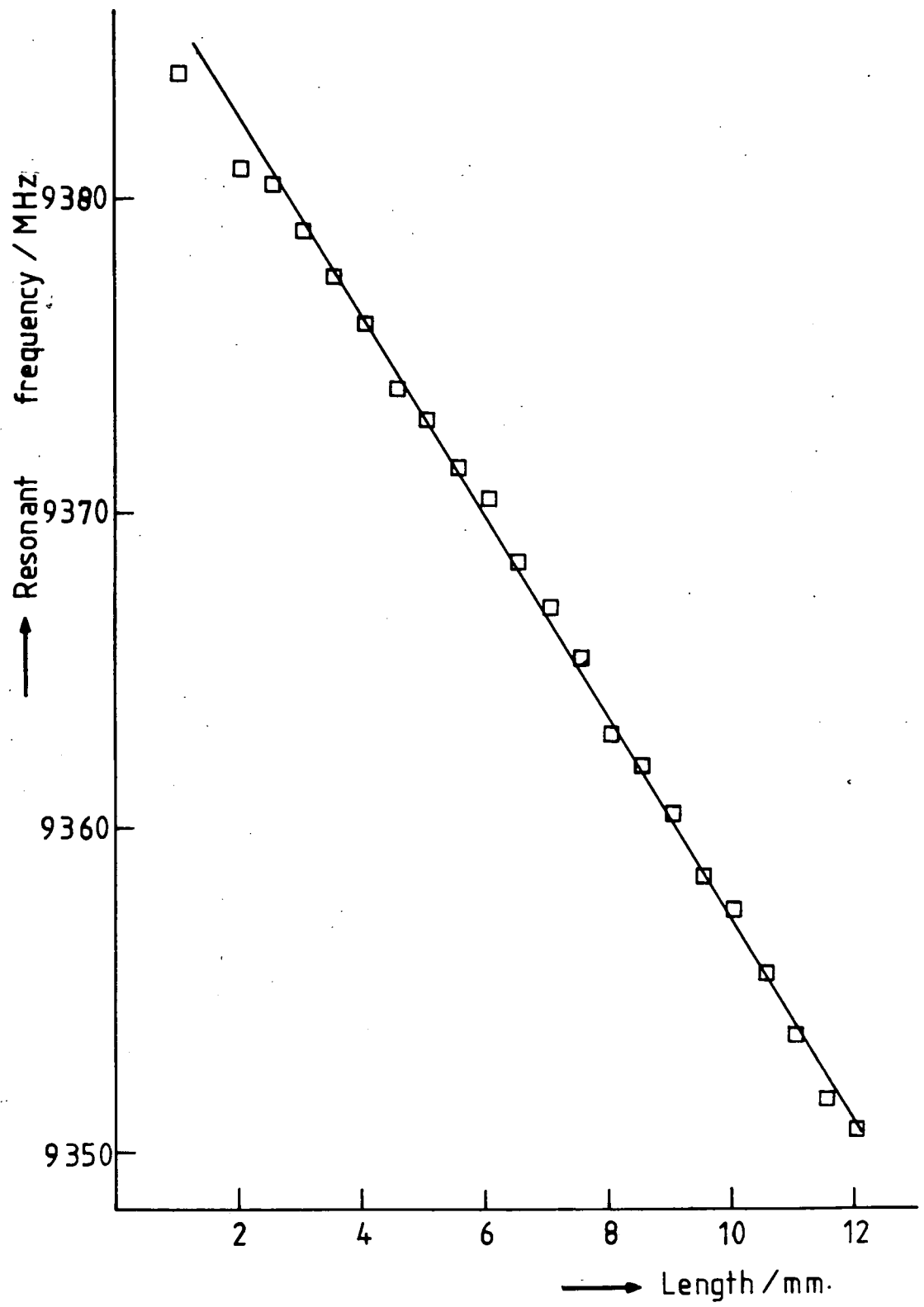


Fig. 6.3 Dependence of resonant frequency on insertion of a length of circular silica rod

frequency shift, Δf was about 40MHz, equation 6.5 still held. Therefore it can be concluded here that the perturbation formulae, or effectively equation 6.5, will hold (for a circular rod sample) if the frequency shift, Δf , is less than 40MHz. However, as a further check that equation 6.5 would give the correct dielectric parameters, two series of measurements were made with standard reference samples.

6.4.2 MEASUREMENTS WITH STANDARD SAMPLES

Two types of sample have been used, namely pure magnesium oxide single crystal (MgO) and vitreosil (SiO_2). The samples were in the form of rectangular rods (since circular rod samples were not easy to produce) and in the case of the pure MgO a number of samples with different dimensions were used. The hole that allows the sample to be inserted into the cavity is only about 2mm. in diameter, therefore the width of the samples is about 1mm. and the thickness of the samples varies from about 0.3mm. to about 0.6mm.. By varying the length of the sample, it was observed that samples having lengths of less than 5mm. (corresponding to a sample volume of less than $2 \times 10^{-9} m^3$) gave results consistent with the reported value. This is shown by Fig.6.4 in which the cavity resonant frequency is plotted as a function of sample volume. The limits below which reliable measurements may be made is shown by the vertical dotted line. Comparing the plots in Fig. 6.3 (for a circular rod) and Fig. 6.4 (for a rectangular rod) it is obvious that the sample size that can be used without violating the criteria is very limited in the case of a rectangular rod. Measurements on

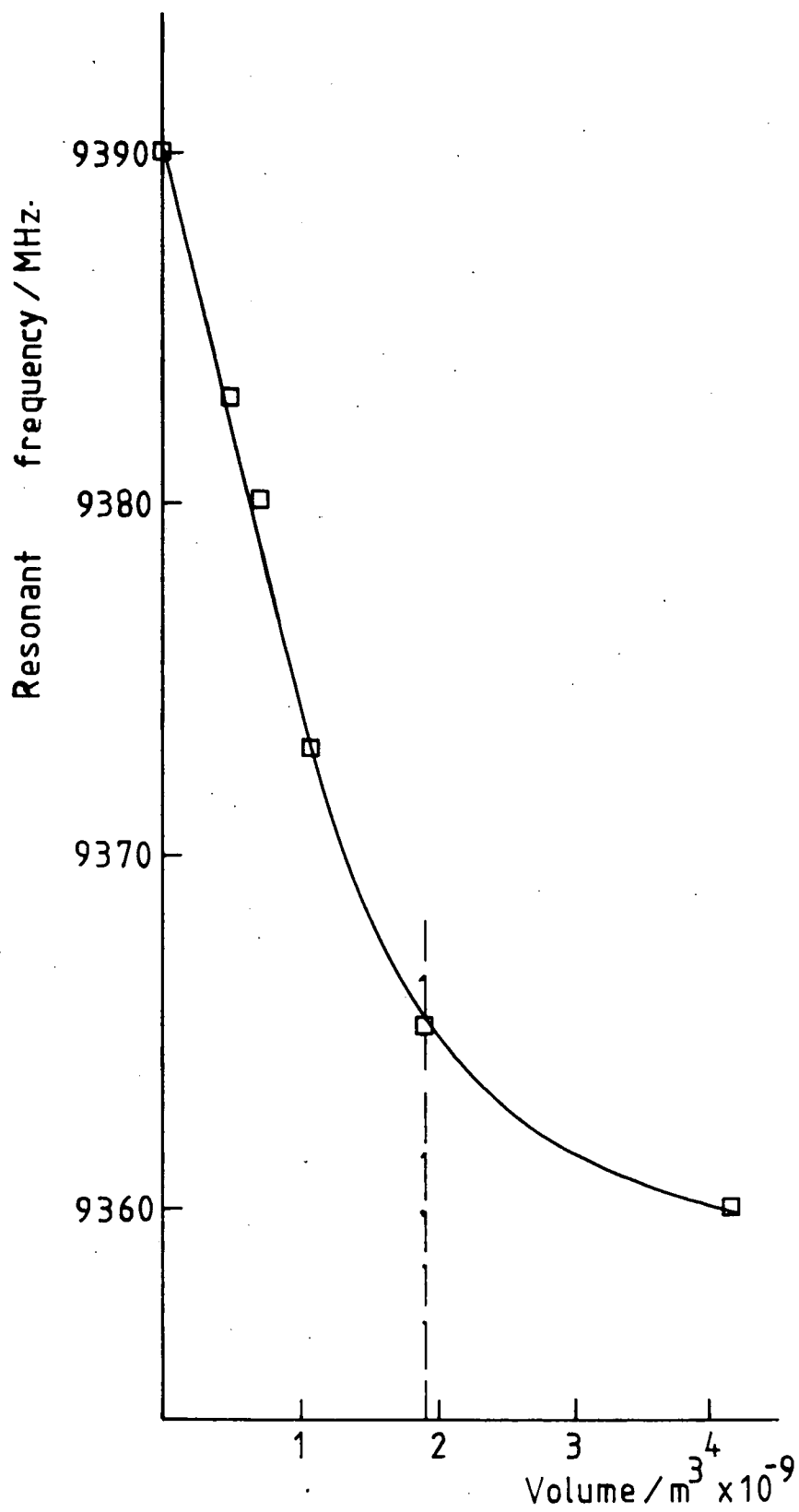


Fig. 6.4 Variation of resonant frequency with sample volume (rectangular MgO rod)

vitreosil produced results which were very consistent with the reported values, i.e the measured values for $\epsilon' = 3.759$ and that of $\epsilon'' = 5.2 \times 10^{-4}$, and the reported values are $\epsilon' = 3.84$ and $\epsilon'' < 10^{-3}$.

6.5 DISCUSSION

The frequency shift formula (eq. 6.3) is valid to a high degree of accuracy. However, the high accuracy of the formula will only be realised if the specimen shape (geometry) is suitably chosen and if the specimen is correctly placed in the cavity. The sample must be placed in a position of zero magnetic field for the measurement of the dielectric properties of the material (or similarly of zero electric field for permeability measurement). It has been shown that, for a sample in the shape of a rod (circular) placed in the cavity so that its length is parallel to the electric field, equation 6.5 will hold even for a frequency shift of about 40MHz but will not if the rod is of rectangular shape. Also, from the measurements on vitreosil, it was found that the accuracy attainable with the carefully assembled cavity perturbation method was about $\pm 2\%$ of the the reported values.

REFERENCES

- 6.1 "Perturbation theory of resonant cavities"
R.A. Waldron - The Institution of Electrical Engineers
Monograph No.373E (1960).
- 6.2 "Note on cavity perturbation theory"
E.G. Spencer, R.C. LeCraw and L.A. Ault
J. Applied Physics, Vol.28, No.1, p130, (1957).
- 6.3 "Handbook of microwave measurements - Vol.2"
M. Sucher and J. Fox - Polytechnic Institute of
Brooklyn press - Interscience publishers - Pennsylvania
(1963)
- 6.4 "A high frequency conductivity study of NiO"
S. Kabashima and S. Kawakubo
J. Phys. Soc. Jap., Vol.24, p493, (1968)
- 6.5 "On the theory of electromagnetic waves in resonant
cavities" - H.B.G. Casimir
Philip Res. Rep. No.6, p162, (1951)
- 6.6 "High frequency dielectric measurements"
G.W. Chamberlain - Science & Technology Press - London
(1967)

CHAPTER 7

PREPARATION AND GENERAL PROPERTIES OF REACTION BONDED
SILICON NITRIDE (RBSN)

7.1 INTRODUCTION

Research and extensive study on Silicon Nitride (Si_3N_4) was initiated in the early 1960s at the Admiralty Materials Laboratory in England. The interest in the ceramic is due to its many good properties which make Si_3N_4 an important technological material. Thermal shock resistance and small high temperature creep, erosion and corrosion resistance make Si_3N_4 attractive for such components of gas turbine engines as rotors, stators, heat exchangers and combustion chambers. It is replacing metal as an engineering material in high temperature applications; it has been successfully used at temperatures up to 1870°C in neutral and reducing atmospheres [7.1]. These properties, and the ability to manufacture to close dimensional tolerances without the use of expensive grinding techniques, make it suitable as an engineering ceramic that might be capable of replacing alumina as a structural material in applications for which intricate shaping and/or superior thermal shock resistance is required. Its low density ($2.3 - 2.6 \text{ g/cm}^3$) makes it useful in applications where the limitation of weight is important; a promising material for rocket nozzles. Si_3N_4 thin films are used extensively for passivation in the semiconductor industry because of their chemical stability (inertness) and high resistance to diffusion of impurities; its high electrical resistivity (about $7 \times 10^{13} \text{ ohm cm}$) makes the material a good insulator ($\text{Tan}\delta$ about $0.001 - 0.01$). Infact

the use of RBSN ceramic as a dielectric has arisen because of its potential use in radomes [7.4], an application which demands a material easy to fabricate to close dimensional tolerances, with good thermal shock resistance and acceptable dielectric properties (transparent to microwave radiation).

Much of the research on the material (RBSN) was done to explain the reaction mechanisms during the nitridation process and to establish the reaction kinetics [7.6 - 7.10]. Some aspects of the reactions are becoming generally accepted but because of the complexity of the system, particularly when considering the role of impurities in both the silicon compact and the nitriding atmosphere, full details of all the reactions are still lacking. Electrical measurements on the material (fully-nitrided) had been published [7.12 - 7.13] and some measurements on a certain range of partially nitrided RBSN have been carried out in this group [7.14], i.e from fully-nitrided RBSN (about 65% weight gain) to partially-nitrided RBSN with a weight gain of around 40%. Further measurements on the whole range of weight gain of RBSN have now been made using the newly developed Fourier method described in earlier Chapters and an improved cavity perturbation technique. It is generally accepted that poor dielectric properties are associated with incomplete nitridation and it is well known that the electrical properties of silicon are very sensitive to very small amounts of cation impurities. It is the aim of the second part of the thesis to study the role of both the unreacted silicon and other impurities in determining the dielectric properties of fully and partially nitrided RBSN.

7.2 MATERIAL PREPARATION

Crystalline Si_3N_4 exists in two hexagonal forms designated the α and β phases. There are three main methods of preparation, depending on the required usage, namely Chemical Vapour Deposition (CVD), Hot Pressing (HPSN) and Reaction Bonding (RBSN). The CVD method produces thin films suitable for use in the semi-conductor industry while HPSN and RBSN are bulk ceramics for engineering applications. Early dielectric studies on CVD-Silicon Nitride [7.15], HPSN [7.16] and RBSN [7.12 -7.14] show significant variations in dielectric properties with different methods of material preparation. To help in explaining the differences in all the measured properties, a brief description of the material preparation is necessary.

7.2.1 CHEMICAL VAPOUR DEPOSITION (CVD)- Si_3N_4

The CVD method is one of the most useful techniques for preparing Si_3N_4 thin-films, with high density and purity at relatively low temperatures (about 750°C) for use as diffusion masks or as insulators in the fabrication of semi-conductor devices. In general ($\text{SiH}_4 + \text{NH}_3$) and ($\text{SiCl}_4 + \text{NH}_3$) reactions are frequently employed for the preparation of thin Si_3N_4 films. X-ray diffraction patterns indicate that all the films are of α - Si_3N_4 type.

7.2.2 HOT PRESSED SILICON NITRIDE (HPSN)

HPSN is produced by hot-pressing (at 1700°C) Silicon Nitride powder in a graphite die at pressures between 150 - 300 MNm^{-2} . Silicon Nitride powders are usually produced by heating fine silicon powder in dry nitrogen at about 1400°C . and this produces mainly α phase powder. However HPSN

mainly contains the β structure, the α to β conversion having taken place during hot-pressing at 1700°C. HPSN ceramics usually are more dense and much less porous than RBSN ceramics and generally have greater strength. The main drawback is that the material has to be machined to produce intricate shaped objects and it has been reported [7.17] that the strength of HPSN is very temperature dependent.

7.2.3 REACTION BONDED SILICON NITRIDE (RBSN)

The fabrication of RBSN usually involves three stages, i.e. :

- 1) production of a silicon powder compact. The particle size and distribution, and the compaction operation (using pressures of about 200 MNm⁻²) each effect the final product.
- 2) Argon-sintering, i.e the compacts are heated to about 1200°C in an argon atmosphere to gain sufficient strength to withstand the machining stresses. It has been reported [7.18] that this process helps in removing the oxide layer on the silicon compact. The silicon powder compact might also be formed directly into the component shape by slip-casting, injection moulding or die casting.
- 3) Nitriding, i.e the already shaped compact is heated in nitrogen at temperatures between 1250°C and 1450°C during which the final ceramic is formed. The nitriding process generally has two stages; namely heating the compact (in a nitrogen atmosphere) at temperatures below 1350°C for a few hours to nitride the surface in order to avoid melting the entire compact (silicon melts at around 1410°C) and finally raising the nitriding temperature higher than the melting point of silicon to complete the nitridation of the inner

layer of the compact. The amount of silicon nitrided in the first stage depends on the impurities present e.g about 10% if aluminium impurities are present and about 40% if iron impurities are present [7.19]. One very important property of RBSN that makes it a very promising engineering material is that the dimensions of the compact remain unchanged (only about 1% increase) during nitridation although there is an increase of about 22% in the solid volume. Both the α and β phases are present in RBSN; the ratio of α/β depends on the nitriding conditions.

7.3 REACTION MECHANISMS OF RBSN

The choice of possible mechanisms for reaction bonding is severely restricted by the well known fact that no change in overall dimensions occurs during the process though the volume of the solid material increases by about 22%. From sintering theory, it is known that the only way to transport materials when a powder compact is heated, without changing the bulk dimensions, is by surface diffusion and evaporation-condensation. However, despite extensive study of the reaction between solid silicon and nitrogen, the mechanisms of the formation of RBSN are still not fully understood. Microstructural and thermogravimetric studies of the material have been made by many workers [7.20 - 7.22] and it has been found that the reaction kinetics for the silicon nitridation experiments are extremely difficult to control, even in high quality laboratory conditions. It has also been reported that nominally identical nitriding of nominally identical silicon compacts can result in differing degrees of silicon to silicon nitride conversion [7.23]. These differences in

nitriding kinetics are believed to be attributable to the many cation impurities such as iron, titanium, aluminium, etc. present in the silicon compact and also the impurities such as oxygen, water vapour and hydrogen in the nitriding atmosphere. It is not intended here to answer all questions but to outline some aspects of the reactions that have been generally accepted and would help to explain the dielectric results of the materials studied.

The first stage of nitridation involves heating the compact at a temperature below 1350°C in a nitrogen atmosphere for a few hours. The silicon nitride formed is generally α -phase and a detailed mechanism has been proposed by Atkinson et. al. [7.24] who suggested a sequence of events schematically illustrated in Fig. 7.1. The formation of the α -matte at the surface of the compact is from the vapour state. An inverse correlation has been made [7.10] between the nitrogen flow rate and the percentage of the α -matte in the final product; a low percentage of the α -matte can be interpreted as a result of a gaseous intermediate being swept away by the flowing nitrogen and a high percentage as a result of the gas continuing to react in stagnant nitrogen.

It has been observed [7.7] that no reaction takes place at the nitride-silicon interface. Therefore, when all the silicon surfaces are covered, the reaction must continue by outward transport of silicon through the product layer or by inward migration of nitrogen through the nitride layer. In the case of migration of nitrogen, the reaction takes place at the inner surface of the nitride layer; in the

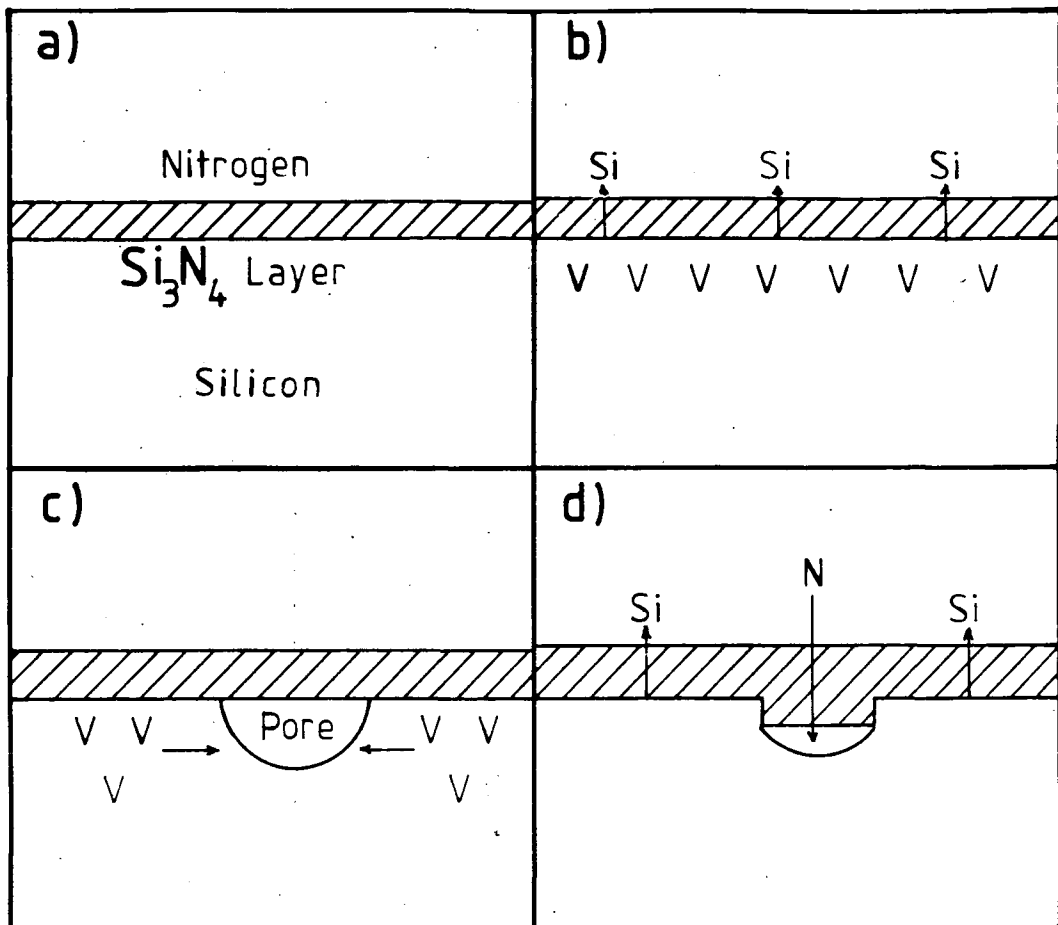


Fig. 7.1 Schematic illustration of formation of α -matte
 a) silicon is first covered with a layer of nitride,
 b) Si migrates out and leaves vacancies behind,
 c) vacancies condense to form a pore at the nitride-silicon interface,
 d) nitride grows into pore which migrates into silicon grain.

pores which are formed as a result of outward transport of silicon. In this second stage of nitridation both α and β phases are present and both usually have needle-like morphology.

The mechanisms for the formation of needles were first suggested by Gribkov et. al. [7.26] and these are illustrated in Fig. 7.2. It was proposed that the only way the needle can grow is by vapour-liquid-solid (VLS) mechanisms and the beads at the termini of some needles often contain impurities which can lower the melting point of silicon. Many needles, however, have no beads attached to their ends but are attached to larger grains. The same formation mechanisms could take place if a pool of liquid were to form on the surface of a large silicon grain and serve as the liquid in the VLS mechanism. This is illustrated in Fig. 7.3. The formation of β needles is illustrated in Fig. 7.4; the β -structure has hexagonal tunnels (1.5\AA) [7.10, 7.27] running in the c direction which will allow the nitrogen through to the reaction site.

The impurities present in the silicon compact and in the nitriding atmosphere play important roles in the nitridation process. The roles of iron impurities, resulting from the machining process, have been studied by many workers [7.8, 7.19, 7.27, 7.28]. Iron appears to serve two important functions:

- 1) devitrification of the silicon surface, i.e to initiate and maintain the open channels (pores) allowing access between the nitrogen and silicon.

- 2) it lowers the melting temperature of silicon by forming

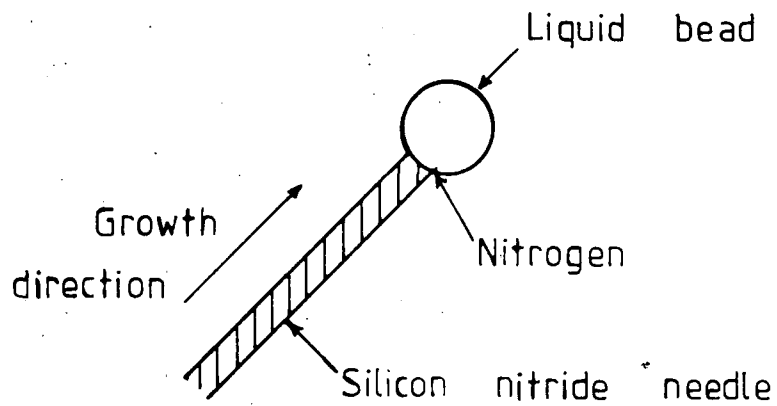


Fig. 7.2 Schematic drawing showing growth of α -needles (with bead) by V-L-S mechanism.

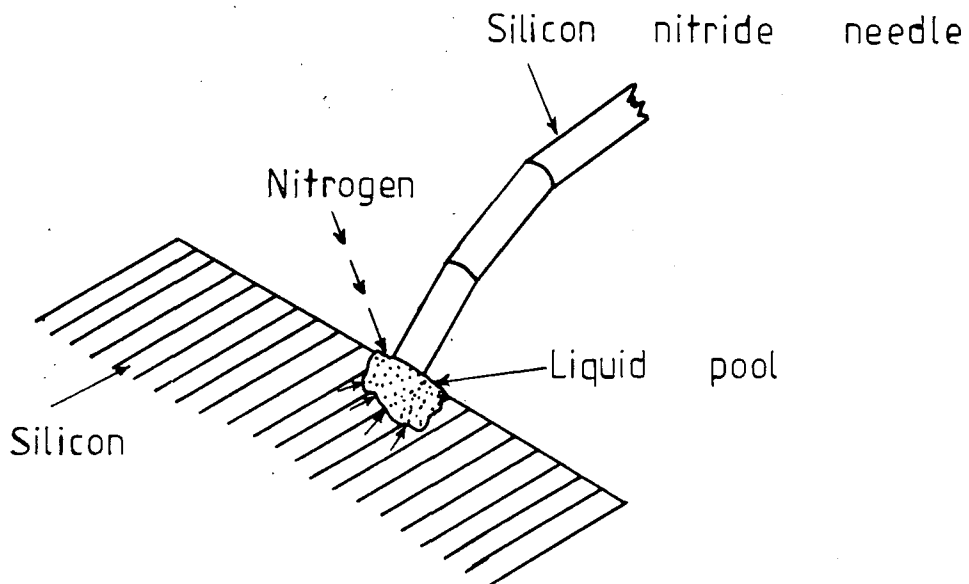


Fig. 7.3 Schematic illustration showing possible mechanism for formation of α -needle (without bead) with liquid phase on surface of silicon grain.

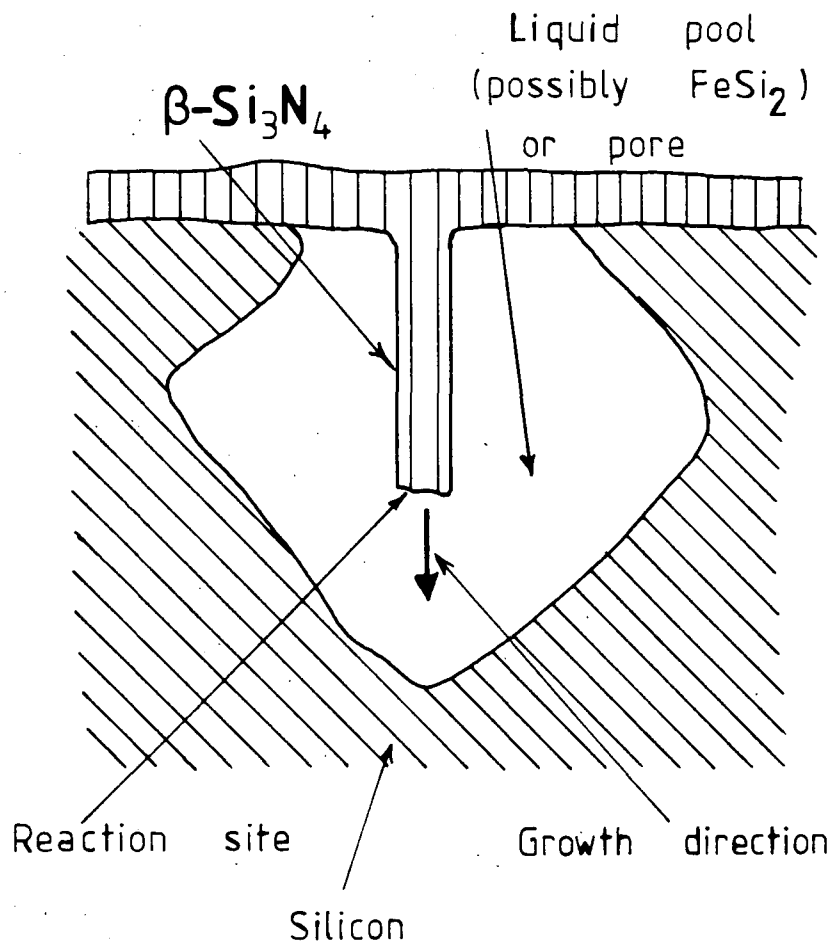


Fig. 7.4 Schematic illustration showing possible mechanism for formation of β -needle. It either grows as nitrogen diffuses to the reaction site through liquid silicon, or it grows into a clean pore as nitrogen slowly diffuses down its length. In the first case the crystal is large and in the second it is small.

Fe-Si liquid phase at a temperature (1208°C) which is lower than the melting point of silicon (1410°C). The liquid phase causes formation of needle-morphology by the VLS mechanism. Messier and Wong [7.11] observed the catalytic acceleration of the nitridation reaction by the addition of Fe and attributed this to the formation of Fe-Si melt.

Mitomo [7.19] reported that aluminium impurities enhance the formation of β phase while Mukerji and Biswas [7.27] found that titanium forms an interstitial compound at 1400°C whose composition varies from $\text{TiN}_{0.6}$ to $\text{TiN}_{1.0}$.

The reaction mechanism for the nitridation of silicon is complex and it was not the intention to present an exhaustive survey of the whole process. Two review papers by Moulson [7.9] and Jennings [7.6] cover most aspects of the reaction mechanisms.

7.4 THE RBSN SAMPLES STUDIED

The RBSN ceramics studied in the present work were supplied by AME Ltd. (Gatehead) and details of their fabrication are described by Bushell [7.30]. The weight gains of the samples used cover the whole range; i.e from 0% (totally unreacted silicon) to 64.5% (fully nitrided). The theoretical maximum weight gain should be 66.5% but in practice this cannot be achieved for two reasons; the presence of small amounts of unreacted free silicon due to incomplete nitridation and secondly volatilization of silicon during nitridation as observed by Messier and Wong [7.11]. Samples with different weight gains have varying percentages of porosity and unreacted free silicon, and the phase compositions for each sample may be calculated using the

following equations [7.9]:

$$C_p = 1 - .281\rho_g - .148\rho_n$$

$$C_{Si} = 1.072\rho_g - .643\rho_n$$

$$C_{Sn} = .791(\rho_n - \rho_g)$$

where C_p , C_{Si} and C_{Sn} are respectively the volume fractions of porosity, silicon and silicon nitride in a nitrided compact, and ρ_n is the density of the green compact while ρ_g refers to the nitrided material. Values of the various volume proportions for the samples studied are shown in Table 7.1.

The samples were cut and polished according to the requirements of the techniques used. For the Fourier analysis technique the samples are in the form of circular discs about 0.3mm thick and 7mm in diameter. Samples for the cavity perturbation method have two sizes depending on how the material disturbs the Q-curve of the cavity. For insulating samples (64.5% - 58% weight gain) the sample is in the form of a rectangular slice of dimensions approximately 0.3mm by 1.5mm by 5mm and for lossy samples (weight gain less than 58%) the dimensions are 0.3mm by 1.5mm by 3mm. Samples for the Fourier analysis method have to be polished whereas this is not necessary for the samples used in the cavity perturbation method.

For the structural and microstructural study two sets of samples were mainly used; namely those with weight gain of 44.44% and 6.5%. For the X-ray diffraction study the same samples used in the cavity perturbation technique were used. Samples studied using electron diffraction and Scanning

	Weight Gain (%)	Nitrided Density (g/cm ³)	Green Ceramic Density (g/cm ³)	Phase Composition			Peak Firing Temperature (°C)
				C _{Sn}	C _{Si}	C _P	
1	64.5	2.52	1.53	.783	.02	.197	1440
2	59.33	2.42	1.60	.649	.159	.192	1440
3	58.27	2.40	1.60	.633	.172	.195	1440
4	49.19	2.27	1.60	.530	.256	.214	1440
5	47.9	2.32	1.60	.570	.223	.207	1370
6	44.08	2.28	1.60	.538	.249	.213	1340
7	42	2.26	1.60	.522	.262	.216	1340
8	39.18	2.11	1.60	.403	.358	.238	1150
9	35.6	2.06	1.60	.364	.391	.245	1150
10	22.49	1.84	1.60	.190	.532	.278	1250
11	0						

Table 7.1 Preparation and composition data for the Si₃N₄ used.

Electron Microscope (SEM) techniques were etched either with hydroflouric acid (HF) or hot phosphoric acid (H_3PO_4). Fracture surfaces were also used for the SEM study.

REFERENCES

- 7.1 "The preparation, properties and structure of Silicon Nitride" - P. Popper and S.N. Ruddlesden
British Ceramic Association, Vol.60, p603, (1961)
- 7.2 "Structure of the nitrides of Silicon and Germanium"
P. Popper and S.N. Ruddlesden
Nature - Vol.180, p1129, (1957)
- 7.3 "Crystal structure of Silicon Nitride" - D. Hardie and
K.H. Jack - Nature - Vol.180, p333, (1957)
- 7.4 "RBSN for high temperature radome applications"
J.D. Walton Jr. - Amer. Ceram. Soc. Bull., Vol.53, p255,
(1974)
- 7.5 "Silicon Nitride as a dielectric material : A short
review" - B. Swaroop - Proc. Inter. Conf., Mater. Tech.
p224, (1975)
- 7.6 "Review - On reactions between silicon and nitrogen.
Part 1 - Mechanism" - H.M. Jennings
J. Mat. Science, Vol.18, p951, (1983)
- 7.7 "A mechanism for the nitridation of silicon powder
compacts" - A. Atkinson, P.J. Leatt, A.J. Moulson,
E.W. Roberts - J. Mat. Science, Vol.9, p981, (1974)
- 7.8 "A mechanism for the nitridation of Fe-contaminated
silicon" - S.M. Boyer and A.J. Moulson
J. Mat. Science, Vol.13, p1637, (1976)
- 7.9 "Review - RBSN : Its formation and properties"
A.J. Moulson - J. Mat. Science, Vol.14, p1017, (1979)

- 7.10 "Structure, formation mechanisms and kinetics of RBSN"
H.M. Jennings and M.H. Richman
J. Mat. Science, Vol.11, p2087, (1976)
- 7.11 "Kinetics of nitridation of Si powder compacts"
D.R. Messier and P. Wong - J. of the American Ceramic
Society, Vol.56, No.9, p480, (1975)
- 7.12 "Silicon nitride as a high-temperature radome material"
W.M. Wells - Reference UCRL 77 95, (1964)
- 7.13 "Microwave dielectric properties of silicon nitride"
G.S. Perry and T.R. Moules - Proc. 12th. Symp.
Electromag. Windows, Georgia Inst. Tech., J.N. Harris
(Ed.), (1966)
- 7.14 "Improved wideband coaxial methods for dielectric
measurements on nitrogen ceramics" - A.B. Ahmad
Ph.D. Thesis, University of Durham, (1983)
- 7.15 "Electrical conduction and breakdown properties of
silicon nitride films" - D. Mangalaraj, M. Radhakrishnan
and C. Balasubramaniam - J. Mat. Science, Vol.17,
p1474, (1982)
- 7.16 "Electrical properties of Hot Pressed Nitrogen Ceramics"
R.I.Sharif - Ph.D. Thesis, University of Durham, (1977)
- 7.17 "Microstructural studies on Silicon Nitride"
A.G. Evans and J.V. Sharp - J. Mat. Science, Vol.6,
p1292, (1971)

- 7.18 "The removal of surface silica and its effect on the nitridation of high purity silicon" - M.N. Rahaman and A.J. Moulson - J. Mat. Science, Vol.19, p189, (1984)
- 7.19 "Effect of Fe and Al additions on nitridation of silicon" - M. Mitomo - J. Mat. Science, Vol.12, p273, (1977)
- 7.20 "Microstructural changes during the argon sintering of silicon powder compacts" - P. Arundale and A.J. Moulson J. Mat. Science Letters, Vol.12, p2138, (1977)
- 7.21 "Handbook of Electronic Materials : Volume 3
Silicon Nitride for microelectronic applications.
Part 1 : Preparation and properties" - J.T. Milek
IFI/Plenum, N.York, Washington, London, (1971)
- 7.22 "Flouride accelerated nitridation of silicon"
D. Campos-Loriz, S.P. Howlett, F.L. Riley, F. Yusof
J. Mat. Science, Vol.14, p2325, (1979)
- 7.23 "Strength, density, nitrogen weight gain relationship for RBSN" - B.F. Jones and M.W. Lindley
J. Mat. Science, Vol.10, p967, (1975)
- 7.24 "Nitridation of high purity silicon" - A. Atkinson, A.J. Moulson, E.W. Roberts - J. of American Ceramic Society, Vol.59, No.7, p285, (1976)
- 7.25 "D.C. electrical conductivity of amorphous silicon nitride-C composite prepared by CVD" - T. Goto and T. Hirai - J. Mat. Science, Vol.18, p383, (1983)

- 7.26 "Growth mechanism of silicon nitride whiskers"
V.N. Gribkov, V.A. Silaev, B.V. Sheetanov, E.L. Umantsev,
A.S. Isaikin" - Soviet Physics - Crystallography,
Vol.16, No.5, p852, (1972)
- 7.27 "Effect of iron, titanium and hafnium on second stage
nitriding of silicon" - J. Mukerji and S.K. Biswas
J. of American Ceramic Soc., Vol.64, No.9, p549, (1981)
- 7.28 "The combined effects of Fe and hydrogen on the
nitridation of silicon" - N.J. Shaw - J. Mat. Science
Letters 1, p337, (1982)
- 7.29 "The electronic structure of silicon nitride"
R.J. Sokel - J. Phys. Chem. Solids, Vol.41, p899, (1980)
- 7.30 "Some properties of Reaction Bonded Silicon Nitride"
T.G. Bushell - Ph.D. Thesis, University of Durham,
(1983)

EXAMINATION OF FULLY NITRIDED RBSN

8.1 INTRODUCTION

Fully nitrided RBSN is known to have good insulating properties and can be measured by most dielectric measuring techniques but partially nitrided RBSN has varying values of dielectric constant and loss tangent, and some techniques fail to measure the dielectric properties because the equivalent circuit assumed for the particular technique becomes invalid. The fact that RBSN changes its dielectric properties with weight gain makes it a good material to test the newly developed Fourier technique. However documentation of the dielectric properties of partially nitrided RBSN is not available. Although a number of publications [8.1 - 8.4] are available for the dielectric properties of fully nitrided silicon nitride, the values quoted vary from 4 to 12. It was accepted that different methods of preparation of silicon nitride would produce samples with different values of dielectric constant. The variations have always been suggested to be due to the free (unreacted) silicon present and the porosity of the sample. However, it is proposed here that impurities make a significant contribution to the dielectric properties of RBSN and must be considered in the analysis of the dielectric study.

Two techniques are use for the dielectric measurements; namely the Fourier analysis technique that covers the range of frequencies from 25MHz, to about 1GHz and the cavity perturbation technique, working at about 9.4GHz . The output

waveform when the sample is inserted in the sample holder is presented for the Fourier method and the dielectric parameters are obtained by comparing the waveform with the theoretically calculated waveforms stored in the computer. The dielectric parameters are plotted against harmonic number (frequency) showing their variation with frequency; the cavity perturbation results give the values at 9.4GHz and thus extend the range of measurements.

8.2 DIELECTRIC MEASUREMENTS

Fig.8.1 shows the output waveform when the fully nitrided RBSN (64.5% weight gain) is inserted in the sample holder (As described in detail in Chapter 3, the input waveform was the standard square-wave signal at 25MHz). The output waveforms for vitreosil and pure MgO are also included in Fig.8.1 to show the differences in the output waveforms for these three materials. Fig.8.2 is a log-log plot of the permittivity against harmonic number (frequency); obtained by comparing the observed output waveform with the range of theoretical waveforms stored in the computer. The theoretical waveforms are obtained by taking different pairs of values of ϵ' and ϵ'' . Here the conduction mechanism is known to be hopping. The data point for the cavity perturbation method is included to cover the frequency range up to about 9.4GHz . The value of the permittivity measured by the Fourier analysis technique is virtually frequency independent and has the value 6.0 ± 0.5 and that measured by the cavity perturbation technique is 5.50 ± 0.05 . The gradient of the log-log plot of the permittivity against frequency is 0.97 ± 0.03 . In the frequency range of 500MHz to about 7GHz data points from

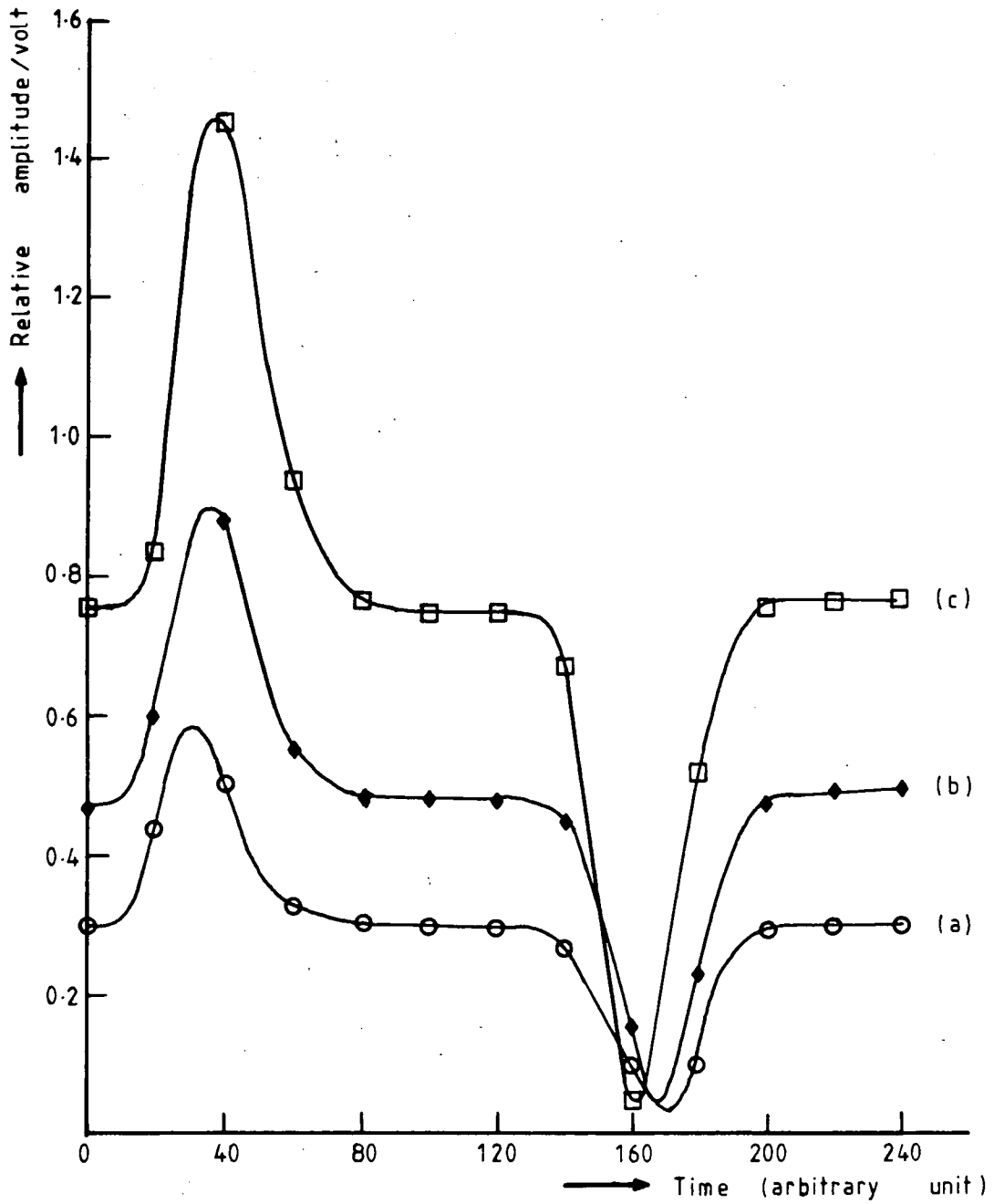


Fig. 8.1 Output waveforms for: a) Vitreosil (○),
 b) 64.5% weight gain RBSN (◆) and c) pure MgO (□)

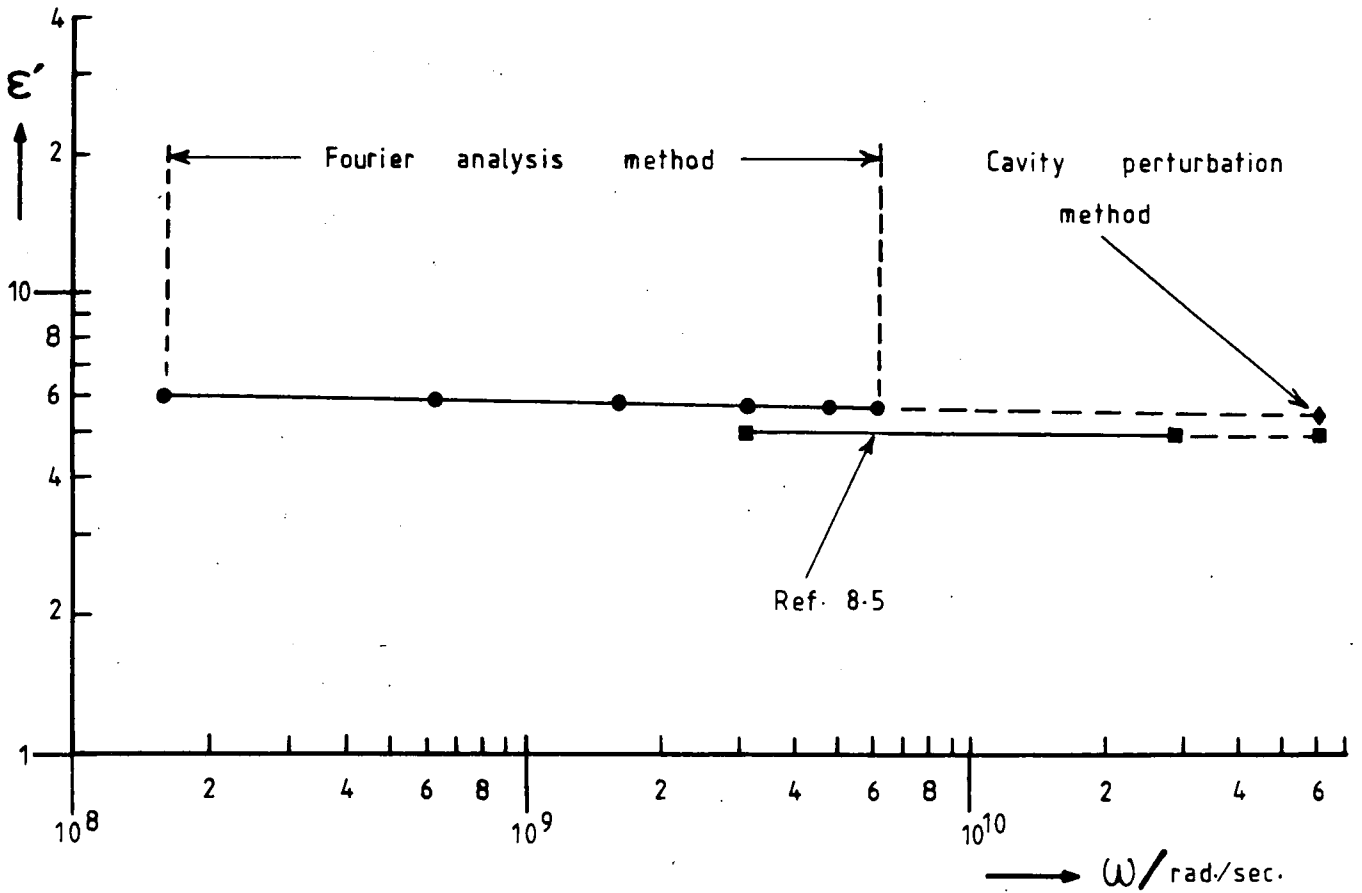


Fig. 8.2 Variation of permittivity with angular frequency for fully nitrated (64.5% weight gain) RBSN.

measurements made by Ahmad [8.5] are included as a comparison and to cover the whole range of frequencies from 25MHz. to 9GHz.. Although the range of frequency covered in the Fourier analysis technique is not the same as that of the short circuit and resonant circuit method used by Ahmad, the small differences in the results are within experimental error; the fact that the n value for the material studied is close to unity makes the variation of the dielectric properties with frequency very small. Thus the present data and the previous work done by Ahmad make a fair comparison.

Fig.8.3 shows the log-log plot of the loss factor, ϵ'' , of 64.5% weight gain RBSN against harmonic number (frequency). The value of the loss factor measured by the Fourier method is 0.015 ± 0.005 and that measured by the cavity perturbation method is 0.01 ± 0.001 . These values agree with that of Ahmad.

The data given in Fig.8.1, 8.2 and 8.3 all refer to the bulk 64.5% weight gain RBSN sample. However the sample is known to contain voids and some free (unreacted) silicon (see Table 7.1) and is also likely to contain other impurities originating from the starting (Si) powder. Corrections for all these items are necessary if one wishes to obtain a meaningful value of permittivity for pure RBSN suitable for example, for comparison with the thin film (CVD) optical measurement data. These correction methods are considered below.

8.3 ANALYSIS OF BULK CERAMIC PERMITTIVITY RESULTS

The RBSN sample studied has a total porosity of approximately 20% (Table 7.1), and there is a fine dispersion of unnitrided material distributed throughout the ceramic.

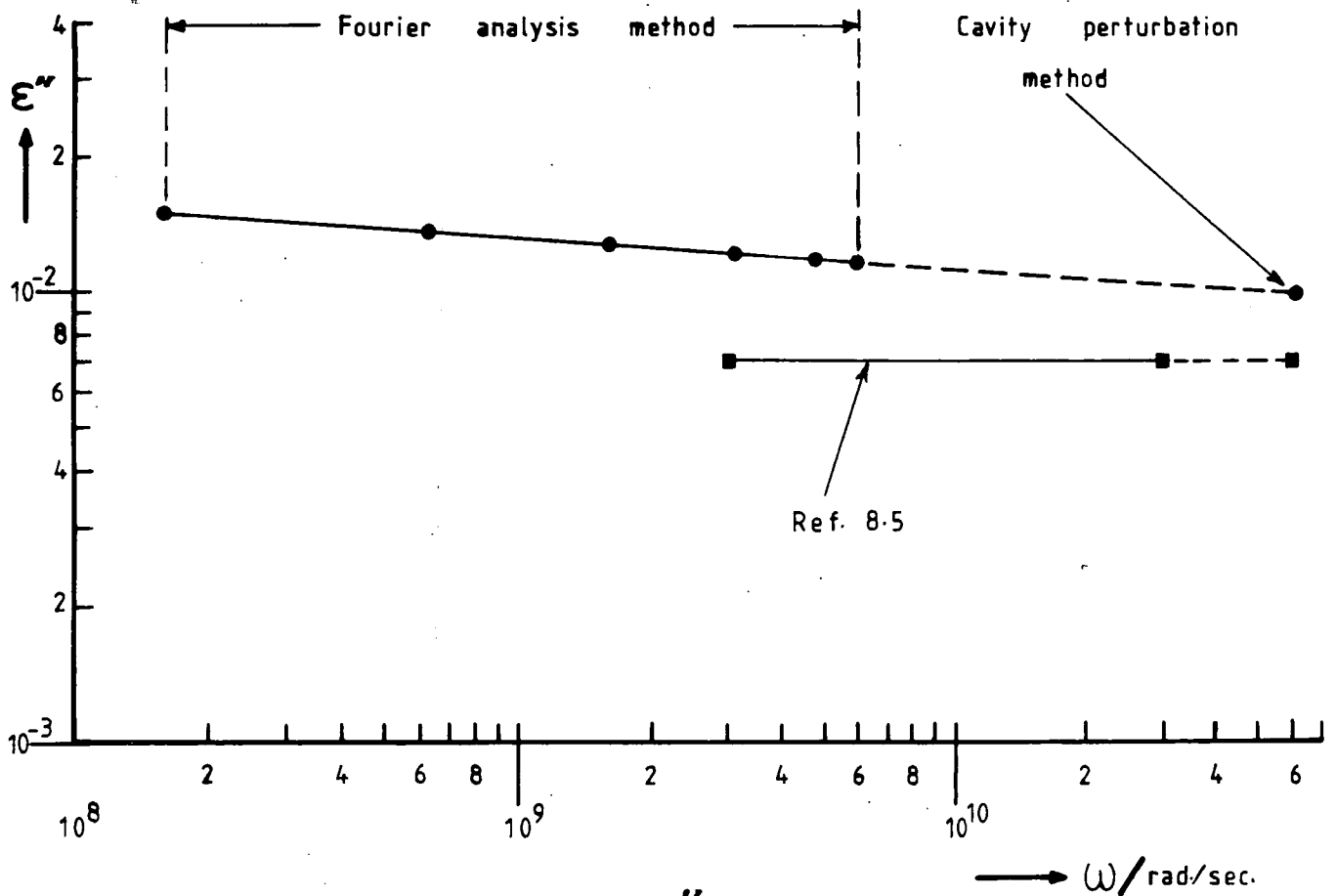


Fig. 8.3 Variation of ϵ'' with angular frequency
for fully nitrated (64.5% weight gain) RBSN

The unnitrided material is usually referred to as 'silicon' but may, at least in part, comprise alloys of silicon with iron and, possibly, other cation impurities associated with the starting silicon powder. Thus the measured parameters are values for the heterogeneous (multi-phase) material. To obtain the true value of permittivity for silicon nitride alone, the contribution from other phases must be deducted from the measured value. Walton [8.1] in his permittivity measurements of RBSN only took into account the effect of porosity present in various samples and calculated his data using the formula:

$$\epsilon = \epsilon_0^{1-p} \quad \text{--- eq. 8.1}$$

where ϵ_0 is the permittivity of the 100% (without pores) dense material and p is the volume fraction of pores.

Walton's measured values; i.e. $\epsilon' = 5.50$ and $\text{Tan}\delta = 0.002$ for samples with porosity around 20%, agree with the present measurements. To repeat the same calculations is insufficient here, because it is thought that taking only porosity into account in treating the results is not enough. The contribution of the so-called 'silicon' must be considered here.

The starting point of this treatment is to assume that the RBSN sample studied is a multi-phase composite material, comprising silicon nitride, voids, unreacted silicon and other impurities (existing most probably as alloys with silicon). Methods of treating composite dielectric materials are given in a review paper on physical properties of composite materials by Hale [8.7] who gives various formulae to calculate the dielectric properties. For the purpose of

treating the present results, one of the appropriate methods is that given by Wiener. This has been chosen for its simplicity and because its upper and lower bounds are the extremes of all the other formulae; i.e calculation using other formulae will give results within the Wiener upper and lower bounds. The Wiener formulae for the permittivity of a composite material are :

$$\epsilon_+ = \epsilon_1 V_1 + \epsilon_2 V_2 + \dots + \epsilon_r V_r + \dots \quad \text{--- eq. 8.2}$$

$$\epsilon_- = \frac{1}{V_1/\epsilon_1 + V_2/\epsilon_2 + \dots + V_r/\epsilon_r + \dots} \quad \text{--- eq. 8.3}$$

where ϵ_+ and ϵ_- are the upper and lower bounds respectively. ϵ_r and V_r are the permittivity and volume proportion of each phase. In this study $r=1$ is for silicon nitride, $r=2$ for voids, $r=3$ for unnitrided silicon and $r=4$ for impurities (silicon alloys).

8.3.1 ANALYSIS USING A THREE-PHASE MODEL

The volume proportions of the three phases (i.e silicon nitride, voids, unnitrided silicon) in composite RBSN are calculated using the formulae quoted in Section 7.4.1 and tabulated in Table 7.1. Using the tabulated volume proportion for each phase and assuming $\epsilon'=1$ for voids and $\epsilon'=12$ for the unnitrided silicon [8.8], the permittivity for silicon nitride is given by :

$$5.50 = \epsilon_1 \times 0.783 + 1 \times 0.197 + 12 \times 0.02$$

from which, for silicon nitride,

$$\epsilon_1 = 6.466$$

Assuming $\epsilon_1 = 6.466$ as the correct value for the permittivity for silicon nitride, the lower bound of the Wiener formula would give for the composite $\epsilon_- = 3.127$.

The accepted reference value for pure silicon nitride (i.e thin film CVD material) obtained from optical measurements is approximately equal to 4; using this value in the Wiener formula would give $\epsilon_+ = 3.569$ and $\epsilon_- = 2.535$. The two ranges of values, i.e the measured values of $\epsilon_+ = 5.50$ and $\epsilon_- = 3.127$ and the calculated values of $\epsilon_+ = 3.569$ and $\epsilon_- = 2.535$, overlap but it is obvious that the measured value is higher than the theoretical prediction (assuming a composite system of only three-phases). However the corrected value of $\epsilon'_1 = 6.466$ is much closer to the reference value (about 4) than is the calculation by Walton which allowed only for porosity and which give values in the region of 9 and 10.

8.4 CONCLUSIONS

The interest in RBSN as a candidate for a radome material was intermittent in the past because generally the electrical properties of the material were considered inadequate. Improvement in fabrication techniques of RBSN has led many workers [8.1 - 8.3] to established the fact that RBSN can be produced with satisfactory dielectric properties for high temperature radome applications. Table 8.1 shows reported values of measured permittivity of silicon nitride. Some values for HPSN [8.9] and thin film [8.10] silicon nitride are included to show that the permittivity of the material depends greatly on the method of preparation. Table 8.2 show some reported values of the loss tangent.

In the present study the measured value of 5.50 for the permittivity of fully nitrated RBSN with 20% porosity,

Frequency GHz.	ϵ'	Fabrication method	Comments	References
(8 -10)	4.5-5.6	reaction-bonded	35%-20% porosity	8.1
9.34	5.65	hot-pressed	5 w/o MgO added	1.3
	4.85	slip-cast		
9.37	6.8	flamed-sprayed		
	8.3	hot-pressed		8.3
0.5-9.34	4.5	reaction-bonded		

Table 8.1 Reported values of the permittivity of Si_3N_4 .

Frequency GHz.	$\text{Tan}\delta$	Fabrication method	References
9.34	1.6×10^{-3}	reaction-bonded	1.14
9.37	7×10^{-3}	hot-pressed	8.3
9.34	4.02×10^{-3}	hot-pressed	1.3
10	1×10^{-2}	reaction-bonded	8.2
8-10	7×10^{-3}	reaction-bonded	8.1

Table 8.2 Reported values of $\text{Tan}\delta$ of Si_3N_4 .

agrees exactly with that of Walton [8.1] and Wells [8.2] and also within experimental error with that of Ahmad [8.5]. The value for loss tangent agrees with that of Walton and Ahmad. This agreement shows that RBSN with nearly the same density and percentage of porosity can have the same dielectric properties although, on the contrary, variation of the dielectric properties has also been reported [8.4]. The agreement here is thought to be co-incidental and the variation is thought to be due to the contribution of uncontrolled (unaccounted) impurities. However, there is at present no data concerning the effect of unreacted 'silicon' (silicon, silicon-impurities) on the dielectric properties of RBSN. Infact, no published work on this aspect of research has been discovered and it is felt that the analysis in this Chapter is the first attempt to include the effect of impurities on the dielectric properties of RBSN. However a detailed quantitative study would present difficulties but the results of such a study would be of great importance to optimize the nitridation process of RBSN and also to serve as a quality control parameter.

REFERENCES

- 8.1 "RBSN for high temperature radome applications"
J.D. Walton Jr. - Amer. Ceram. Soc. Bull., Vol.53,
p255, (1974)
- 8.2 "Silicon nitride as a high-temperature radome material"
W.M. Wells - Reference UCRL 77 95, (1964)
- 8.3 "Microwave dielectric properties of silicon nitride"
G.S. Perry and T.R. Moules - Proc. 12th. Symp.
Electromag. Windows, Georgia Inst. Tech.,
J.N. Harris, (Ed), (1974)
- 8.4 "Silicon nitride : a promising material for radome
applications" - Proc. 12th. Symp. Electromag. Windows,
Georgia Inst. Tech., J.N. Harris, (Ed), (1974)
- 8.5 "Improved wideband coaxial methods for dielectric
measurements on nitrogen ceramics" - A.B. Ahmad
Ph.D. Thesis, University of Durham, (1983)
- 8.6 "Silicon nitride as a dielectric material" - B. Swarop,
Proc. 4th. Interim. Conf. Mater. Tech., 224, (1975)
- 8.7 "Review - The physical properties of composite materials"
D.K. Hale, J. Mat. Science, Vol.11, p2105, (1976)
- 8.8 "Dielectric anomalies in Si single crystal" - K.V. Rao
and A. Smakula, J. Appl. Phys., Vol.37, p2840, (1966)
- 8.9 "Electrical properties of HPSN" - R.I. Sharif
Ph.D. Thesis, University of Durham, (1977)
- 8.10 "Handbook of Electronic Materials : Vol.3" - J.T. Milek
IFI/Plenum, N.York, Washington, London, (1971)

CHAPTER 9

EXAMINATION OF PARTIALLY NITRIDED RBSN

Partially nitrided RBSN samples are produced by varying the firing schedule and the nitrogen partial pressure in the furnace. Details of the process have been fully described in Bushell's thesis [9.1]. The samples studied in this section varied from 0% weight gain (pure silicon) to about 64.5% weight gain (almost fully nitrided). Both the Fourier analysis method and an improved cavity perturbation method have been used in the dielectric measurements. In the cavity perturbation method, smaller sample sizes have to be used for lossy material to obtain a measureable Q-curve on the oscilloscope. Results for fully nitrided RBSN (Chapter 8) are included where it is appropriate to show variations over the whole range of weight gain. Structural studies were made using X-ray diffraction and Reflection High Energy Electron Diffraction (RHEED). Microstructural studies were also undertaken using the Scanning Electron Microscope (SEM) coupled with its Energy Dispersive Analysis by X-ray (EDAX) facility. The results from both studies are helpful in explaining the dielectric measurements of RBSN samples having various degrees of nitridation.

9.1 RESULTS

9.1.1.1 FREQUENCY VARIATION OF ϵ' AND ϵ''

The results for the partially nitrided RBSN are presented in almost the same format as for the fully nitrided sample in Chapter 8. Five samples with different weight

gains have been investigated using the Fourier analysis method. For this method the size of all the samples was kept the same, i.e. a circular disc with a diameter of about 7mm. and 3mm. thick. Fig. 9.1 shows the output waveforms when successive samples with different weight gains were inserted in the sample holder. Similarly, the dielectric parameters were obtained by comparing with the theoretical waveforms stored in the computer. For the cavity perturbation technique, eight samples with different weight gains have been used. The size of the sample for this technique cannot be kept the same as samples with low weight gain absorb much of the microwave energy and thus cause extremely large broadening of the absorption curve of the cavity. Sample sizes have to be reduced so that a reasonable absorption curve can be displayed on the oscilloscope and the Q-factor of the cavity can be determined. Smaller samples mean the uncertainty or errors in determining the volume of the sample are higher and thus the measurements of the dielectric parameters are less accurate as compared to the measurements of the fully nitrated RBSN with bigger sample size.

Fig. 9.2 combines all the results and shows the log-log plot of permittivity, ϵ' , against frequency for samples with different weight gain. Fig. 9.3 shows the log-log plot of the loss factor, ϵ'' , against frequency for the same set of samples. The gradients of all the plots in Fig. 9.2 and Fig. 9.3 are all about 0.97 ± 0.03 , similar to that of the fully nitrated RBSN in Chapter 8. Thus it appears that a hopping process is the dominant conduction mechanism for the whole range of partially and fully nitrated RBSN. There is,

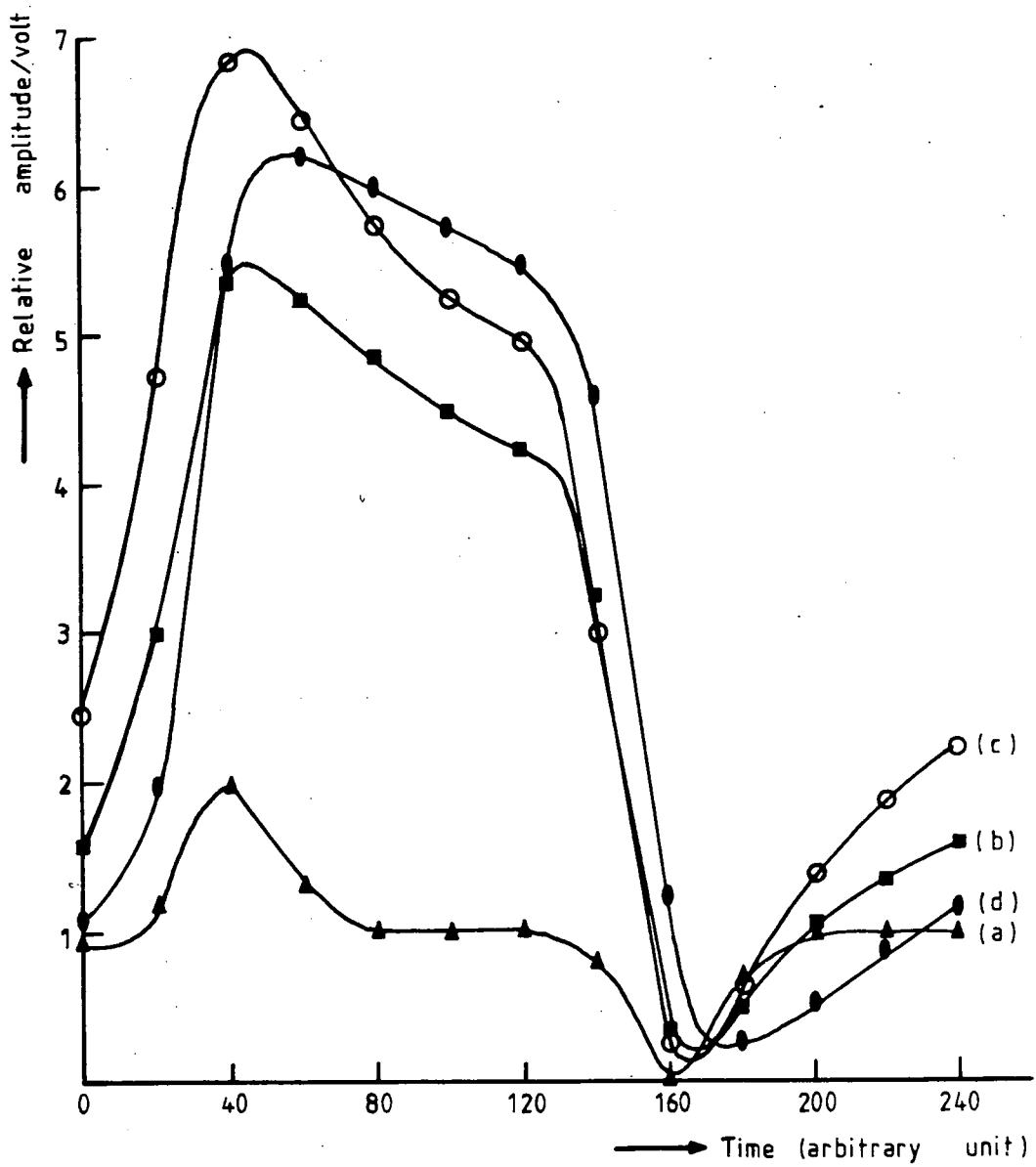


Fig. 9.1 Output waveforms for partially nitrided RBSN; a) 59.33% weight gain (▲), b) 48.18% weight gain (■), c) 39.18% weight gain (○) and d) 22.47% weight gain (●). [Waveform for 0% weight gain (silicon) is the same as b)]

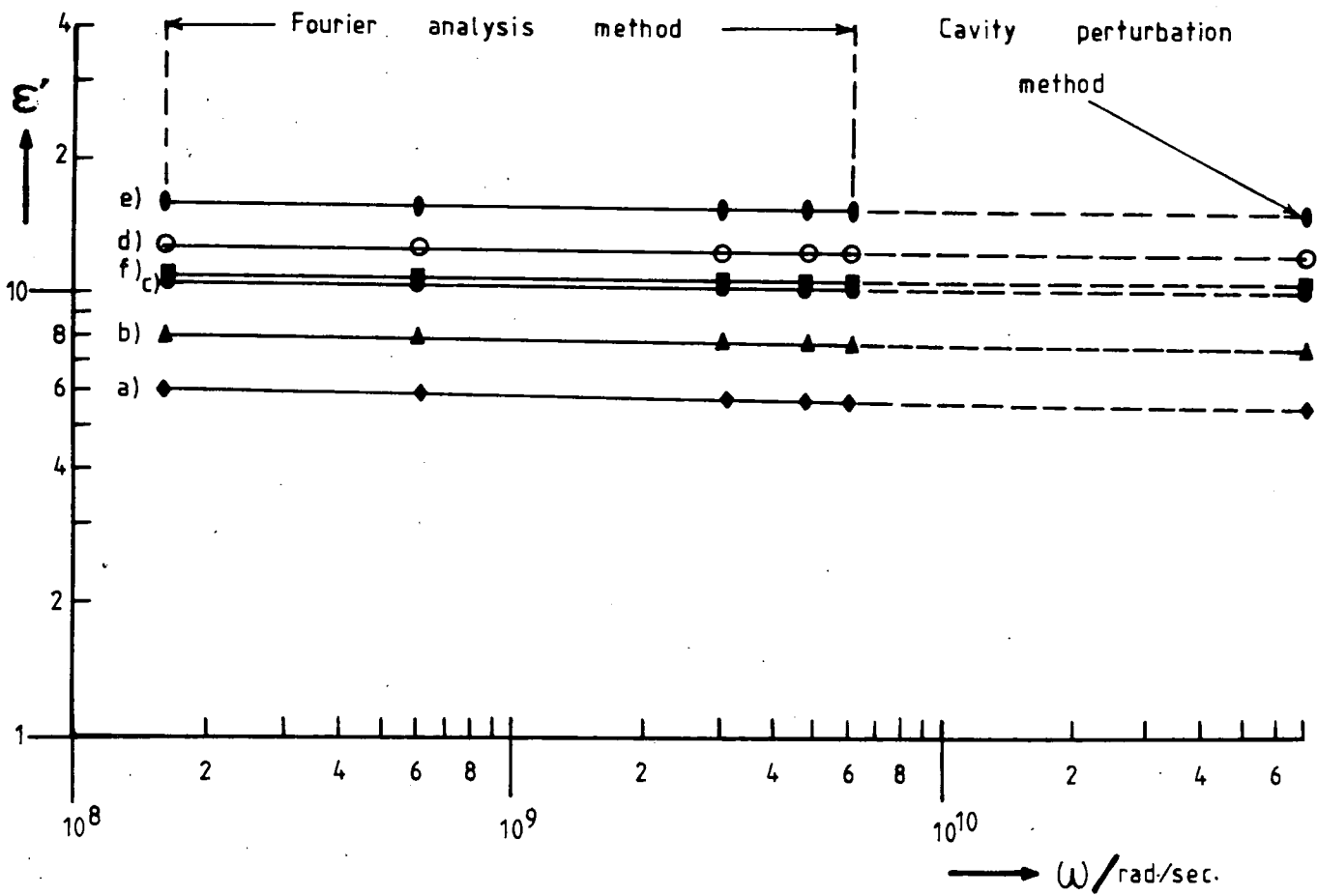


Fig. 9.2 Variation of ϵ' with angular frequency;

- a) 64.5% weight gain (\blacklozenge), b) 59.33% weight gain (\blacktriangle),
 c) 49.18% weight gain (\bullet) d) 39.18% weight gain (\circ),
 e) 22.47% weight gain (\bullet) and f) 0% weight gain (\blacksquare).

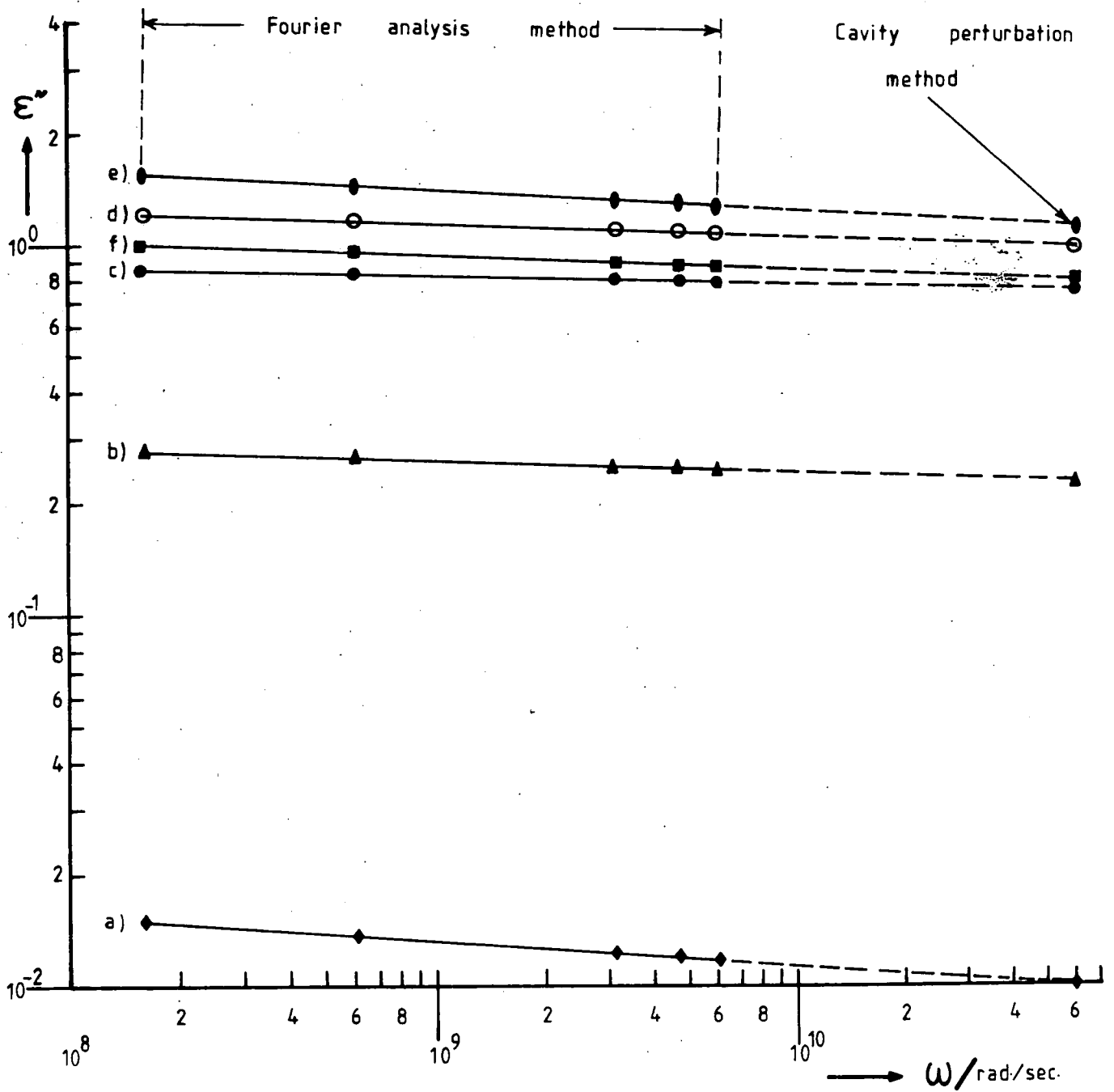


Fig. 9.3 Variation of ϵ'' with angular frequency;

- a) 64.5% weight gain (◆), b) 59.33% weight gain (▲),
 c) 49.18% weight gain (●) d) 39.18% weight gain (○),
 e) 22.47% weight gain (●) and f) 0% weight gain (■).

however, no previous reference with which to compare the dielectric properties results for the whole range of weight gain of RBSN. Ahmad [9.2] made measurements on the partially nitrided RBSN from about 63% to about 38% weight gain and these results are used as a comparison with the present measurements.

9.1.1.2 VARIATION OF MEASURED PERMITTIVITY WITH WEIGHT GAIN

The variation of the measured permittivity with frequency is the same for all the weight gains. Therefore, the variation of the measured permittivity with weight gain at a particular frequency is the same at any other measured frequency. The cavity perturbation method is chosen to show this variation because it is more accurate and the samples are much easier to prepare since they do not need to be polished nor cut into circular shapes. Eight samples with weight gains ranging from 0% (pure silicon) to 64.5% (almost fully nitrided RBSN) have been used to show this variation. The values of the measured permittivity are presented in Fig. 9.4 which shows the plot of the measured permittivity against weight gain.

The variation of the measured permittivity with weight gain for RBSN goes through a peak at about 22% weight gain. The value of the permittivity at the peak is about 15, higher than that of pure silicon, which has a value of 12 [9.3]. The accuracy of the measurements on the lossy partially nitrided RBSN is about ± 0.5 and the difference between the peak and the value for the 0% (pure silicon) weight gain sample is about 4.5; the peak is thus genuine. Ahmad's

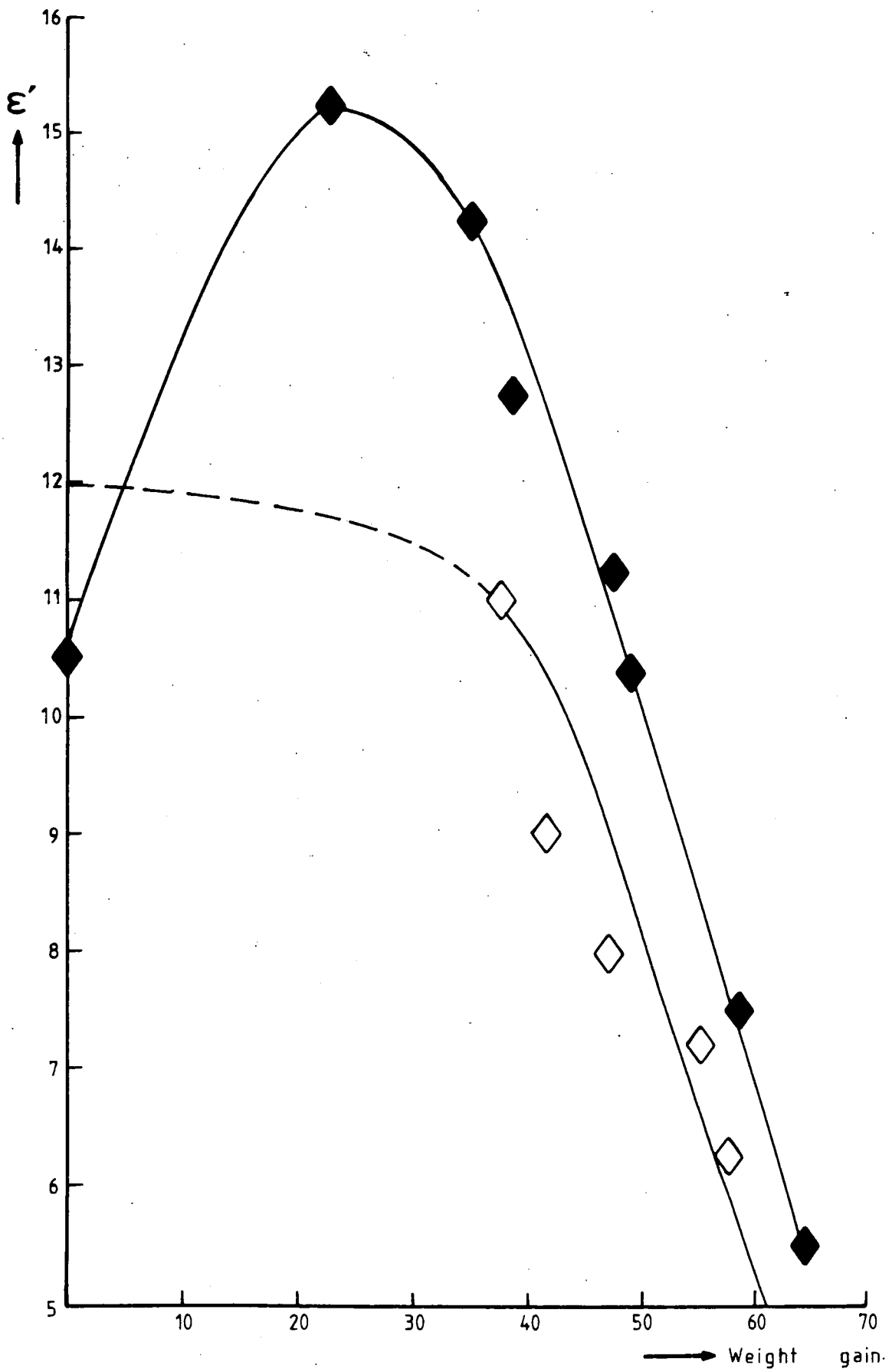


Fig.9.4 Variation of ϵ' with weight gain; present (◆), Ref.9.2 (◇)

results, for samples with weight gain ranging from 63% to 38% show the same trend in this restricted range of weight gain and have been included in Fig. 9.4.

The presence of this peak is one of the most interesting aspects of the present study of RBSN. It does not agree with the extrapolation made by Ahmad. The implication that the value of the permittivity would increase continuously from that of the fully nitrided RBSN to the higher value for pure silicon, (due to the increasing amount of unnitrided silicon) cannot be fully accepted. The reasons for not accepting Ahmad's previous explanation are complex and will be given in the next sections. Infact the rest of this Chapter will be devoted to establishing the background for an explanation of the variation of the measured permittivity with weight gain, as shown in Fig. 9.4. It will be seen that only a semi-quantitative treatment could be undertaken because attempts to explain the variation in detail would have required full control of the material preparation and monitoring all the constituents present in the starting material and in the nitriding atmosphere, factors which were beyond the available range of feasibility and control.

An empirical equation describing the curve shown in Fig. 9.4 has been obtained. A least square method of curve fitting was used [9.5]. The variation was taken to be of the form:

$$y = a + bx + cx^2 \quad \text{--- eq. 9.1}$$

Given this assumption, successive partial differentiation with respect to the coefficients gave three equations in each of which the co-ordinate values of the experimental

points could be substituted in order to determine the best-fit values of the three coefficients, a , b and c respectively. The values found were $a = 10.767$, $b = 0.3058$ and $c = -0.0061$. Therefore the resultant equation that empirically describes the variation of permittivity of RBSN with weight gain is :

$$\epsilon' = 10.767 + 0.3058W_g - 0.0061W_g^2 \quad \text{--- eq. 9.2}$$

where W_g is the percentage weight gain. It may be noted that the 'a' value of 10.767 represents ϵ' for pure silicon. Further, if the same variation holds for higher weight gains than were examined here, the ϵ' value for fully nitrided material (i.e $W_g = 66.5\%$) should be reduced to 4.0.

9.1.2.1 STRUCTURAL AND MICROSTRUCTURAL STUDIES OF RBSN

Crystalline silicon nitride exists in two forms referred to previously as α and β . Both structures are hexagonal and both have a basic building unit of the silicon-nitrogen tetrahedron joined so that each nitrogen is shared by three tetrahedra [9.6]. The lattice parameters, for the α -phase are, $a=7.755$, $c=5.616$, and for the β -phase are, $a=7.606$, $c=2.907$ [9.7]. It is not the aim here to check these parameters but to try to identify and study the impurities present in RBSN. Knowledge of the structure of the impurities present in RBSN not only will help to explain the dielectric measurement results but will also help to clarify the reaction mechanism during the nitridation process which produces RBSN.

Three methods have been used to study the impurities present in RBSN. The X-ray powder method has been used to obtain the diffraction patterns of the bulk material, the RHEED

technique examines the region close to the surface of the ceramic and a SEM coupled with an EDAX facility has been used to study the microstructure of etched surfaces and identify the impurities present in the sample. Basically two different samples were investigated; fully nitrided RBSN (64.5% or 63% weight gain) and partially nitrided RBSN (44.44% or 35.6% weight gain).

9.1.2.2 X-RAY DIFFRACTION

In the conventional X-ray powder technique, the specimen is ground to a fine powder and mounted in such a way that it can be irradiated by a monochromatic X-ray beam. However RBSN is polycrystalline material with a very small grain size, i.e a small piece of the sample is made up of a very large number of small grains comprising of both phases and including impurities and voids. Consequently, it is not necessary to grind such a sample in order to make it polycrystalline but it is simply adequate to prepare a rod-like sample thin and small enough to minimise X-ray absorption. Moreover the thin slice sample used in the cavity perturbation technique can also be used for the X-ray diffraction measurements. The sample is fixed at the end of a glass (Lindermann) rod and mounted as in the normal X-ray powder method. Details of the powder technique can be obtained in many texts.

Two samples with weight gains of 64.5% and 44.44% were investigated. Table 9.1 gives the measured d-spacings for a sample with 44.44% weight gain and Table 9.2 gives those for similar measurements from the 64.5% weight gain sample. Analysis of the diffraction lines produced is very difficult

Expt. results			Si	α -Si ₃ N ₄	β -Si ₃ N ₄	CaSi ₂	FeSi ₂
R/cm	I	d/Å	d/Å	d/Å I/I ₀	d/Å I/I ₀	d/Å I/I ₀	d/Å I/I ₀
2.150	s	4.072		4.320 50			
2.355	s	3.80		3.88 30			
2.375	w	3.76			3.82 20		
2.72	w	3.32		3.37 30			
2.75	w	3.23			3.31 85	3.31 12	
2.92	vs	3.055	3.09			3.08 12	
2.95	w	3.034				3.08* 12	
3.175	m	2.83		2.89 85			
3.45	s	2.604		2.599 75	2.668 100	2.66 40	
3.52	s	2.53		2.547 100		2.55 28	
3.6	s	2.492			2.492 100		
3.65	ms	2.465					2.37 60
3.95	ms	2.28		2.32 60	2.312 9		
4.0	w	2.25			2.18 35		
4.25	m	2.13		2.158 30		2.13 16	
4.425	m	2.05		2.083 55	1.904 5		
4.8	vs	1.893	1.893		1.892 5	1.92 100	1.89 30
4.85	w	1.88		1.884 8			
4.95	m	1.843			1.827 20		1.84 100
5.125	w	1.782		1.806 12	1.753 70		1.78 15

Table 9.1 Interplanar spacings (X-ray) for 44.44% weight gain RBSN compared with ASTM data. [s= strong, w= weak, m= medium, vs=very strong, ms= medium strong, d= interplanar spacing, I= intensity]

Expt. results			Si	α -Si ₃ N ₄	β -Si ₃ N ₄	CaSi ₂	FeSi ₂
R/cm	I	d/Å	d/Å	d/Å I/I ₀	d/Å I/I ₀	d/Å I/I ₀	d/Å I/I ₀
2.15	m	4.147					
2.18	s			4.32 50			
2.34	m	3.797		3.88 30			
2.4	s				3.82 20		
2.42	w	3.673					
2.7	m	3.298		3.37 30			
2.75	s	3.239			3.31 85	3.31 12	
2.85	s	3.128	3.09			3.08 12	
3.15	m	2.837					
3.25	s	2.76		2.89 85			
3.3	w	2.711		2.823 5			
3.425	s	2.616			2.668 100	2.66 40	
3.5	s	2.561		2.599 75		2.55 28	
3.575	s	2.509		2.547 100			
3.65	s	2.459			2.49 100		
3.725	m	2.412					2.37 63
3.95	w	2.279			2.312 9		
4.025	s	2.238		2.32 60			
4.1	w	2.199		2.283 8			
4.275	w	2.113		2.244 5			
4.325	w	2.09					
4.45	m	2.034		2.158 30	2.18 35	2.13 16	
4.5	s	2.012		2.083 55			
4.75	s	1.912				1.92 100	1.89 30
4.875	s	1.866					1.84 100

Table 9.2 Interplanar spacings (X-ray) for 64.5% weight gain RBSN compared with ASTM data.

considering that so many components are present causing many diffraction lines from one component to overlap with those from another. The measured d-spacings have been compared with the values given by the ASTM (American Society for Testing Materials) index for the pure α and β phases of silicon nitride. In addition, pure silicon is also expected to be present and its ASTM d-spacings are also included in both the Tables. Examination of the two Tables shows that these three materials account for most of the lines present in the diffraction photographs. It should be noted that the relative intensity I/I_0 of each component can be misleading mainly because the values given by the ASTM index are for single crystals of each material. But when a sample comprising several components is studied, for example RBSN, then the amount of each component present in the ceramic will determine the relative intensity of each line.

Returning to the extra lines not accounted for by the presence of silicon and α and β phases (see Table 9.1 and 9.2) consideration was given to other possible materials which might be present. From the papers which discuss the reaction mechanism, it is known that iron silicide is frequently observed as an impurity in this type of material. In addition, SEM studies (described below) show that calcium compounds are present. Accordingly, ASTM data for the silicides of iron and calcium have been considered and those with the particular chemical composition of FeSi_2 and CaSi_2 give the best fit to the extra lines. For this reason the ASTM data for FeSi_2 and CaSi_2 are included in Table 9.1 and 9.2. Unfortunately each of the compounds has several lines which overlap with either the pure silicon, or the $\alpha\text{-Si}_3\text{N}_4$.

or β - Si_3N_4 and in addition the ASTM data for the α - Si_3N_4 does not include high Θ lines. Thus no further conclusive identification could be made from the X-ray diffraction study.

Comparing the relative intensities of pure silicon diffraction lines produced by the partially and fully nitrided RBSN, it is obvious that the amount of pure silicon in the fully nitrided sample is much less than in the partially nitrided sample. This agrees with the variation given in Table 7.1. Also, the β - Si_3N_4 diffraction lines are much more easily identifiable in the fully nitrided sample. This is due to the fact that during the first stage of nitridation (that produces lower weight gain samples) the α - Si_3N_4 is mainly formed. However, fully nitrided RBSN has about 15% β -phase. The conclusion that FeSi_2 is tentatively identified as the particular phase of iron silicide present as an impurity in RBSN agrees with the proposals by Moulson [9.7]. The new observation of this study is the identification of CaSi_2 as an included impurity in the RBSN studied.

9.1.2.3 REFLECTION HIGH ENERGY ELECTRON DIFFRACTION

The RHEED method works on the same principle as X-ray diffraction (in both cases Bragg's law is obeyed i.e

$= 2d_{hkl} \sin\theta$) but instead of having $\lambda = 1.54$ (for Cu-K α) as in the powder method, an electron beam with energy 100KeV. has an associated wavelength $\lambda = 0.04$, which results in the Bragg diffraction angle being $< 1^\circ$. Fully nitrided (64.5% weight gain) and partially nitrided (35.6% weight gain) samples have been investigated but polished surfaces did not give any distinctive diffraction patterns. In fact polishing

the surface of the sample probably made it completely amorphous. To remove the polished surface, the samples have been etched with HF and hot (160°C) phosphoric acid (H_3PO_4). Two etchants have been used with the hope that either one or both have preferential reactions to dissolve either the pure silicon or silicon nitride; leaving the surface with a higher concentration of the impurity phases.

Plates 9.1a and 9.1b illustrate the diffraction patterns of the sample (35.6% weight gain) etched in HF and H_3PO_4 respectively. The analyses of these patterns are tabulated in Table 9.3 and 9.4 respectively. All the lines in Table 9.3 are attributable to the α - Si_3N_4 and pure silicon. This is in complete agreement with the results of the X-ray study. However, for the sample etched in H_3PO_4 (see Table 9.4) there are extra lines not attributable either to the silicon nitride (α and β) or the pure silicon. The ASTM data for CaSi are in good agreement with the extra lines present. Thus the tentative identification (which was provided by the X-ray diffraction measurement) of $CaSi_2$ as an impurity in the RBSN studied is convincingly confirmed.

Plates 9.2a and 9.2b show the comparison of the diffraction patterns of two samples, with 64.5% and 35.6% weight gain, both etched in HF for 18 hours. The analyses of the diffraction patterns in plate 9.2a and 9.2b are presented in Table 9.5. The sample with 35.6% weight gain consists predominantly of α - Si_3N_4 and pure silicon. In fact, the presence of β -phase cannot be identified in this particular sample. However the fully nitrated sample is predominantly α - Si_3N_4 and the β - Si_3N_4 can now be identified easily; the pure silicon lines are not seen in this case.



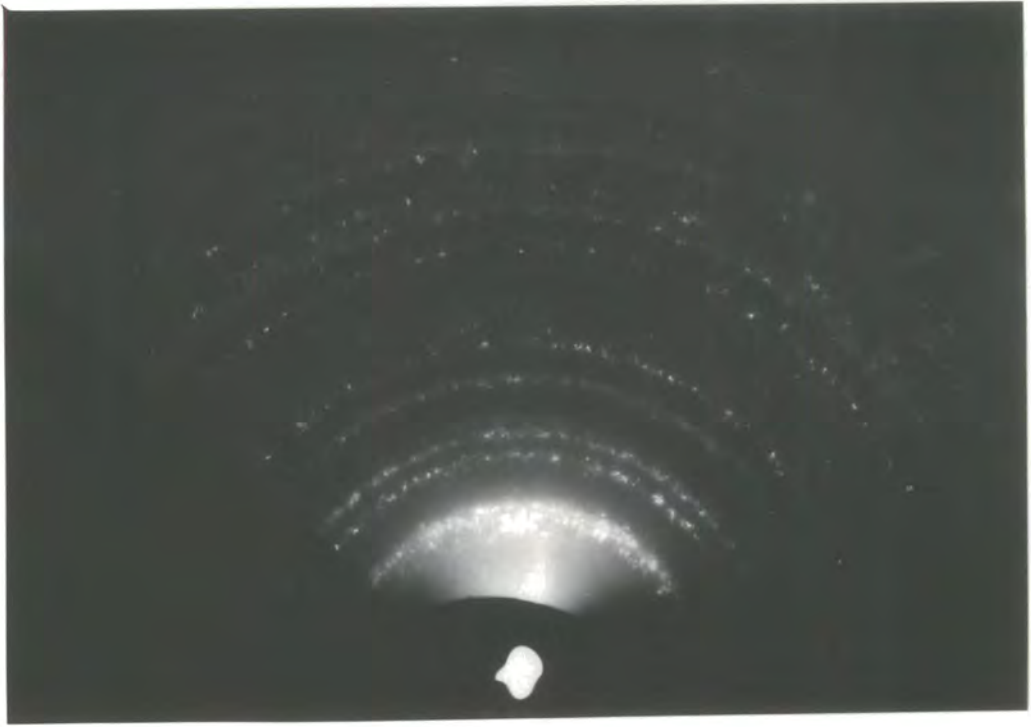


Plate 9.1a RHEED pattern for 35% weight gain RBSN; HF etched.

Expt. results			Si	α -Si ₃ N ₄	
R/cm	I	d/Å	d/Å	d/Å	I/I ₀
1.75	vs	4.23		4.32	50
2.25	s	3.29		3.37	30
2.45	s	3.02	3.089		
2.55	w	2.90		2.89	85
2.95	s	2.51		2.547	100
3.3	s	2.24		2.32	60
3.55	w	2.085		2.158	30
3.95	w	1.873	1.892	2.083	55
4.25	m	1.741		1.771	25
4.5	m	1.64	1.613		
4.7	m	1.57		1.596	35

Table 9.3 RHEED data for 35% weight gain RBSN; HF etched.

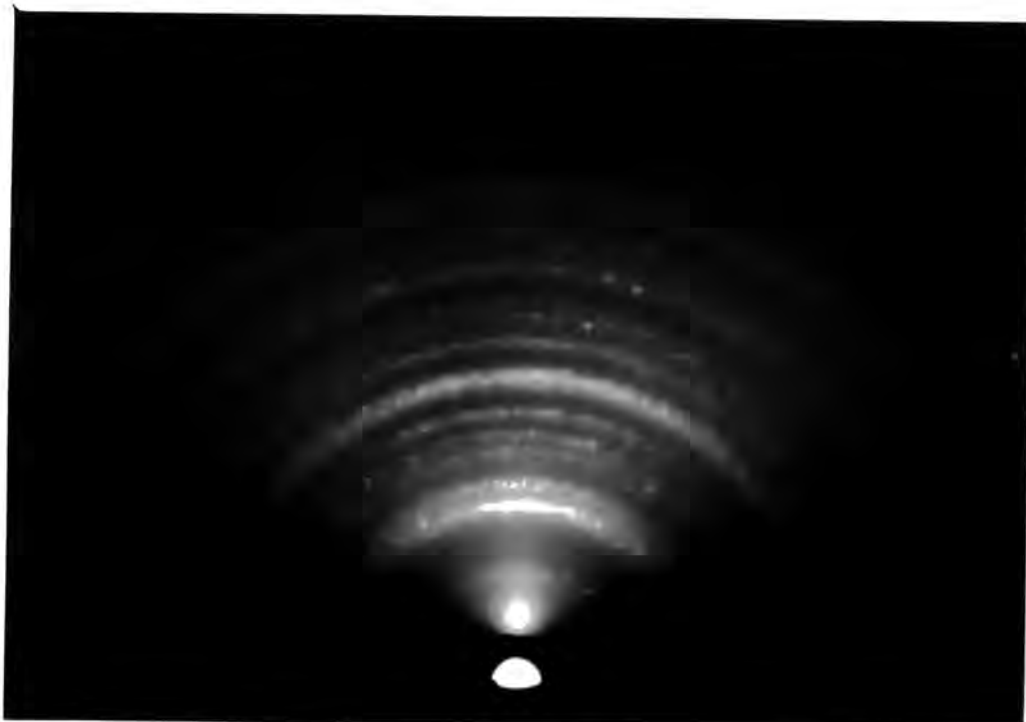


Plate 9.1b RHEED pattern for 35% weight gain RBSN; H_3PO_4 etched

Expt. results			Si	$\alpha-Si_3N_4$		CaSi ₂	
R/cm	I	d/Å	d/Å	d/Å	I/I ₀	d/Å	I/I ₀
1.05	w	7.03		6.69	8		
1.70	vs	4.35		4.32	50		
1.85	s	4.00		3.88	30		
2.20	vs	3.30		3.37	30	3.31	12
2.30	s	3.22	3.089			3.08	12
2.55	s	2.90		2.893	85		
2.85	vs	2.596		2.599	75	2.66	40
3.20	s	2.31		2.547	100	2.55	28
3.45	w	2.145				2.13	16
3.85	s	1.92	1.892			1.92	100
4.20	w	1.76		1.771	25		
4.55	w	1.626				1.64	16
4.60	w	1.608	1.613	1.596	35	1.55	12

Table 9.4 RHEED data for 35% weight gain RBSN; H_3PO_4 etched.

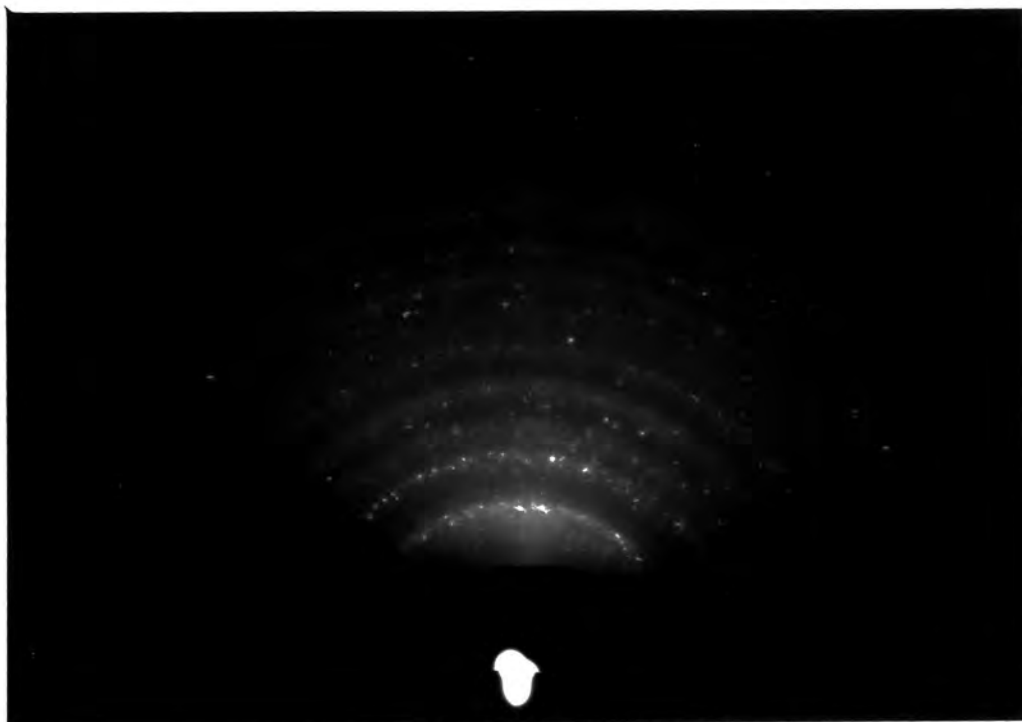


Plate 9.2a RHEED pattern for 35% weight gain RBSN, HF etched

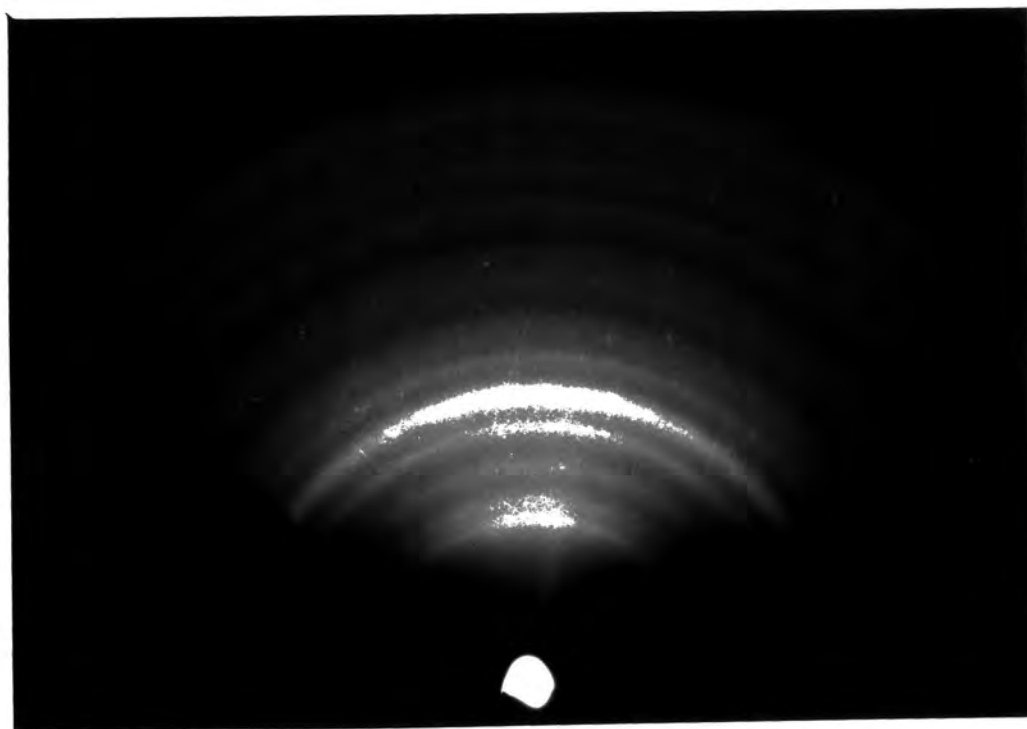


Plate 9.2b RHEED pattern for 64.5% weight gain RBSN, HF etched

35% weight gain					64.5% weight gain					
Expt. results			Si	α -Si ₃ N ₄		Expt. results			β -Si ₃ N ₄	
R/cm	I	d/Å	d/Å	d/Å	I/I ₀	R/cm	I	d/Å	d/Å	I/I ₀
1.35	s	4.133		4.32	50	1.3	s	4.29		
						1.45	s	3.85	3.82	20
1.675	s	3.33		3.37	30	1.67	s	3.34	3.31	85
1.90	m	2.94		2.893	85	1.95	s	2.84	2.668	100
2.2	m	2.54		2.547	100	2.20	vs	2.54	2.49	100
2.45	m	2.27		2.32	60	2.45	s	2.27		
2.65	w	2.106		2.158	30	2.65	m	2.106		
				2.083	55	2.75	m	2.03		
2.90	m	1.924	1.892							
						3.05	w	1.83	1.83	20
3.15	m	1.771		1.771	25	3.20	m	1.74	1.75	70
3.45	m	1.617	1.613							
3.50	w	1.594		1.596	35	3.55	m	1.572	1.57	35

Table 9.5 Comparison of RHEED data for the 35% weight gain and 64.5% weight gain RBSN; both etched with HF for 18 hours.

[Refer to Plate 9.3 and Plate 9.4]

These observations are consistent with the X-ray diffraction studies.

Thus in summary the structural studies on RBSN using the X-ray powder photograph technique and the RHEED technique identify the main impurities present in the partially nitrated samples (35.6% and 44.44% weight gain) as FeSi_2 and CaSi_2 . Other impurities may be present but insufficient in quantity to be identified by these diffraction techniques. To explore further possibilities, the SEM together with its EDAX facility was employed as described in the next section.

9.1.2.4 SCANNING ELECTRON MICROSCOPE AND EDAX STUDY

The Energy Dispersive Analysis by X-ray facility of the SEM has been used to analyse the impurities present on the etched or fractured surfaces of the samples. The microstructure of the surface of the sample was revealed by the secondary emission of the spectrum of the SEM; magnifications from about 50X to about 10,000X have been used. The electron beam can be focussed on a very small area of a distinct feature of the surface and the EDAX facility is able to print out the X-ray emission spectrum of the elements present in that small area. Three types of surface have been examined; two of these were etched surfaces where the etchants were HF and H_3PO_4 respectively (note that these were the same samples used in the RHEED study) and the third type of surface was produced by fracturing the samples. The presentation of the observations and their analysis is given according to the type of surfaces studied; i.e :

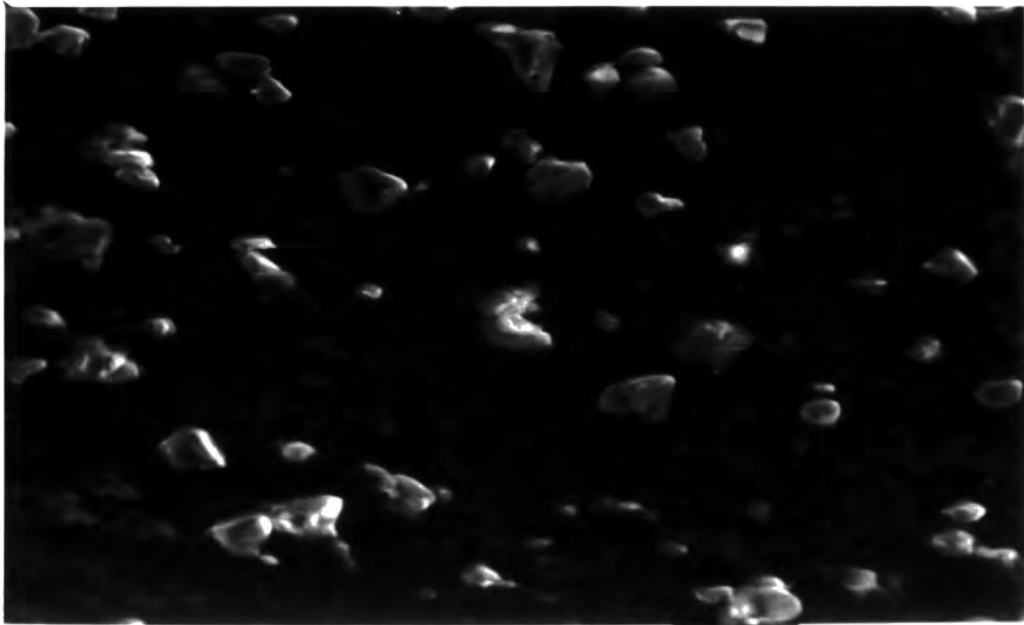
a) HF etched surface

In the semiconductor industry HF is regularly used to

remove the silicon oxide layer from the surface of silicon, leaving a matrix of pure silicon on the surface. Samples with 44.44% and 63.29% weight gain have been etched in 40% HF for two hours. Plate 9.3a shows the general microstructural features of RBSN (44.44% weight gain) etched in HF. The evenly distributed features on the surface of the sample are pure silicon. Almost the same general microstructural features can be seen for the sample with 63.29% weight gain; but there was much less evidence of pure silicon. The micrograph of the surface of the 63.29% weight gain sample could not be recorded without applying a conducting coating to the surface. This is due to the highly insulating nature of the sample which gets easily charged up when the electron beam is focussed on the surface, thus making the image unstable.

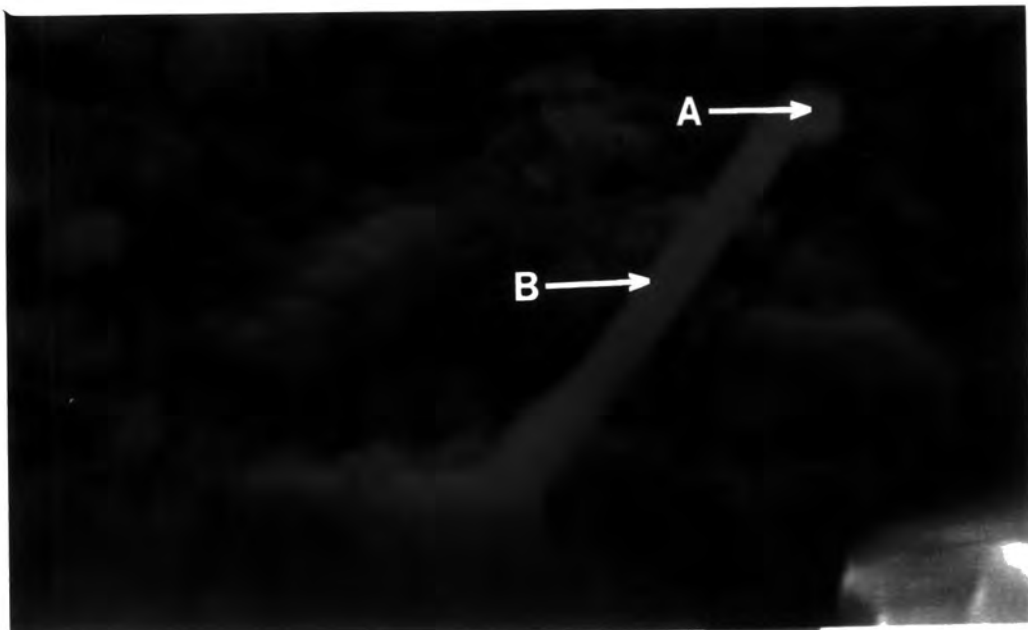
Plate 9.3b shows a whisker (filament) with a globule at its end. The EDAX trace of the globule [Fig. 9.5] shows the presence of iron (Fe-K α) but no iron can be observed along the filament. Plate 9.4a shows two filaments resting on the pure silicon feature and Plate 9.4b shows that one of these filaments has disappeared during examination. This can be explained by the fact that the filaments are very insulating and this particular one become charged by the electron beam causing its ejection from the field of view.

Fig. 9.6 shows an EDAX plot from a globule-like feature of the 63.29% weight gain sample etched in HF. The plot is a comparison between the background (shaded) and the globule (dotted). The background is the EDAX analysis outside the globule and the spectrum from the globule is taken by focussing the electron beam onto it. Both traces have a rather



40 μ

Plate 9.3a Microstructural features of 44.44% weight gain RBSN, HF etched



4 μ

Plate 9.3b A whisker and globule in 44.44% weight gain RBSN, HF etched

SB CNT

4060 EU

Link Systems 860 Analyser

1K FS: B

10 EU/CHAN

7-Feb-84

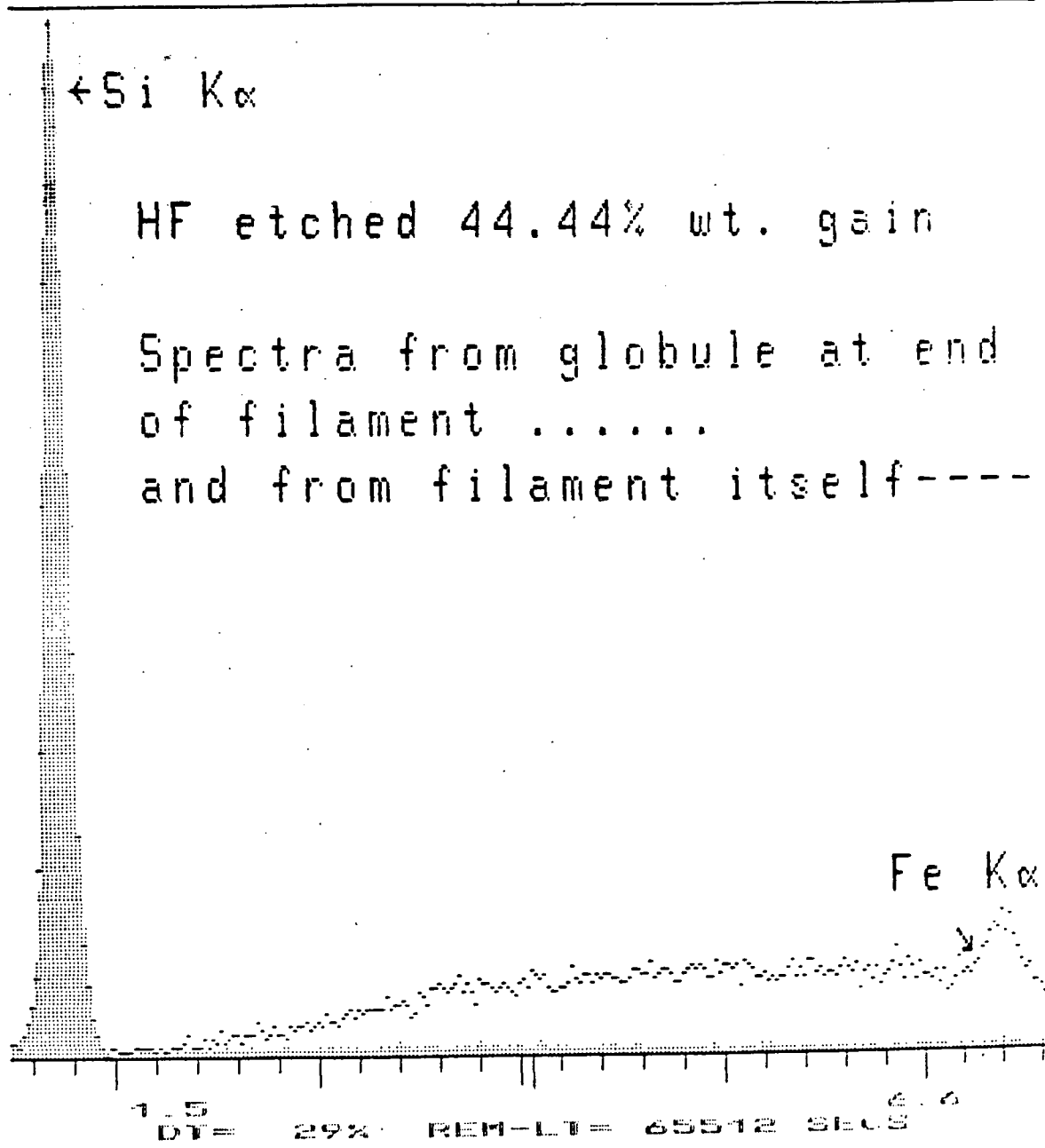


Fig. 9.5 EDAX spectra from 44.44% weight gain RBSN after etching in HF [Refer to Plate 9.3b].

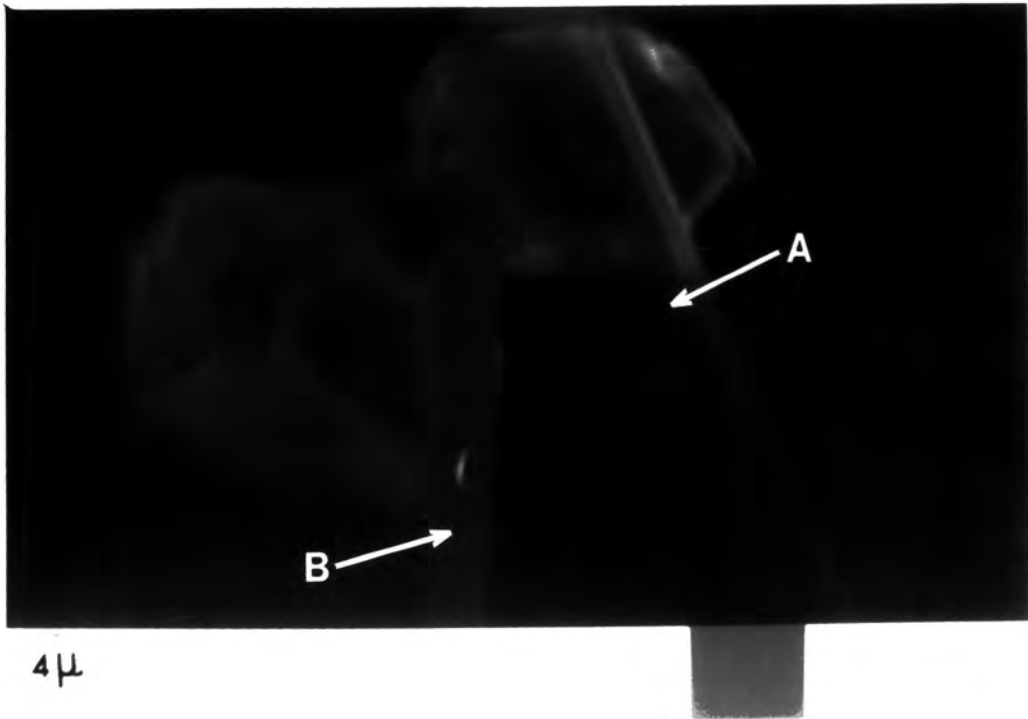


Plate 9.4a Two filaments on pure silicon features (44.44% weight gain RBSN, HF etched)

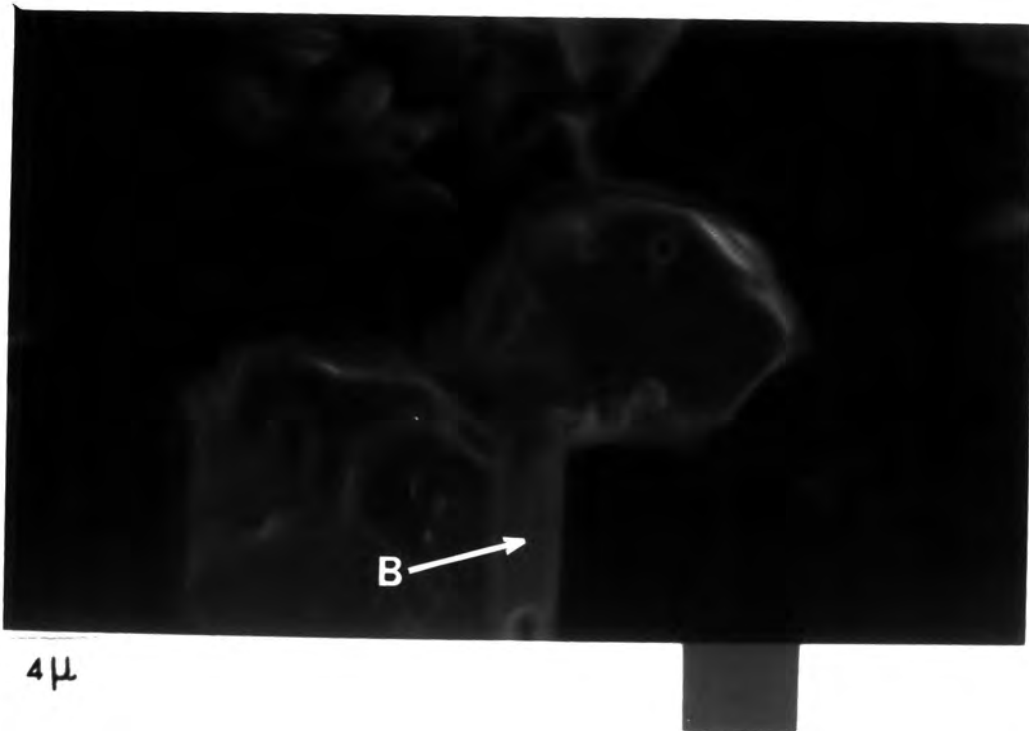


Plate 9.4b Subsequent examination of region shown in Plate 9.4a

99 CNT

2K FS: B

4540 EU

10 EU/CHAN

Link Systems 860 Analyser

8-Feb-84

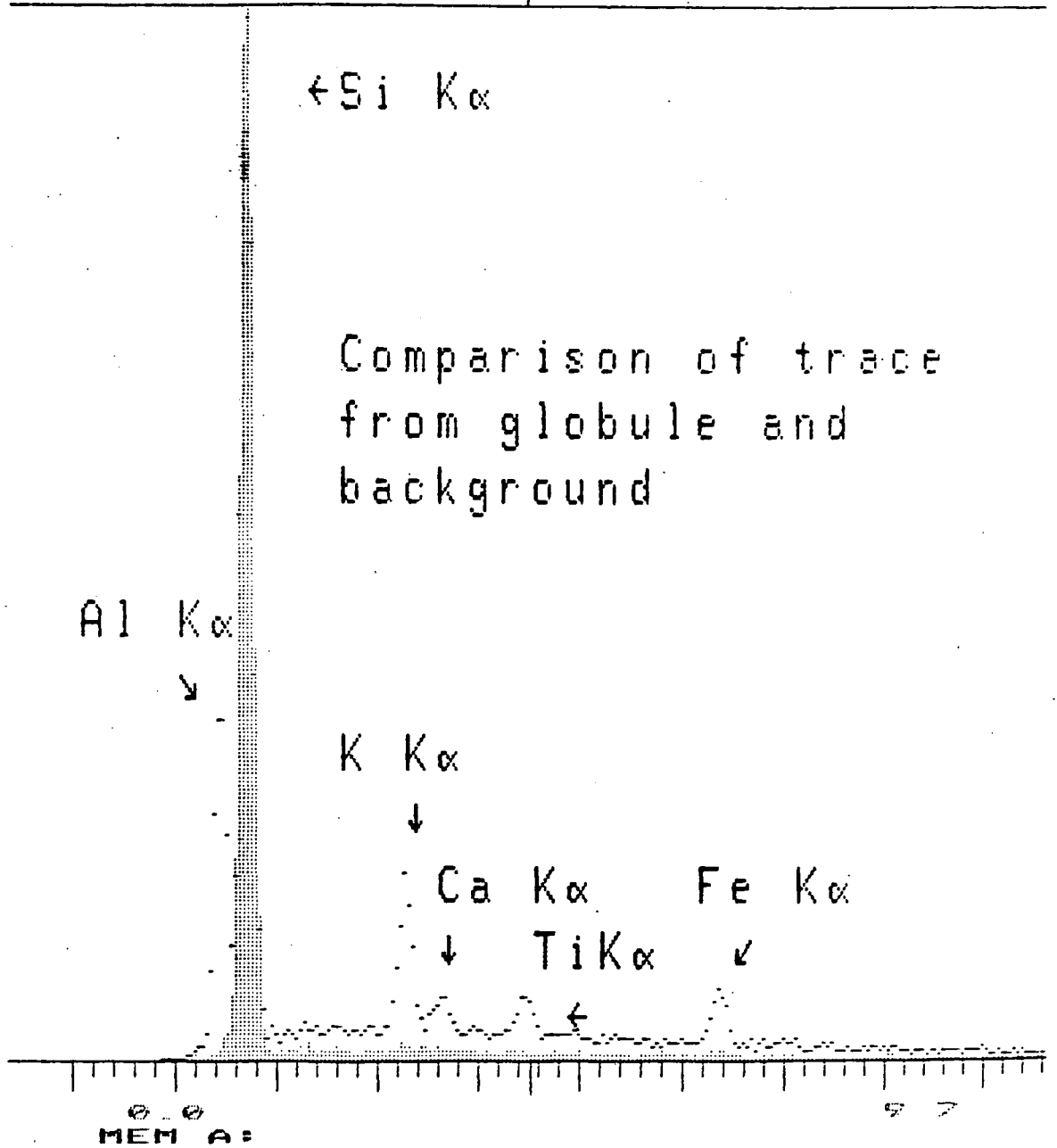


Fig. 9.6 EDAX spectra from 63.29% weight gain RBSN after etching in HF. The spectrum indicated by the dotted trace was recorded from the globule while the shaded one represents the background spectrum.

intense of Si-K α line; probably a contribution from Si₃N₄. The background trace does not show any presence of impurities. However, aluminium (Al-K α), potassium (K-K α), Calcium (Ca-K α), titanium (Ti-K α) and iron (Fe-K α) are definitely present in the globule. This would suggest that all the impurities present in the sample tend to form precipitates indicating that during the nitridation process, a liquid pool of pure silicon and impurities is probably formed. In the nitridation process the silicon is converted to silicon nitride, leaving the pool of impurities to form precipitates as the final product. This observation is consistent with the mechanisms of formation of RBSN that have previously been reported.

b) H₃PO₄ etched surfaces

Samples with 44.44% and 63.29% weight gain have been studied and the etching was carried out at a temperature of 160°C for about half an hour. Plate 9.5a shows some distinct features (large fibre) on the H₃PO₄ etched surface of the 44.44% weight gain sample. At higher magnification (Plate 9.5b) it can be seen that the sample is very porous. Fig.9.7 shows the background EDAX trace of samples with 35.6% and 44.44% weight gain. No impurities are observed except phosphorus which is likely to have been introduced into the sample by the H₃PO₄ etchant.

Plate 9.6a shows a large fibre joined to another. The EDAX plot from this (Fig. 9.8) shows that calcium is the main impurity present in the large fibre. Also traces of aluminium (Al), potassium (K) and titanium (Ti) are observed. Plate 9.6b shows another feature on the H₃PO₄ etched surface. The EDAX plot (Fig. 9.9) from this feature again shows

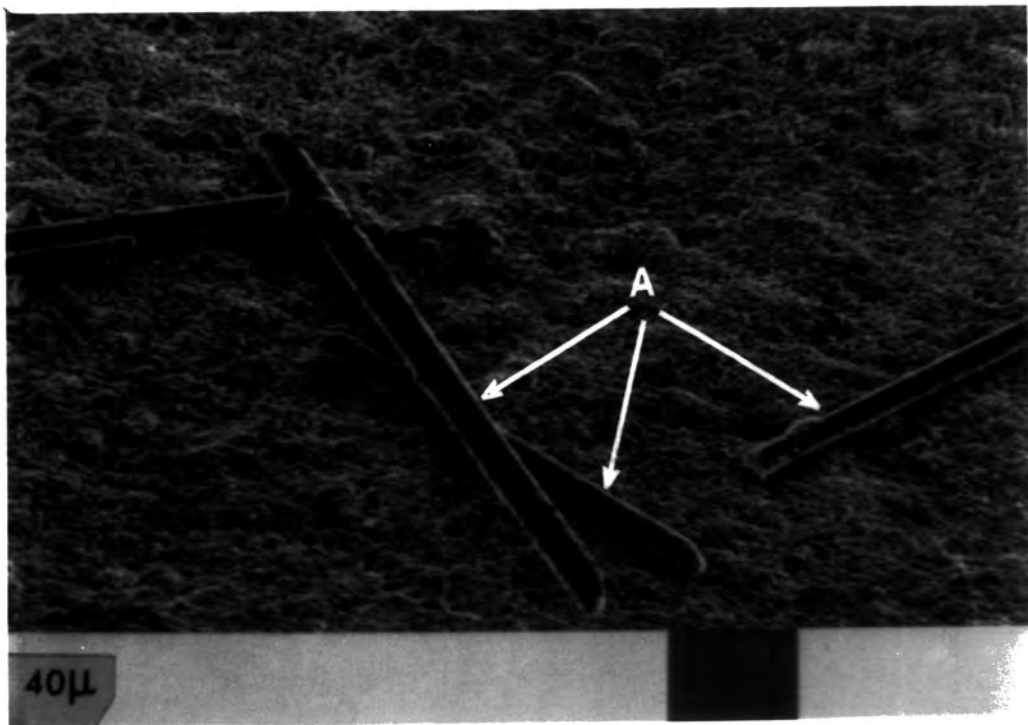


Plate 9.5a Features on 44.44% weight gain RBSN ,
 H_3PO_4 etched

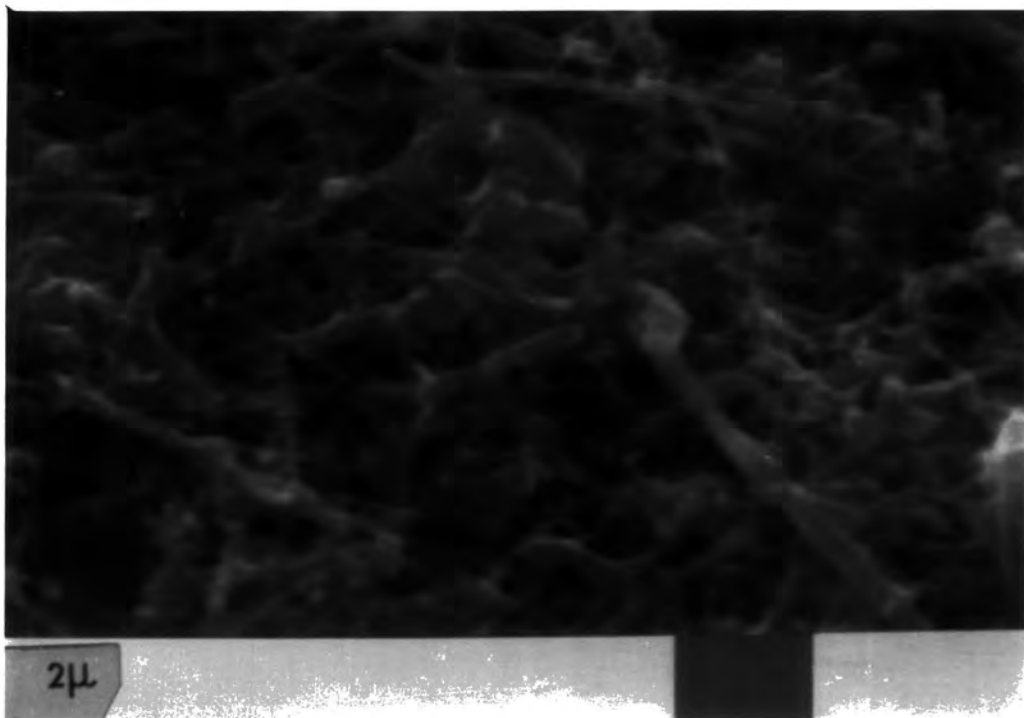


Plate 9.5b Higher magnification micrograph of Plate 9.5a

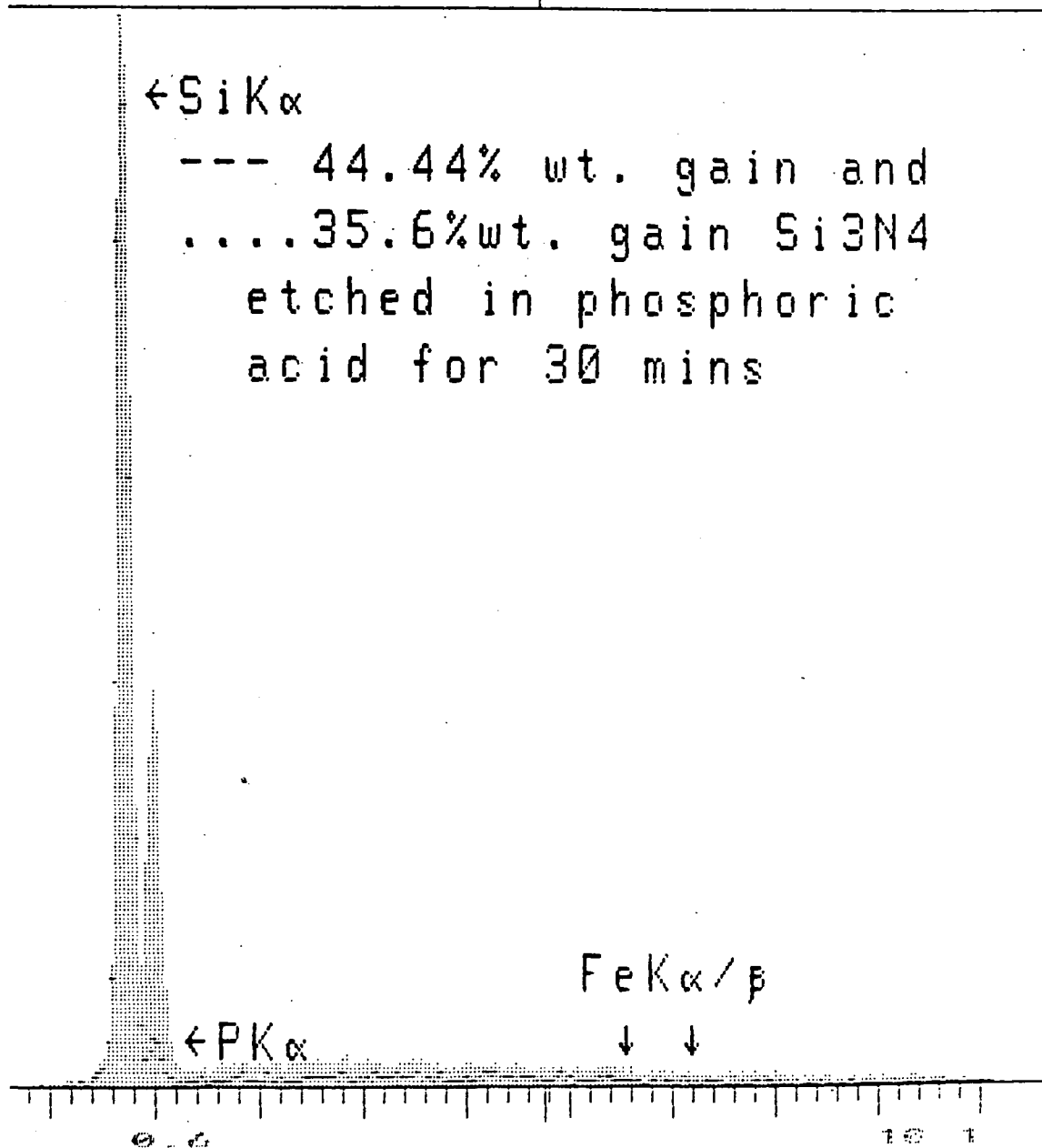


Fig. 9.7 EDAX spectra from backgrounds of samples with 44.44% and 35.6% weight gain.

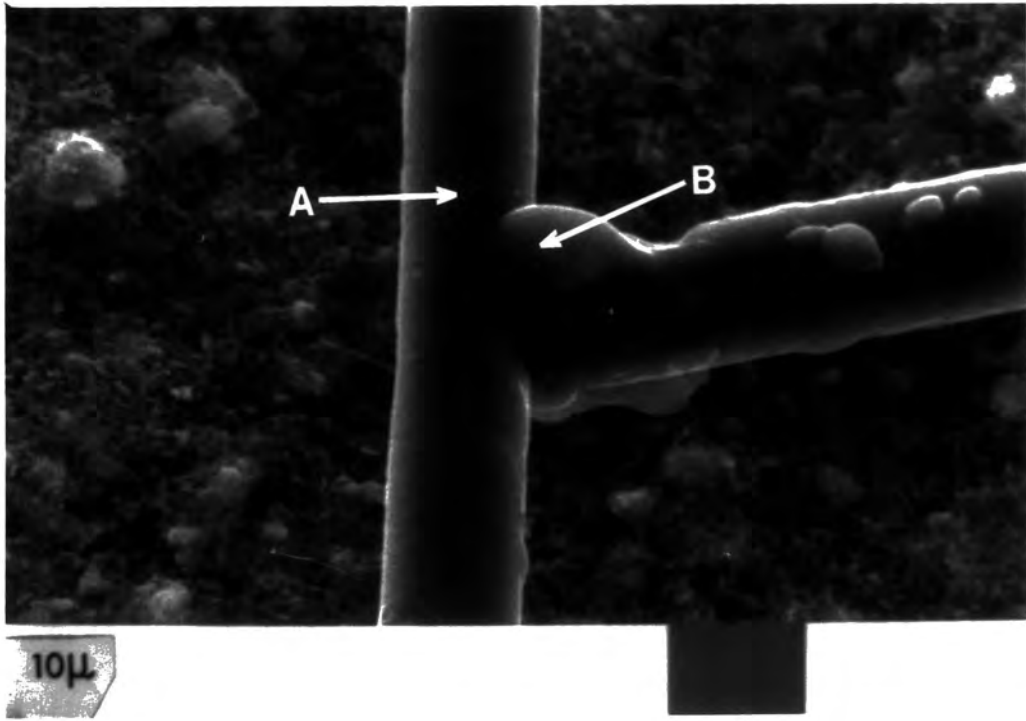


Plate 9.6a Junction of two large fibres (44.44% weight gain
RBSN, H_3PO_4 etched)

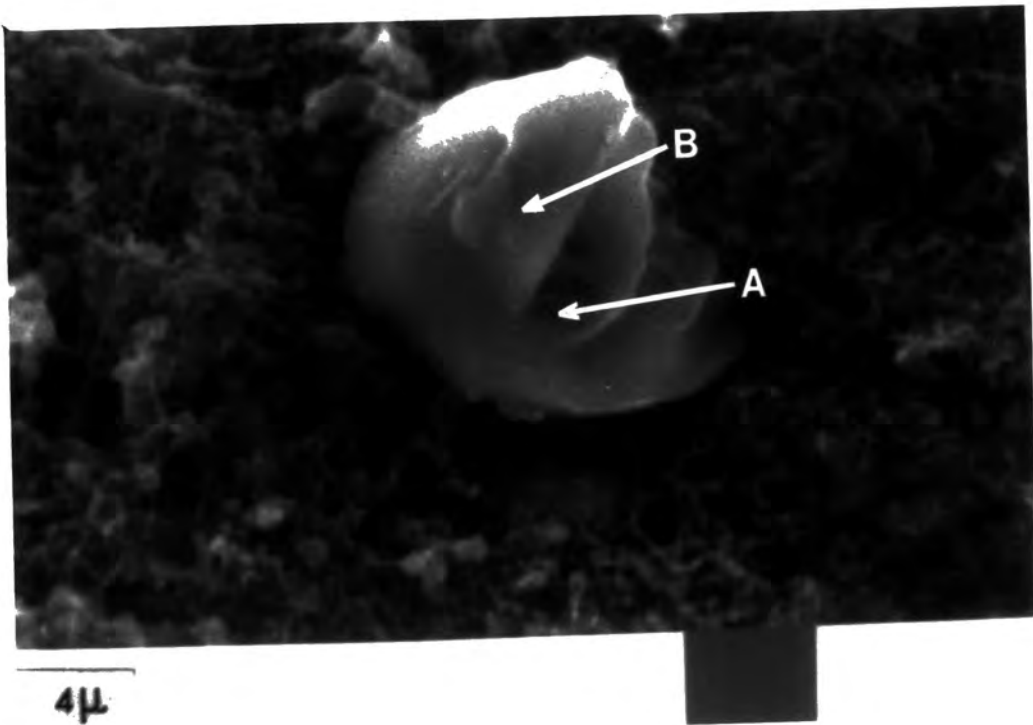


Plate 9.6b Surface feature, H_3PO_4 etched surface (44.44%)

22 CNT

511 FS: B
3100 EV 10 EV/CHAN
Link Systems 660 Analyser 26 Jan 84

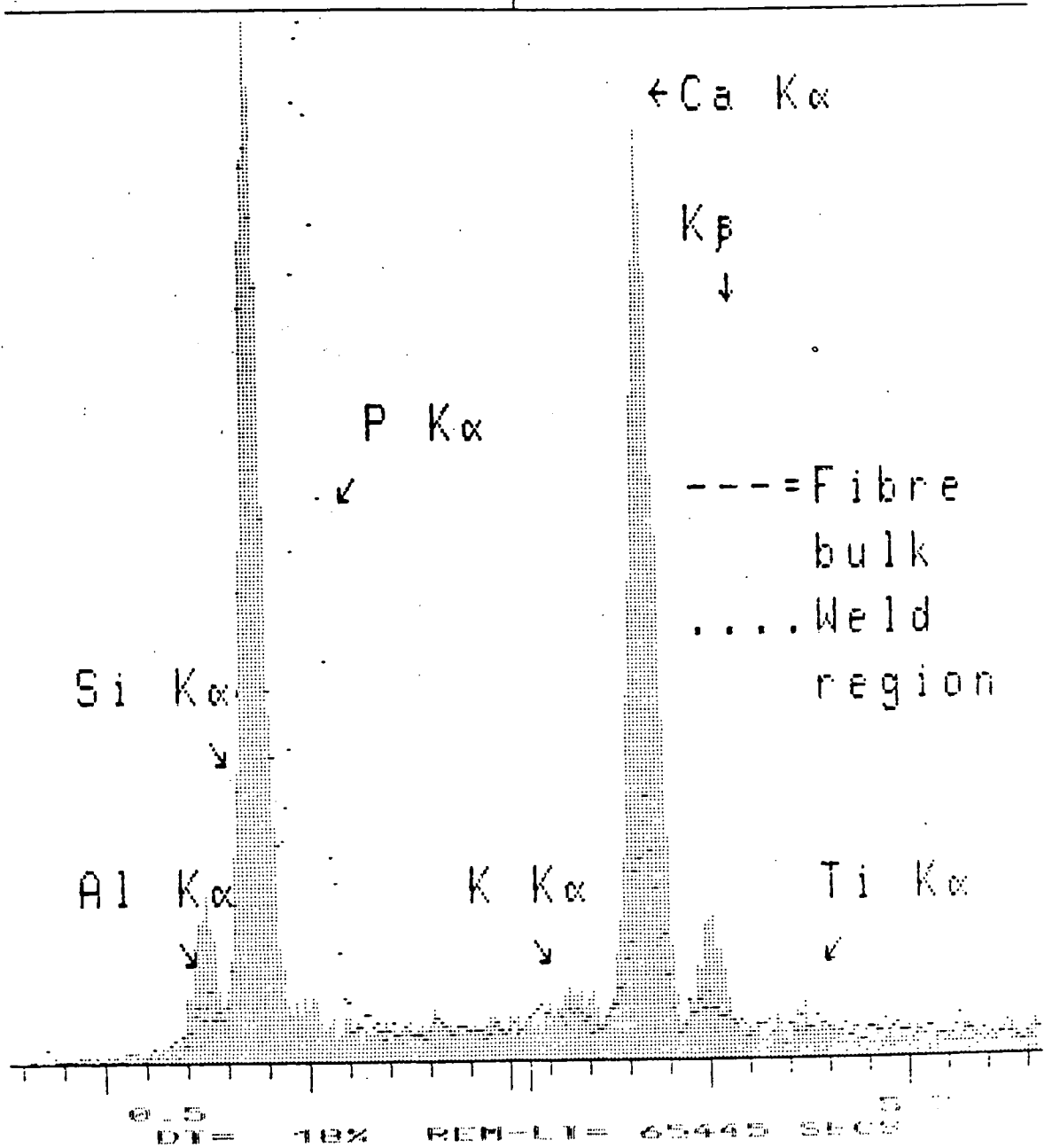


Fig. 9.8 EDAX spectra of a feature (large fibre joined to another) from 44.44% weight gain RBSN; H₃PO₄ etched. [Refer to Plate 9.6a].

33 CNT

511 P3: D

3290 EV

10 LUCHAN

Link Systems 800 Analyser

25 Jan 84

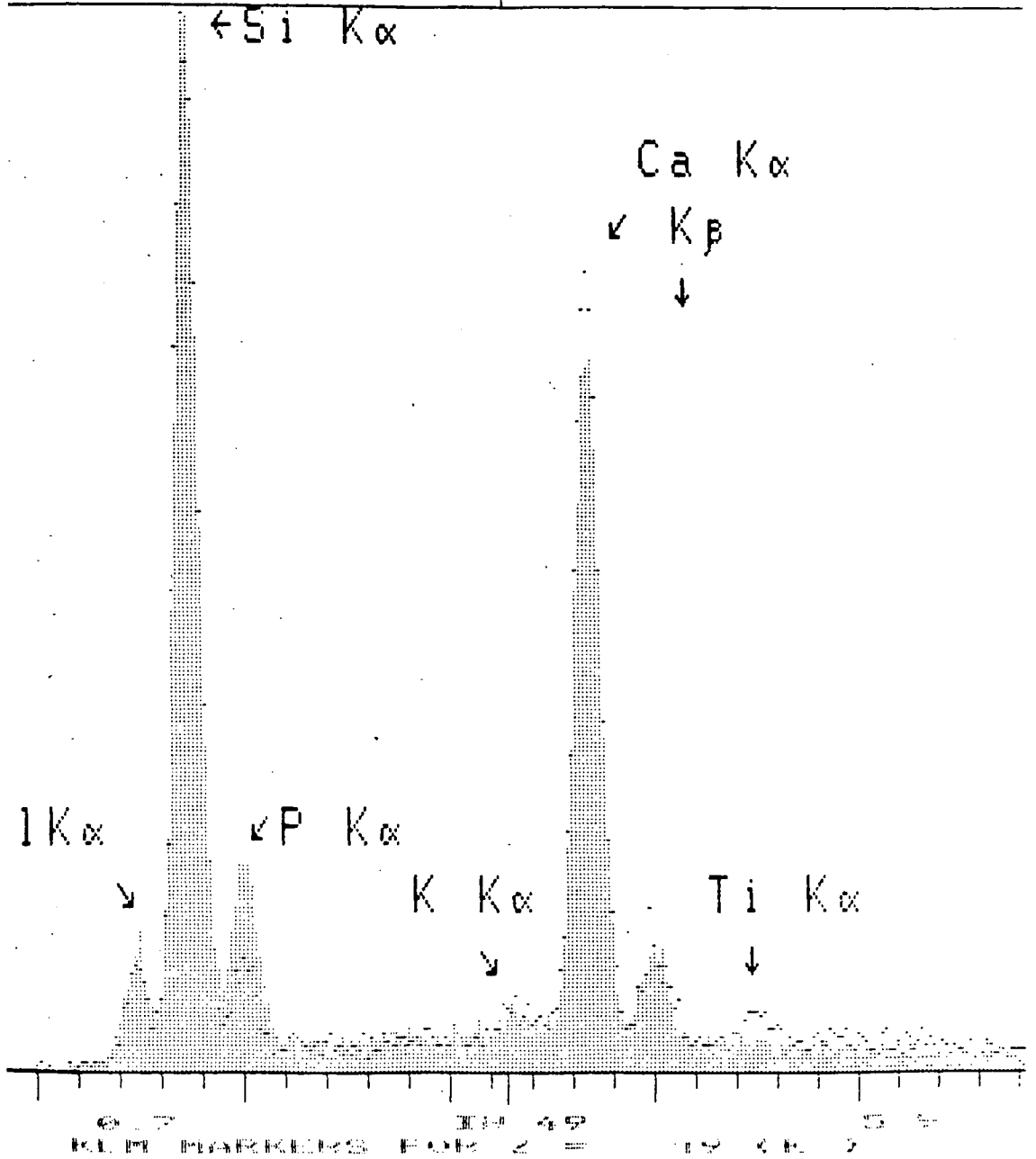


Fig. 9.9 EDAX spectra of two regions of a feature [Plate 9.6b] from 44.44% weight gain RBSN; H₃PO₄ etched.

calcium as the main impurity with traces of Al, K, and Ti present. Plates 9.7a and 9.7b show two more distinct features on the same surface and EDAX plots (Fig. 9.10 and 9.11) show that calcium is again the main impurity in both these features and traces of Al and Ti are present as well. It can be concluded here that etching the surface of the sample with hot H_3PO_4 has left the surface with distinct features containing impurities, mainly calcium with traces of Al, K and Ti. This supports the conclusion of the RHEED study on H_3PO_4 etched samples, that the extra diffraction lines not attributable to pure silicon and silicon nitride can be attributed to $CaSi_2$.

Because of the charging effects mentioned above in the case of the 63.29% weight gain sample, no micrograph is available for this specimen. However, the sample was carefully studied and it was found that the surface did not reveal the presence of any calcium fibres as seen in the sample with 44.44% weight gain. The EDAX plot, Fig. 9.12, of a precipitate on the surface of the sample shows the presence of sulphur and chlorine. The calcium peak cannot be distinguished from the background. Thus it can be assumed that most of the impurities must have volatilized during the long nitridation process of necessary to produce the fully nitrided sample.

c) fracture surface

The general microstructure of a fracture surface of a sample with 44.44% weight gain is shown in Plate 9.8a. Plate 9.8b shows a typical precipitate seen on the fracture surface. The corresponding EDAX plot, Fig. 9.13 shows the

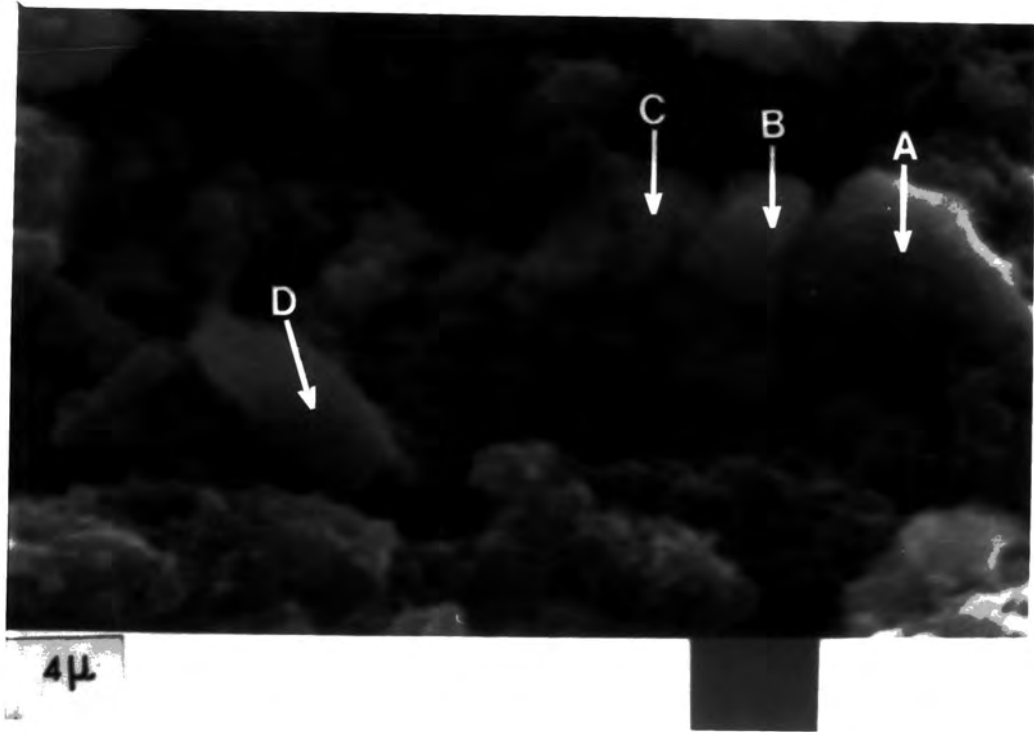


Plate 9.7a Surface features, H_3PO_4 etched surface (44.44%)

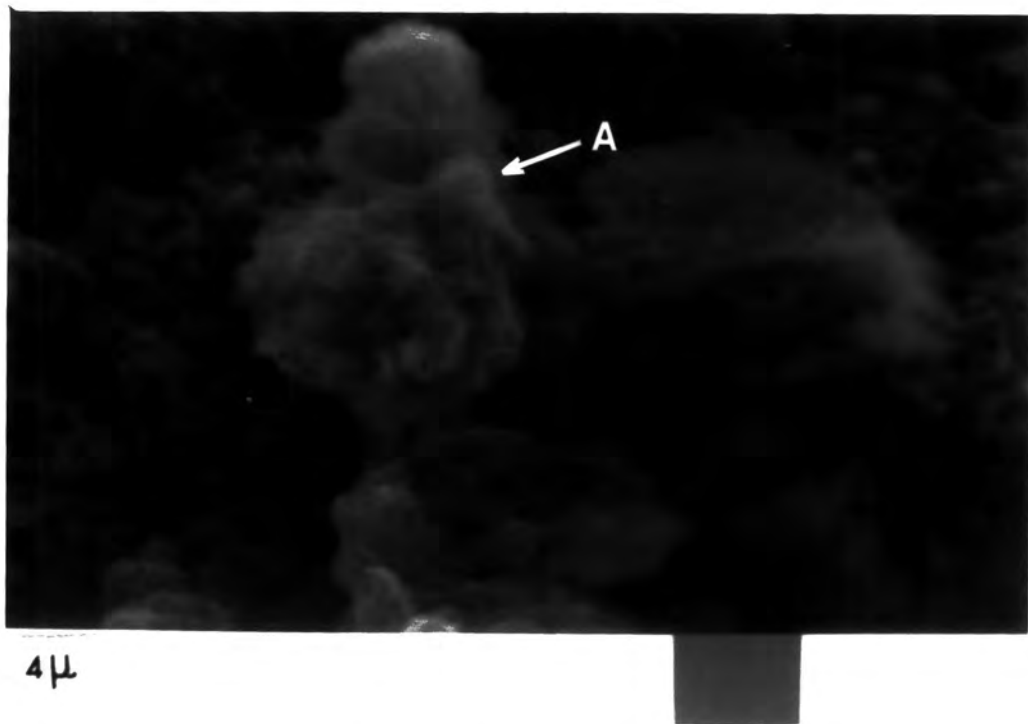


Plate 9.7b Surface feature, H_3PO_4 etched surface (44.44%)

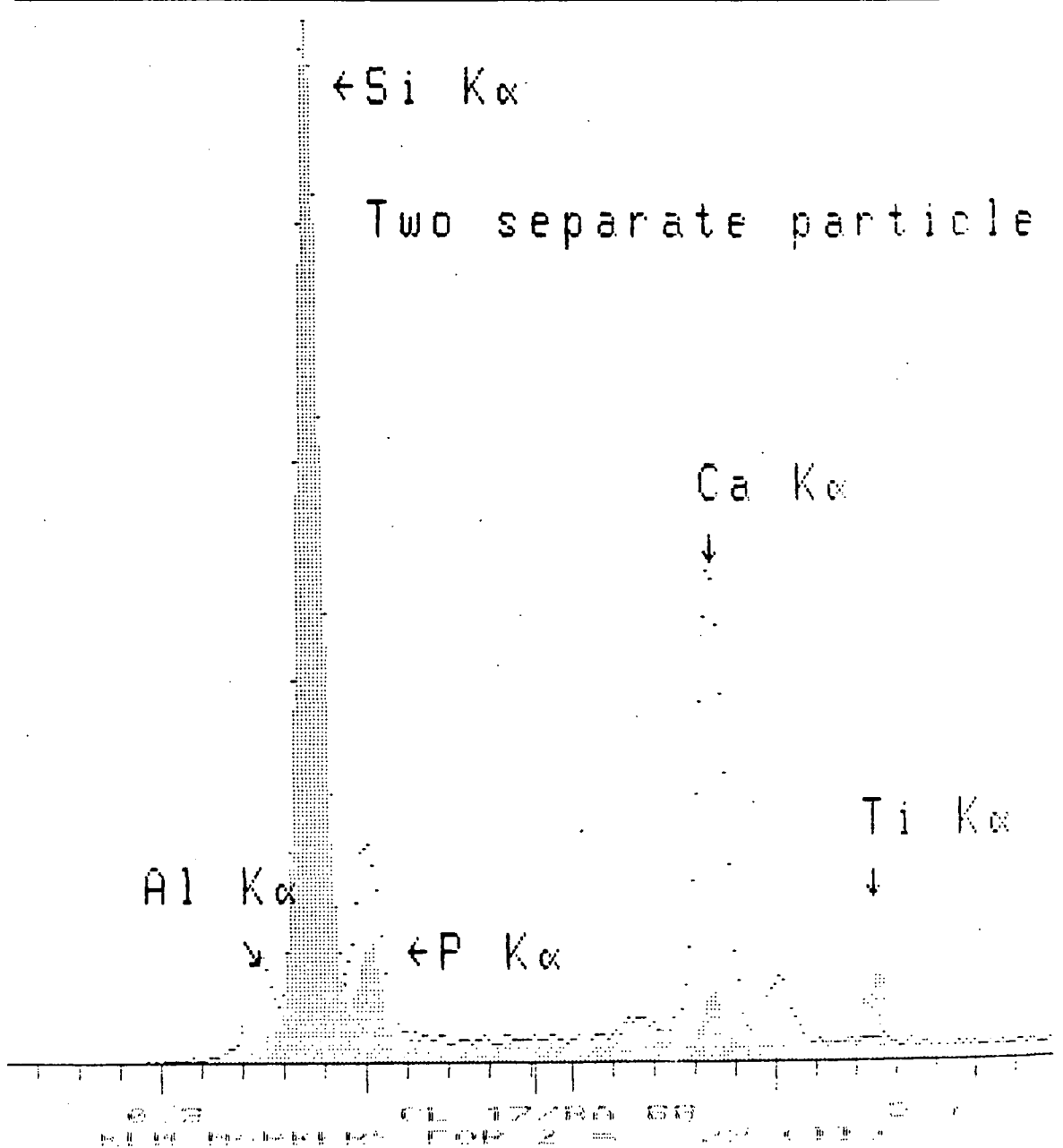


Fig. 9.10 EDAX spectra of a feature [Plate 9.7a] from 44.44% weight gain RBSN; H₃PO₄ etched.

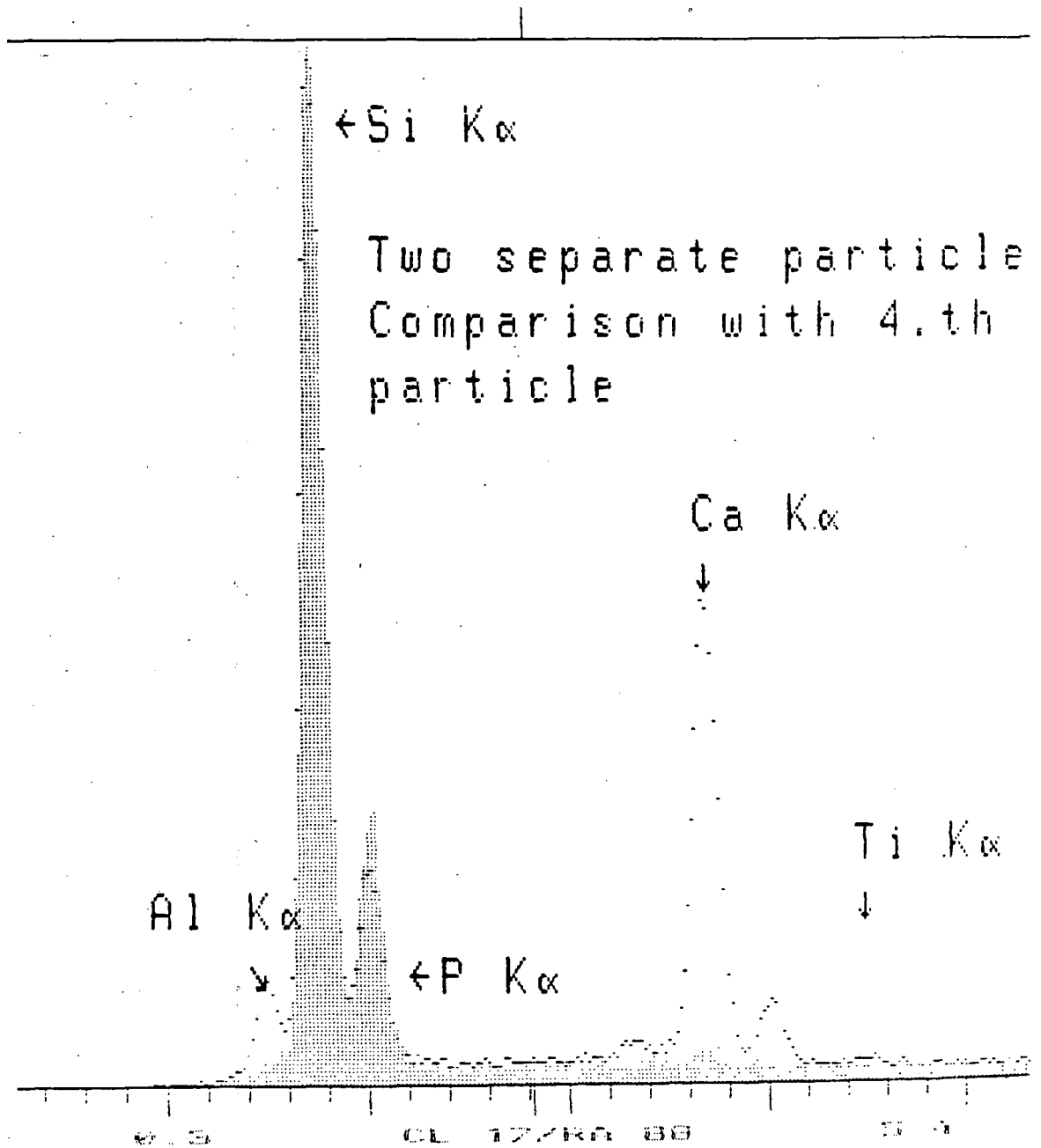


Fig. 9.11 EDAX spectra of a feature [Refer to Plate 9.7b] from 44.44% weight gain RBSN; H_3PO_4 etched.

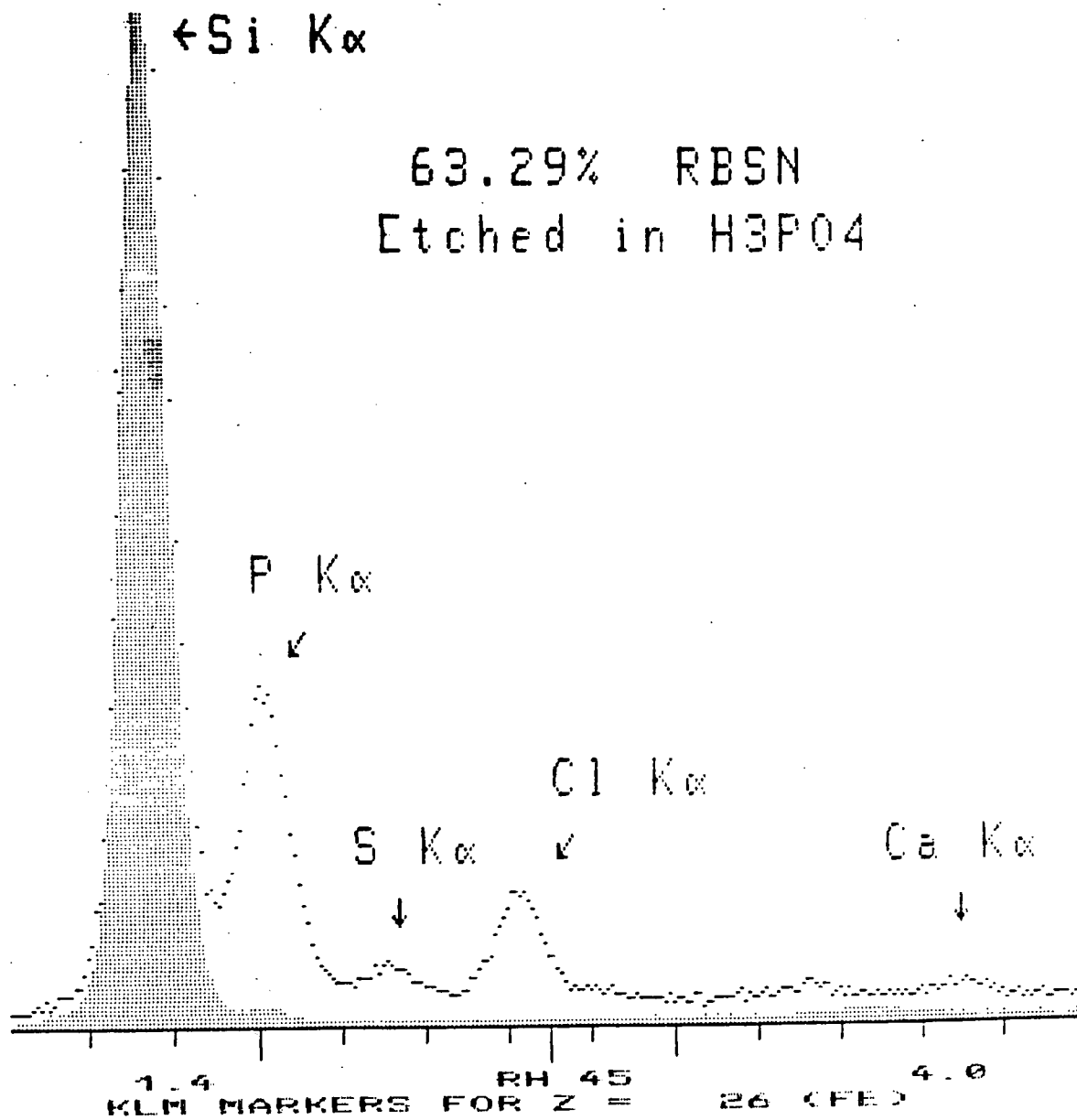
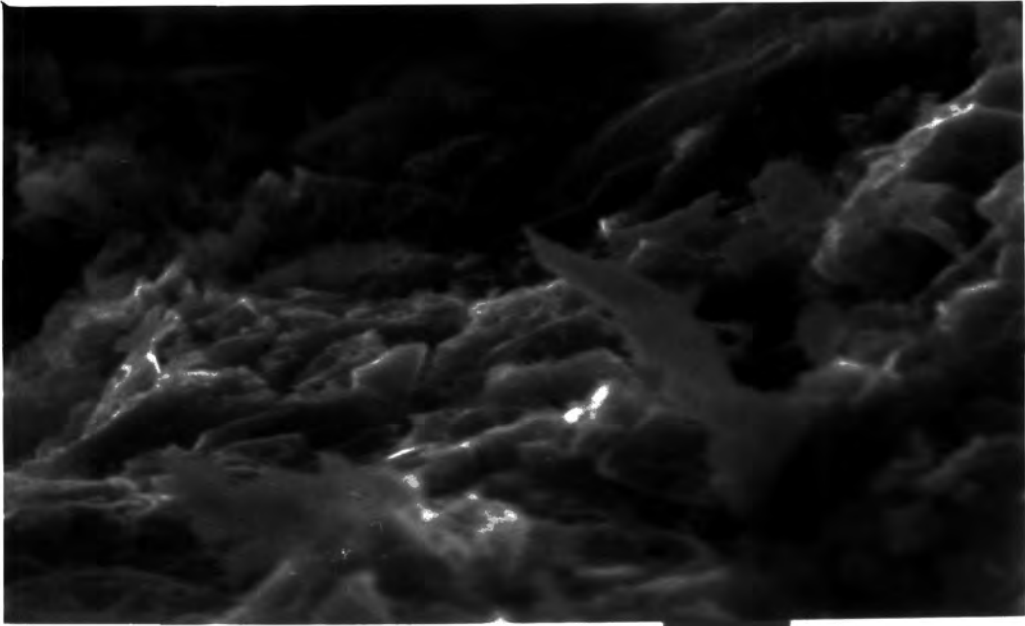
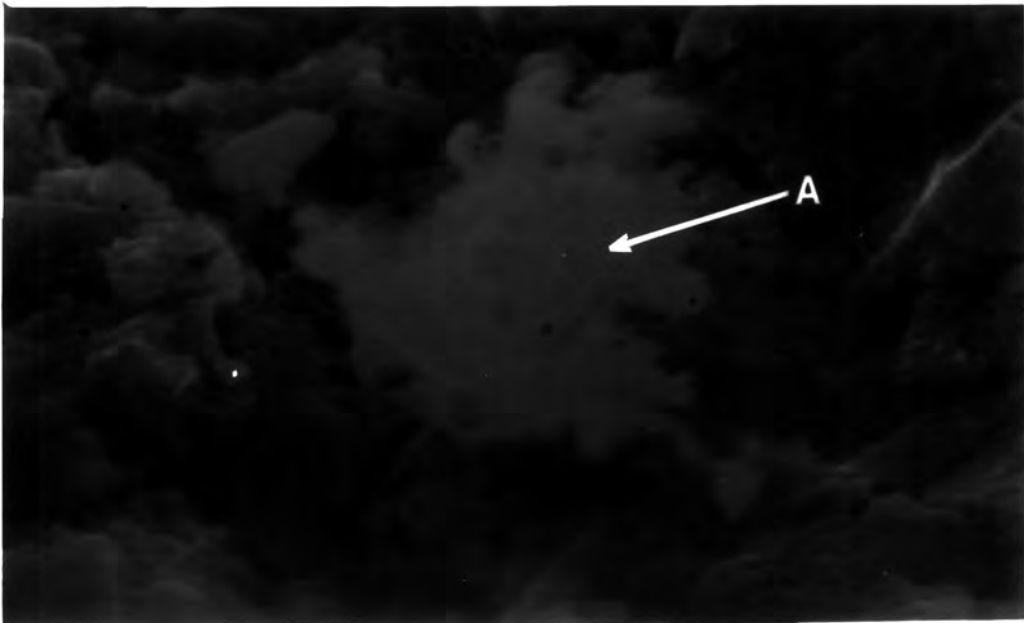


Fig. 9.12 EDAX spectra of a precipitate on the surface of 63.29% weight gain RBSN (H₃PO₄ etched); shaded trace represent the background.



4 μ

Plate 9.8a Micrograph of fracture surface (44.44% weight gain RBSN)



4 μ

Plate 9.8b Precipitate seen on fracture surface (44.44%)

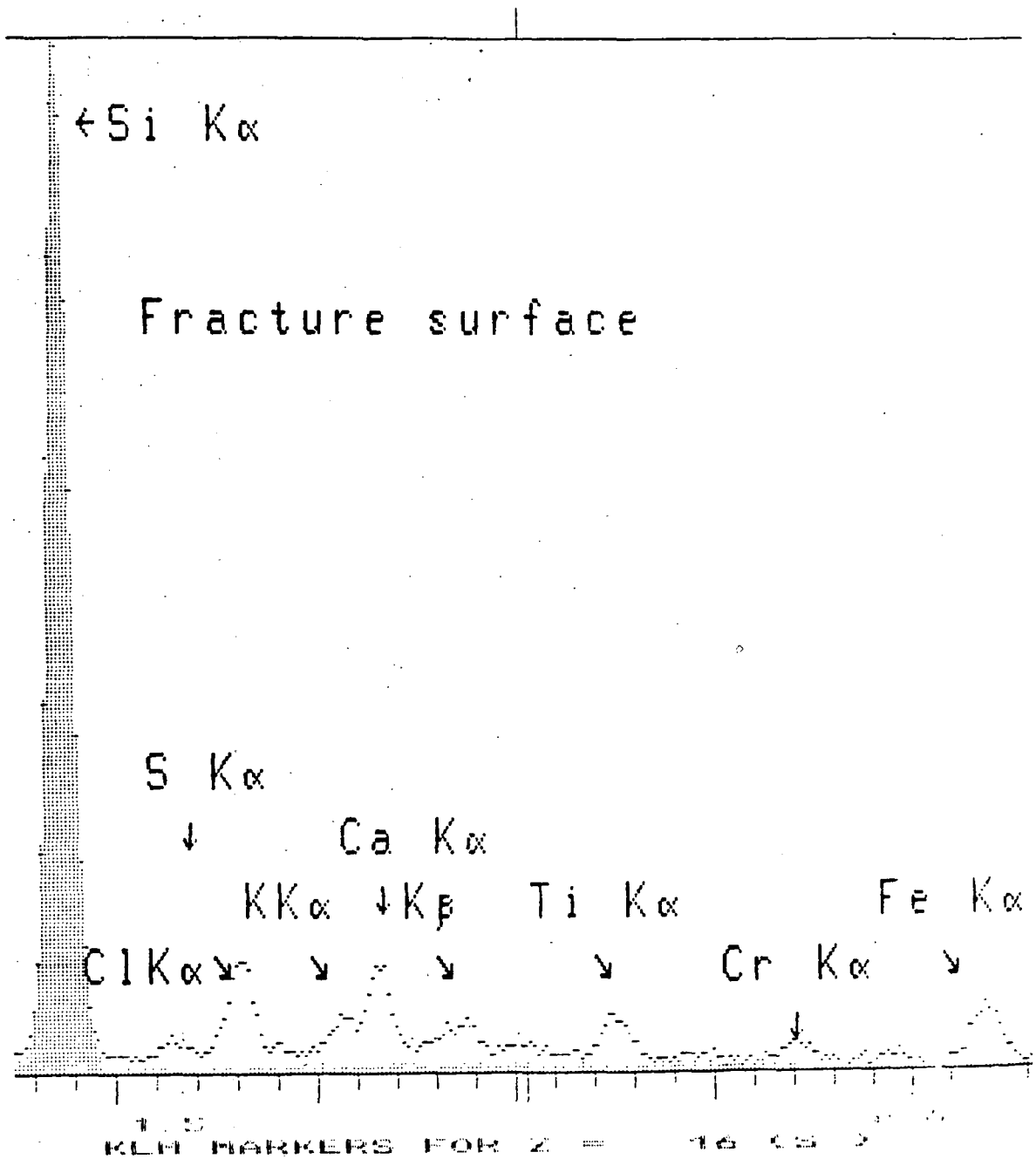


Fig. 9.13 EDAX spectra of a precipitate on the fracture surface of 44.44% weight gain RBSN [Refer to Plate 9.8]; shaded trace represents the background.

presence of sulphur (S), chlorine (Cl), potassium (K), calcium (Ca), titanium (Ti), chromium (Cr) and iron (Fe) in this precipitate. There was no phosphorus observed; thus the assumption that the phosphorus seen in the EDAX plot of the surface etched with H_3PO_4 came from the acid itself is valid. Apart from phosphorus all the other mentioned impurities present on the etched surfaces can be detected in the fracture surface; thus all the impurities are genuinely present in the bulk of the samples studied.

In conclusion, the structural studies on the RBSN samples supplied by AME (Gateshead) revealed the two major impurities to be $FeSi_2$ and $CaSi_2$. Further, the microstructural studies using the SEM and EDAX facility showed traces of aluminium, chlorine, sulphur, potassium, calcium, titanium, chromium and iron present in the sample. Furthermore the impurities are much more easily detected in the partially nitrified sample. The fact that the impurities tend to conglomerate into large precipitates, instead of being distributed evenly in the sample, makes their contribution to the dielectric properties of the sample much more significant. This experimental evidence suggests strongly that the contribution from impurities must be considered in the analysis of the dielectric measurement results.

9.2 DIELECTRIC THEORY OF COMPOSITE MATERIALS

A brief review is first given of previous work on the permittivity of composite materials consisting of separate known phases such that the material can be considered in the same way as a mixture of different powders. The permittivity of a composite material depends not only on the permittivity

of each phase and its volume fraction but also on the geometry of each of the particles of the composite phases. However, the permittivity of a two phase composite material must be between certain limits whatever the geometry of each constituent and if some knowledge of the particle geometry is available, still closer bounds can be set on the possible values of the permittivity. The theoretical work on the dielectric behaviour of heterogeneous systems has been described in a review by Van Beek [9.7]. A review paper on the physical properties of composite materials by Hale [9.9] gives some of the more important permittivity relationships for two phase composite materials. Hale's values given in Tables I and II and Fig. 2 of Reference 9.9 are respectively reproduced in Tables 9.6 and 9.7 and Fig. 9.14. The permittivity of the composite is represented by ϵ^* , the upper and lower bounds by ϵ_+ and ϵ_- , the volume fractions of the two phases by V_1 and V_2 , and the permittivity by ϵ_1 and ϵ_2 ($\epsilon_2 > \epsilon_1$).

From the plot in Fig. 9.14 it is obvious that ϵ^* , the permittivity of the composite material, does not go higher than ϵ_2 . In fact all the traces in the plot show ϵ^* slowly decreases from the value at ϵ_2 to the value of ϵ_1 , i.e the values of ϵ^* lie between the two limits, ϵ_2 and ϵ_1 . However, the salient feature of the experimental results (Fig. 9.4) is that the measured permittivities for medium weight gain RBSN samples are substantially higher than the value of permittivity for pure silicon. The voids have a permittivity value equal to unity, thus contributing very little to the overall permittivity of the ceramic. Therefore a three-phase RBSN regarded as a mixture of silicon nitride, pure silicon and voids should not have a permittivity value

TABLE 9.6

System	Dilute suspension $\epsilon_m = \epsilon_2$	
Spheres	$\epsilon^* = \epsilon_2 \frac{2\epsilon_2 + \epsilon_1 + 2V_1(\epsilon_1 - \epsilon_2)}{2\epsilon_2 + \epsilon_1 - V_1(\epsilon_1 - \epsilon_2)}$	Eq.9.1
	$\epsilon^* = \epsilon_2 + \frac{3V_1\epsilon_2(\epsilon_1 - \epsilon_2)}{2\epsilon_2 + \epsilon_1}$	Eq.9.2
Discs or lamellae	$\epsilon^* = \epsilon_2 + \frac{V_1(\epsilon_1 - \epsilon_2)(\epsilon_2 + 2\epsilon_1)}{3\epsilon_1}$	Eq.9.3
Rods, needles or fibres	$\epsilon^* = \epsilon_2 + \frac{V_1(\epsilon_1 - \epsilon_2)(5\epsilon_2 + \epsilon_1)}{3(\epsilon_1 + \epsilon_2)}$	Eq.9.4
SCS approximation $\epsilon_m = \epsilon^*$		
	$\epsilon^* = \epsilon_2 + \frac{3V_1\epsilon^*(\epsilon_1 - \epsilon_2)}{2\epsilon^* + \epsilon_1}$	Eq.9.5
	$\epsilon^* = \epsilon_2 + \frac{V_1(\epsilon_1 - \epsilon_2)(\epsilon^* + 2\epsilon_1)}{3\epsilon_1}$	Eq.9.6
	$\epsilon^* = \epsilon_2 + \frac{V_1(\epsilon_1 - \epsilon_2)(5\epsilon^* + \epsilon_1)}{3(\epsilon^* + \epsilon_1)}$	Eq.9.7

TABLE 9.7

Bounds for the dielectric constants of isotropic two-phase composites

Wiener

$$\epsilon_{(+)}^* = \epsilon_1 V_1 + \epsilon_2 V_2 \quad \text{Eq. 9.8}$$

$$\epsilon_{(-)}^* = \frac{1}{(V_1/\epsilon_1) + (V_2/\epsilon_2)} \quad \text{Eq. 9.9}$$

Hashin and Shtrikman

$$\epsilon_{(+)}^* = \epsilon_2 + \frac{V_1}{[1/(\epsilon_1 - \epsilon_2)] + (V_2/3\epsilon_2)} \quad \text{Eq. 9.10}$$

$$\epsilon_{(-)}^* = \epsilon_1 + \frac{V_2}{[1/(\epsilon_2 - \epsilon_1)] + (V_1/3\epsilon_1)} \quad \text{Eq. 9.11}$$

where $\epsilon_2 > \epsilon_1$

Beran

$$\epsilon_{(+)}^* = \left[\langle \epsilon \rangle - \frac{\langle (\epsilon')^2 \rangle}{3\langle \epsilon \rangle + (9\langle \epsilon \rangle^2 / \langle (\epsilon')^2 \rangle)} \right] \quad \text{Eq. 9.12}$$

$$\epsilon_{(-)}^* = \left[\left\langle \frac{1}{\epsilon} \right\rangle - \frac{(4/9\langle \epsilon \rangle^2) \langle \epsilon' / \epsilon \rangle^2}{(1/3\langle \epsilon \rangle^2) \langle (\epsilon')^2 / \epsilon \rangle + J} \right]^{-1} \quad \text{Eq. 9.13}$$

where

$$I = \frac{1}{16\pi^2 \langle \epsilon \rangle^2} \int_{V_s} \int_{V_r} \left(\frac{\delta^2 \langle \epsilon'(0) \epsilon'(r) \epsilon'(s) \rangle}{\delta r_s \delta s_s} \right) \frac{r_i s_i}{r^3 s^3} dr ds$$

$$J = \frac{1}{16\pi^2 \langle \epsilon \rangle^2} \int_{V_s} \int_{V_r} \left(\frac{\delta^2 \langle \epsilon'(r) \epsilon'(s) / \epsilon(0) \rangle}{\delta r_s \delta s_s} \right) \frac{r_i s_i}{r^3 s^3} dr ds$$

$\epsilon(x)$ = dielectric constant at point x

$\epsilon'(x)$ = $\epsilon(x) - \langle \epsilon \rangle$

$\langle \epsilon \rangle$ = ensemble average of $\epsilon(x)$ (assumed to be equal to the spatial average)

$\langle \epsilon'(0) \epsilon'(r) \epsilon'(s) \rangle$ = ensemble average of the product of ϵ' at some co-ordinate origin within the composite, ϵ at a position r from the origin and ϵ' at position s

r, s = sets of three orthogonal space vectors with a common origin.

V_r, V_s = volumes of infinite spheres in vector spaces denoted by subscripts.

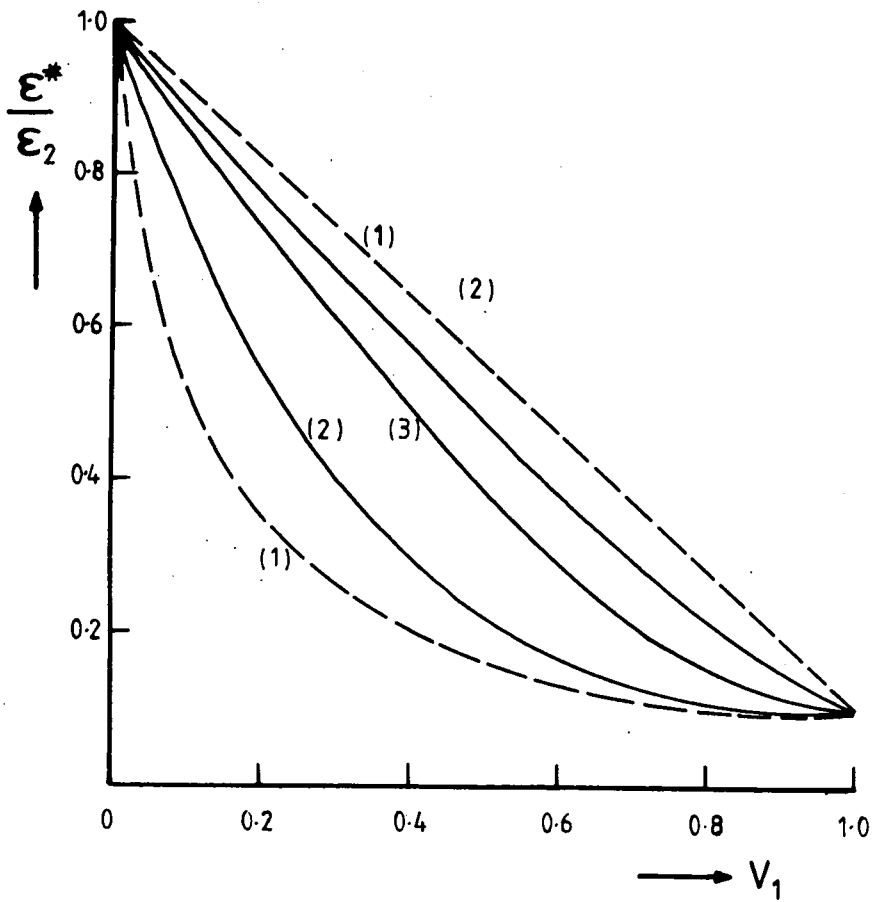


Fig. 9.14 Dielectric constant of composite materials ($\epsilon_1/\epsilon_2 = 0.1$). (1) Weiner bounds (equations 9.8 and 9.9), (2) Hashin and Shtrikman bounds for arbitrary geometry (equations 9.10 and 9.11), (3) Bottcher SCS approximation for spheres in a continuous matrix (equation 9.5).

higher than that of the pure silicon. Thus, in the samples examined the most likely explanation is that other phases are present which have permittivity values much higher than that of silicon. This is partially supported by the results of the structural and microstructural studies of the material, which show the presence of both FeSi_2 and CaSi_2 phases, though it is unfortunate that a literature search has not revealed published data for the permittivity of these silicides.

Considerable care must be taken however in attempting to apply the Wiener theory directly to the situations which arise in partially-nitrided RBSN. In the first place it must be borne in mind that the temperature and time conditions used for nitriding differ for each different weight gain (c.f. Table 7.1). Consequently the variation of composition with weight gain is complex and the occurrence of certain additional silicide phases may well be important only in certain regimes. There is also evidence that evaporation of certain phases may occur during high temperature nitriding such as would be used for producing high weight gain material. Thus Messier and Wong [9.14] in a thermo-gravimetric study on RBSN have reported the loss of silicon during controlled nitridation, attributing this to volatilization. The nitridation temperature used to make high weight gain samples can go up to at least 1450°C ; it is known that the melting point of FeSi_2 is 1208°C , so it is possible that vapourisation may also apply to some silicide phases under similar conditions.

9.5 CONCLUSIONS AND SUGGESTIONS

The dominant a.c conduction mechanism for the whole range of weight gain of RBSN is a hopping process. The log-log plots of the dielectric parameters against frequency for all the samples studied are straight lines with gradients of about 0.97 ± 0.03 . However the plot of the measured permittivity against the weight gain goes through a peak at about 22% weight gain. A three phase model consisting only of silicon nitride, pure silicon and voids cannot account for the peak. It is suggested that the contribution of the impurities must be considered to explain the presence of the peak. Structural studies on the ceramic using the X-ray diffraction and RHEED techniques reveal that the main impurities are FeSi_2 and CaSi_2 . The microstructural study using the SEM with the EDAX facility showed traces of aluminium, sulphur, chlorine, potassium, calcium, titanium, chromium and iron to be present. It would be of considerable interest to analyse the permittivity data of Fig. 9.4 by making a more detailed characterisation of the properties of each phase present at each particular weight gain and to attempt to correlate the shape of the permittivity curve with the growth and decay of impurity phases.

REFERENCES

- 9.1 "Some properties of Reaction Bonded Silicon Nitride"
T.G. Bushell - Ph.D thesis - University of Durham (1983)
- 9.2 "Improved wideband coaxial methods for dielectric measurements on nitrogen ceramics" - A.B. Ahmad
Ph.D thesis - University of Durham (1983)
- 9.3 "Dielectric anomalies in silicon single crystals"
K.V. Rao and A. Smakula - J. Applied Physics Vol.37,
p2840, (1966)
- 9.4 "Statistical methods for technologists" - C.G. Paradine
and P.H.P. Rivett - The English Universities Press, (1960)
- 9.5 "A second course in statistics" - R. Loveday
Cambridge University Press, (1961)
- 9.6 "The electronic structure of silicon nitride"
R.J. Sokel - J. Phys. Chem. Solids Vol.41, p899, (1980)
- 9.7 "Dielectric behaviour of heterogeneous system"
L.K.H. Van Beek - Progress in Dielectric 7, p71, (1967)
- 9.8 "Solid mixture permittivities" - W.F. Brown Jr.
J. Chemical Physics Vol.23, No.8, p1514, (1955)
- 9.9 "Review - The physical properties of composite materials" - D.K. Hale
J. Mat. Science Vol.11, p2105, (1976)
- 9.10 "A variational approach to the theory of the effective magnetic permeability of multiphase materials"
Z. Hashin and S. Shtrikman
J. Applied Physics Vol.33, No.10, p3125, (1962)

- 9.11 "Bounds for effective electrical, thermal and magnetic properties of heterogeneous materials" - M.N. Miller
J. Mathematical Physics Vol.10, No.11, p1988, (1969)
- 9.12 "The dielectric constant of fibre composite"
W.E.A. Davies - J. Phys. D Vol.7, Appl. Phys. p120,(1974)
- 9.13 "Effect of Iron, Titanium and Hafnium on second stage nitriding of silicon" - J. Mukerji and S.K. Biswas
J. of the American Ceramic Soc. Vol.64, No.9, p549,(1981)
- 9.14 "Kinetics of nitridation of silicon powder compacts"
D. R. Messier and P. Wong
J. of the American Ceramic Soc. Vol.56, No.9, p480,(1975)

